الجمهورية الجزائرية الديمقراطية الشعبية
REPUBLIQUE ALGERIENNE DEMOCRATIQUE ET POPULAIRE
وزارة التعليم العالي والبحث العلمي
MINISTERE DE L'ENSEIGNEMENT SUPERIEUR ET DE LA RECHERCHE SCIENTIFIQUE
جامعة فرحات عباس سطيف 1
UNIVERSITE FERHAT ABBAS SETIF1
UFAS1 (ALGERIE)

THESE

Présentée à la Faculté de Technologie

Pour l'Obtention du Diplôme de

Doctorat

Domaine : Science et Technologie
Filière : Electronique
Option : Electronique et commande industrielle

Par

Mr. LAIB Abdelbaset

Commande robuste de systèmes photovoltaïques interconnectés au réseau avec convertisseurs multi niveaux

Soutenue le : 02/05/2019 devant un jury composé de :

AMARDJIA Noureddine	Professeur	Univ. Sétif 1	Président
KRIM Fateh	Professeur	Univ. Sétif 1	Directeur de thèse
REKIOUA Toufik	Professeur	Univ. Bejaia	Examinateur
LACHOURI Abderrazak	Professeur	Univ. Skikda	Examinateur
BADOUD Abdessalam	MCA	Univ. Sétif 1	Examinateur

A Robust Control for Grid-Connected PV Systems using Multilevel Inverters

by

LAIB Abdelbaset

A thesis
presented to the University of Sétif 1
in fulfillment of the
thesis requirement for the degree of
Doctor of Philosophy
in
Electronics and Industrial Control

To my mother

To my Father

To my brother and my sisters

Acknowledgement

*In the name of **ALLAH**, the Most Gracious and the Most Merciful. Thanks to **ALLAH** who is the source of all the knowledge in this world, for the strengths and guidance in completing this thesis.*

*I express my deep sense of gratitude and heart-felt thanks to my supervisor, Prof. **KRIM Fateh**, for his invaluable guidance, patience, kindness and consistent encouragement throughout the course of this work. I am very glad that I have pursued my doctoral studies under his excellent supervision.*

*I would like to express my appreciation to my thesis committee members: Prof. **AMARDJIA Noureddine**, Prof. **REKIOUA Toufik,** Prof. **LACHOURI Abderrazak** and Dr. **BADOUD Abdesslem,** for their discussions, suggestions, and feedbacks to improve my thesis.*

*I cannot forget to mention all my friends, **LEPCI** group, Dr. **TALBI Billel**, **SAHLI Abdeslem**, **KIHAL Abbes,** Dr. **FEROURA Hamza**, Dr. **BELAOUT Abdesslam**, **BOUYAHIA Semcheddine,** Dr.**ARABI Abderrazak, MEDKOUR Hicham**, **BELGUIDOUM Fouzi,** and **BARA Seif**, for their great friendship, help and support.*

LAIB Abdelbaset

Abstract

Several grid-connected PV topologies are investigated in this dissertation for low, medium and high-power applications. Furthermore, an effective controller has been proposed for these topologies instead of conventional control strategies. The latter's suffer from several drawbacks such as bad MPPT tracking, inaccurate grid power control, low grid current quality, hard implementation practically and variable switching frequency. To overcome these drawbacks, a model predictive control (MPC) strategy is proposed to control the power converters employed in the investigated grid-connected PV topologies. The major drawbacks of MPC strategy are variable inherent switching frequency and computational burden especially in case of high-level inverters. Therefore, these drawbacks are taking into account in the design of proposed controllers.

Firstly, an improved control strategy based on fixed switching predictive control strategy for three-phase dual-stage grid-connected PV system is proposed. A variable incremental current step size of an MPPT current oriented loop based on fixed-switching predictive current control is proposed and employed to control the DC-DC converter. While, a modified VOC based on predictive control strategy and space vector modulation (SVM) is employed to control the DC-AC converter.

Afterwards, High-level NPC inverters are employed in grid-connected PV system in order to inject a high produced PV power into the grid with high performance operation. On the other hand, a simple and effective model predictive control (MPC) algorithm is proposed for grid-connected PV system using high-level NPC inverter (six-level) that permits to inject the active power generated by the PV system, the reactive power demanded by the grid operator and assure the balance of DC-link capacitor voltages. Then, an optimized model predictive control (O-MPC) is proposed in order to achieve the same performance control provided by the MPC algorithm but with a significant reduction in computational burden.

Finally, a topology that divided the large PV array to string modules with individual DC-DC converter connected to a centralized multilevel inverter is investigated in order to overcome the problems resulted by connecting the PV modules as large PV array. Simple and effective controllers for this topology based on finite control set model predictive control (FCS-MPC) strategy is proposed. A voltage oriented maximum power point tracking (VO-MPPT) performed by an FCS-MPCC is applied for each DC-DC converter to draw the maximum power point from each string PV modules. In addition, an FCS-MPC controller is proposed to control the centralized multilevel NPC inverter connected to the grid.

The simulation and HIL results validate the proposed control schemes for the investigated grid-connected PV topologies.

Keywords: Photovoltaic energy, Grid-connected PV systems, Multilevel inverters, Maximum power point (MPPT), Model predictive control.

Table of Contents

List of Figures

List of Tables

List of Acronyms

AC	Alternating Current
ANN	Artificial neural network
AI	Artificial intelligence
CHB	Cascaded H-Bridge
CO-MPPT	Current based MPPT
DC	Direct Current
DPC	Direct power control
EPIA	European Photovoltaic Industry Association
FCS-MPC	Finite control set model predictive control
FLC	Fuzzy logic control (controller)
GA	Genetic algorithm
GW	Gigawatt
HIL	Hardware in the loop
IGBT	Insulated Gate Bipolar Transistor
INC	Incremental conductance
IncCon	Incremental conductance
I-V	Current-voltage
MPC	Model Predictive Control
MPP	Maximum Power Point
MPPT	Maximum Power Point Tracking
NPC	Neutral-Point Clamped
P&O	Perturb and observe
PC	Predictive Control
PCC	Predictive Current Control

PI	Proportional-Integral
PID	Proportional-integral-derivative
PS-VOC	VOC based on predictive control strategy and SVM
V-DPC	Voltage based direct power control
VFOC	Voltage flux-oriented control
PLL	Phase Locked Loop
VS-INC	Variable step-size incremental conductance
PSO	Particle swarm optimization
PV	Photovoltaic
P-V	Power-voltage
PWM	Pulse Width Modulation
SVM	Space Vector Modulation
THD	Total harmonic distortion
V-DPC	Voltage based direct power control
VFOC	Voltage flux-oriented control
VOC	Voltage oriented control
VS-INC	Variable step-size incremental conductance
VSI	Voltage Source Inverter

List of Symbols

i_{pv} , $i_{pv}(k)$	Measured PV array current (A)
$i_{pv}(k-1)$	Previous measured PV array current (A)
v_{pv} , $v_{pv}(k)$	Measured PV array voltage (V)
$v_{pv}(k-1)$	Previous measured PV array voltage (V)

p_{pv}, $p_{pv}(k)$	Measured PV array power (W)
$\Delta p_{pv}(k)$	Measured PV array power variation (W)
$\Delta i_{pv}(k)$	Measured PV array current variation (A)
$\Delta v_{pv}(k)$	Measured PV array voltage variation (V)
i_{ref} , $i_{ref}(k)$	Reference PV array current (A)
$i_{ref}(k-1)$	Previous reference PV array current (A)
$\Delta i_{ref}(k)$	Step of reference PV array current (A)
$d(k), d(k+1)$	Actual and predicted duty cycle
G	Irradiance (W/m²)
i_{inv} , $i_{inv}(k)$	Inverter input current (A)
S	Control action of boost converter
v_{dc}, v_{dc_ref}	Measured DC-link voltage & reference DC-link voltage (V)
v_{ga}, v_{gb}, v_{gc}	Grid voltages (V)
v_{gd}, v_{gq}	Grid voltages in d-q frame (V)
i_{ga}, i_{gb}, i_{gc}	Grid currents (A)
i_d, i_q	Measured grid current in d-q frame (A)
$i_d(k+1), i_q(k+1)$	Predicted grid current in d-q frame (A)
i_{d_ref}, i_{q_ref}	Reference grid current in d_q frame (A)
v_α, v_β	Voltage vector in α-β frame (V)
v_d, v_q	Voltage vector in d-q frame (V)
Q_{ref}	Reactive power reference (VAR)
Q	Reactive power (VAR)
S_g	Grid apparent power (VA)
a,b,c	Natural frame quantities
d,q	Synchronous frame quantities

α,β	Stationary frame quantities
$S_{a1}, S_{a2}, S_{b1}, S_{b2}, S_{c1}, S_{c2}$	Control action of the inverter
f_g	Grid frequency (Hz)
ω_g	Grid angular frequency (rad/s)
θ	Grid voltage angle (rad)
T_s	Controller sampling time (s)
g	Cost function
k	Discrete-time present sampling instant
$k-1$	Discrete-time past sampling instant
$k+1$	Discrete-time future sampling instant
t	Continuous-time
λ_{dc}	Weighting factor for dc-link capacitor voltages balancing
λ_{swc}	Weighting factor for switching frequency reduction
$\frac{d}{dt}$	Derivative operator
S_x	Level of voltage vector of phase $x = a, b, c$
S_{xj}	Switching states of phase $x = a, b, c$, $j = 1, 2, \cdots$
swc_x	Number of switch changes in inverter phase $x = a, b, c$

Chapter 1

Introduction

1.1 INTRODUCTION

The world has been suffering from several environmental problems in the last decades (air pollution, global warming …), this was due to the massive incontrollable use of oil and carbon as energy sources [1]. For this reason, clean energy sources were emerged like the suitable solution in order to circumvent the present problems, since, they possess inherent benefits towards the environment [1-3].

Solar energy through PV array systems is one of the most commonly used from renewable power sources. Where, a latest statistic study [4] shows the exponential increase in PV global capacity beside to wind global capacity from 2007 to 2017 in the world compared to other renewable sources as illustrated in Figure 1.1. The world solar PV global capacity increased exponentially from 8 GW in 2007 to 402 GW in 2017. While, the annual additions are increased from 2.5 GW in 2007 to 98 GW in 2017 as shown in Figure 1.2. For that, the solar PV global capacity would reach 1100 GW by 2030, according to the European Photovoltaic Industry Association (EPIA) [5].

This exceptional growth in PV arrays utilization is due to the cost reduction of PV modules and the introduction of economic incentives or subsidies. Moreover, PV arrays can range it easily as small scale for low power systems (individual utilizations) or large scale for high power systems, compared to other renewable energy sources that have higher costs [6]. According to the connection into the public grid, the PV systems can be divided in two categories: stand-alone PV systems and grid-connected PV systems.

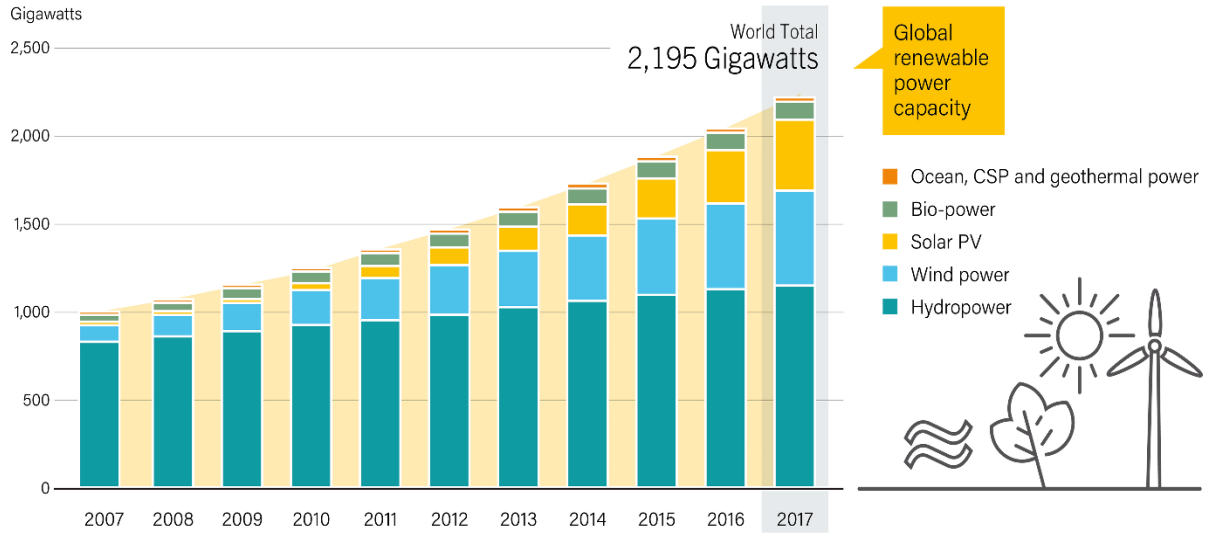

Figure 1.1: Global renewable power capacity, 2007-2017.

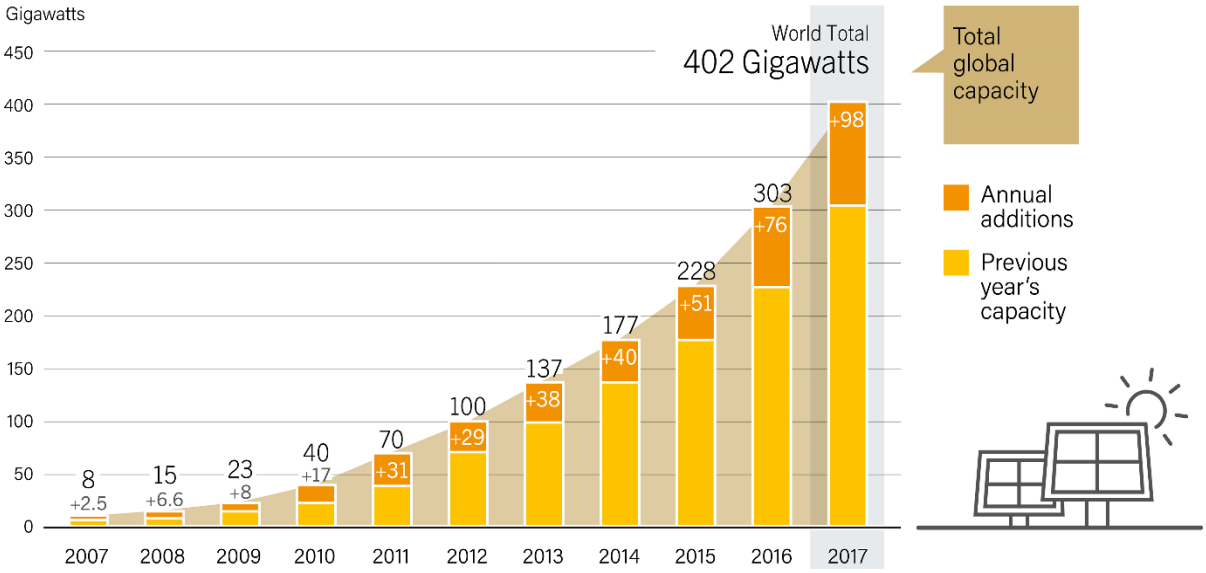

Figure 1.2: Solar PV global capacity and annual additions, 2007-2017.

1.1.1 Stand Alone PV systems

Stand-alone PV systems or namely Off-grid PV systems, are designed to function independently of the public grid [7-9]. These systems are contained of several components (PV arrays, power converters, storage components) that convert solar energy into electric energy and then delivered it to supply a DC or AC loads or to the storage system. For remote or isolated regions that are far from the conventional sources, stand-alone PV systems have been considered as a good alternative solution for meeting electricity demands where utility power is costly or unavailable. Stand-alone PV systems found numerous applications such as solar home systems (SHS), water pumping system in domestic, livestock water supplies, small-scale irrigation systems and fish farms [7-9].

1.1.2 GRID-CONNECTED PV SYSTEMS

Grid-connected PV systems are designed to be able to inject the extracted PV power into the public grid. These systems are contained numerous power conversion stages (power converters) that used to extract the power from PV array and then inject it into the public grid [10-13]. The aims of these systems are to feed the grid-connected customer or offer bulk power in order to reduce fuel sources dependency and greenhouse gases. Also, the injection of power into grid should follow the standards given by the utility companies. Power quality, detection of islanding operation, grounding, etc. are the issues deal by these standards. The international standard IEC61727 [14], EN61000-3-2 [15] and IEEE1547 [16] standards are summarized and listed in Table I [17].

TABLE 1.1: Summary of the most interesting standards dealing with interconnections of PV systems to the grid.

ISSUE	*IEC61727* [14]	*IEEE1547* [16]	*EN61000-3-2* [15]
Nominal power	10 kW	30 kW	16A*230V=3.7 kW
Harmonic currents (Order-h) Limits	(3-9) 4.0% (11-15) 2% (17-21) 1.5% (23-33) 0.6%	(2-10) 4.0% (11-16) 2.0% (17-22) 1.5% (23-34) 0.6% (>35) 0.3%	(3) 2.30 A (5) 1.4 A (7) 0.77 A (9) 0.40 A (11) 0.33 A (13) 0.21 A (15-39)0.15*8/h
	Even harmonics in these ranges shall be less than 25% of the odd harmonic limits listed.		Approximately 30% of the odd harmonics.
Maximum current THDi %	5.0%		-
Power factor at 50% of rated power	0.9	-	
DC current injection	Less than 1.0% of rated output current.	Less than 0.5% of rated output current.	<0.22A- corresponds to 50 W half-wave rectifier.
Voltage range for normal operation.	85%-110% (196 V-253 V)	88%-110% (97 V- 121 V)	-
Frequency range for normal operation.	50 ± 1 Hz	59.3 Hz to 60.5 Hz	-

1.2 BACKGROUND OF GRID-TIED PHOTOVOLTAIC SYSTEM TOPOLOGIES

The main electrical components in grid-connected PV systems are the PV arrays and power electronic converters in addition to the grid-side filter. The key to improve the efficiency of PV arrays and assure the injection of the produced PV power into the grid with high quality is power electronic conversion. These systems are classified depending on the number of conversion stage into two categories single and dual-stages [18]. These categories commonly used power electronic topologies in PV systems.

1.2.1 SINGLE-STAGE GRID CONNECTED PV SYSTEM

Single-stage grid-connected PV system as its name implies, contain only one conversion stage as described in Figure 1.3. This conversion stage is a DC-AC converter which used to extract the maximum power from PV arrays and inject it into the grid at the same time. The utilization of minimum number of conversion stage in this topology reduced weight, volume and cost [17]. To implement this topology practically and assure the injection of produced PV power, the input voltage of the inverter (output PV voltage) must be higher than the grid peak voltage. This reason requires choosing one of the two methods:

- Employ a step-up transformer after the inverter in order to achieve a grid-connection with low grid peak voltage [19].
- Connect large number of PV modules as string of series in order to achieve a PV array with sufficiently high PV voltage [20].

These methods are practically realized. But the adding of transformer in conversion chain will increase the volume, weight and cost of the system, besides increase the losses [21]. On the other hand, the connection of large number of PV modules suffers from several drawbacks such as hot-spots during partial shading of the PV array, reduced safety and increased probability of leakage current through the parasitic capacitance between the panel and the system ground. Furthermore, the control design in both methods is complicated due to the MPPT must be added with inverter control [21].

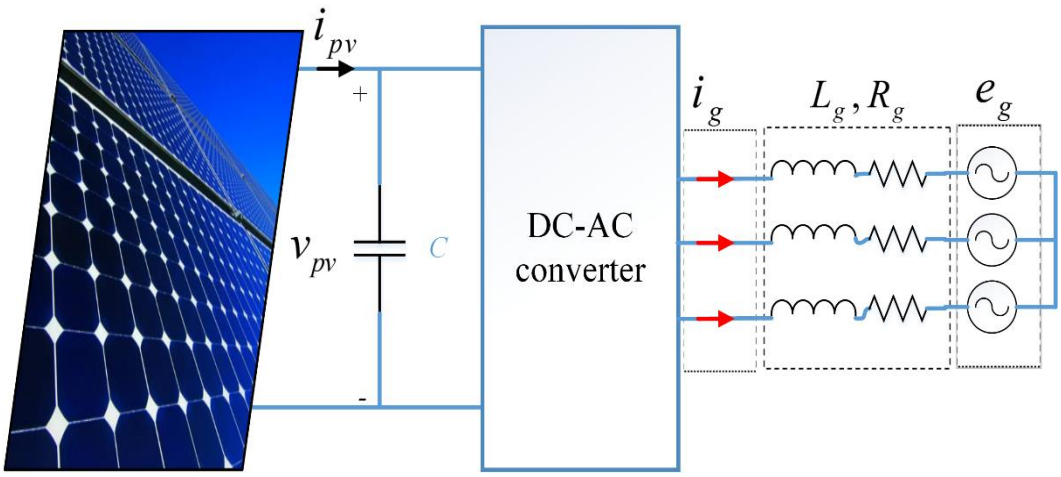

Figure 1.3: Single-stage grid-connected PV system topology.

1.2.2 DUAL-STAGE GRID CONNECTED PV SYSTEM

Dual-stage grid-connected PV system contains two conversion stages as described in Figure 1.4. The first stage is a DC-DC converter (generally boost converter) used to track the maximum power point (MPP). While, the second stage is a DC-AC converter (inverter) used to inject the extracted PV power from the first stage into the grid. The weight, volume and cost of this topology are high in comparison with single-stage topology [18]. Also, the losses in the conversion chain are increased due to the increase in number of components. However, it has been widely used due the fact that, the maximum power point tracking (MPPT) and current injection controls are decoupled at different converters which simplify the control design and achieve high harvesting energy capability. As well as, it provides the capacity to boost the DC-link voltage value above the grid voltage peak value whatever the PV modules connection and quantity of produced PV power [10].

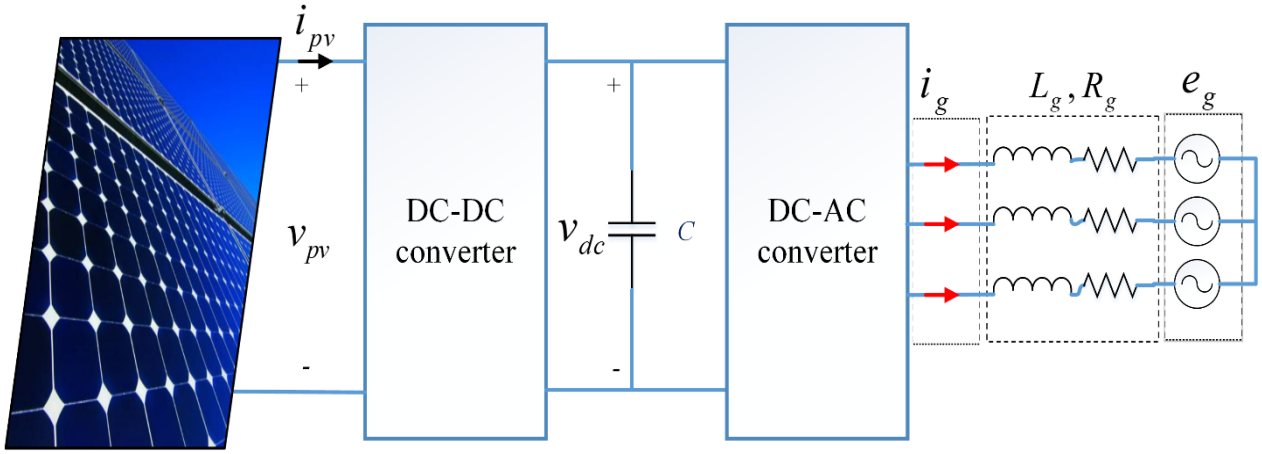

Figure 1.4: Dual-stage grid-connected PV system topology.

1.2.3 OTHER TOPOLOGIES

Several grid-connected PV system topologies are developed based on single and dual-stage topologies in medium and high power range. Multi-string inverters and multi maximum power point trackers with centralized inverter are the most used topologies [22-24].

Multi-string inverters topology is shown in Figure 1.5. In this topology, the large PV array is divided into several single string of PV modules, each one connected to their inverter. All the inverters are connected to the grid through an inductive filter. This topology suffers from the same drawbacks of single-stage topology [24].

The multi maximum power point trackers with centralized inverter topology is composed of two conversion stages as shown in Figure 1.6, the first stage contains number of PV modules, each one connected to an individual DC-DC converter. In the second stage, a centralized inverter tied to the grid is used. Each output of the DC-DC converter is connected to the input of the centralized inverter. This topology offers the same advantages as the dual-stage topology. However, it requires a high cost [22].

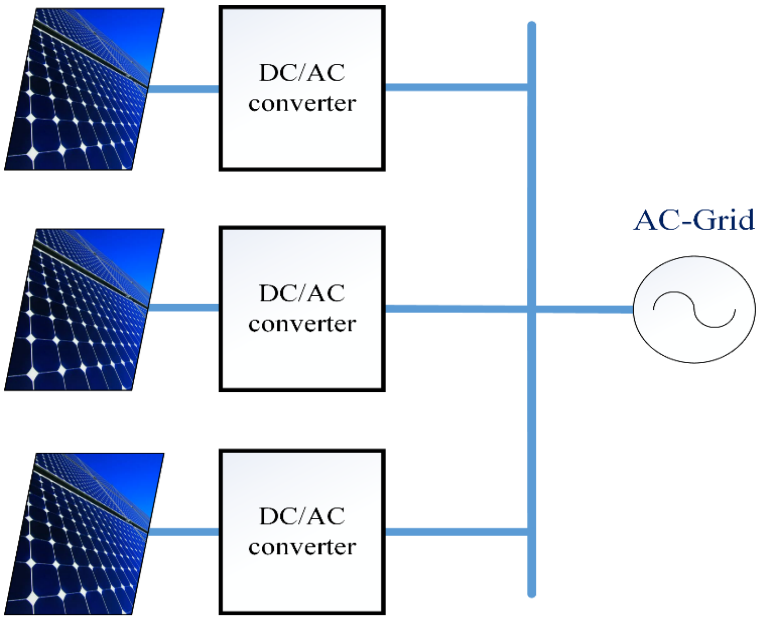

Figure 1.5: Multi-string inverters topology.

In medium and high power range, the use of two-level inverter in these topologies require the operation at low switching frequency which creates many disadvantages such as large ripple, high values for grid-side filter, and rich harmonic content of the output voltage and

current [25]. For this reason, the multilevel inverters are widely introduced in these topologies [26]. Where, the cascaded modular multilevel converters are suitable to modify the first topology. On the other hand, multilevel Neutral Point Clamped (NPC) inverters are proper to employ as centralized inverter. NPC inverters use the semiconductor switches connected in series, which allow the operation at higher DC voltages [27].

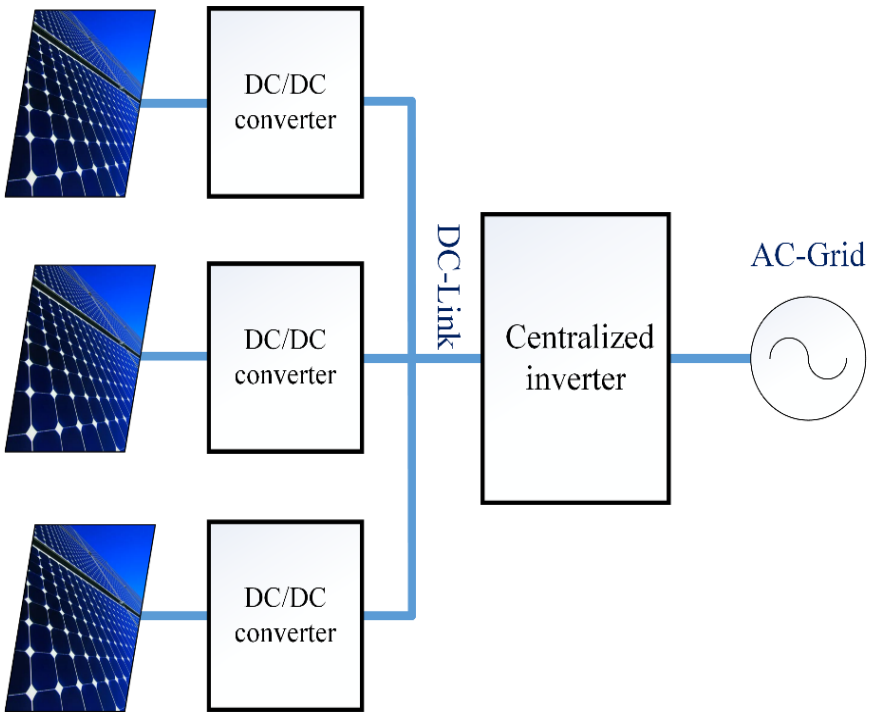

Figure 1.6: Multi MPPTs with centralized inverter topology.

1.3 DISSERTATION MOTIVATION AND OBJECTIVES

The selection of suitable grid-connected PV system topology and design of effective control schemes are considered as great challenges. It is necessary to select the suitable topology depending on the quantity of power injected into the grid in addition to the offers provided by topology advantages in term of energy harvesting capability. On the other hand, the development of effective controllers is crucial due to the effect of different operating conditions on the overall selected topology. So, this dissertation has two research directions which are: investigate sustainable grid-connected PV system topologies; and design effective control schemes.

1.3.1 INVESTIGATION OF SUSTAINABLE GRID-TIED PV SYSTEM TOPOLOGIES

As detailed in background of grid-connected PV system topologies section, the selection of single-stage grid-connected PV system suffers from several drawbacks especially in term of

energy harvesting capability. Motivated by this reason, the first objective is to investigate the advantages of applying dual-stage configuration in low power PV systems.

Then, the advantages of this configuration are combined with efficient grid-side multilevel converters in order to inject the produced PV power with high performance as well as assure the operation in medium and high power range.

The connection of PV modules as large PV array suffers from partial shading problem which reduce the effective energy harvesting and complicate the control design [21]. Also, due to high switching frequency provided by MPPT unit, DC-DC converter components do not support high power range. In order to overcome these problems, another objective of this dissertation is to investigate a topology that divides the large PV array to string modules with individual DC-DC converter and connects them to a centralized multilevel inverter.

1.3.2 Investigation of Effective Control Schemes

Generally, the control scheme for the grid-connected PV systems is divided into three control steps, maximum power point tracking (MPPT), DC-link regulation and control of power injected into the grid. These control techniques have been investigated in several research and considered as an ongoing research topic.

PV arrays still do not provide a maximum efficiency, since their characteristics are highly nonlinear and are affected by climatic conditions. The random changes of these conditions reduce the PV array output power [3, 18]. Therefore, it is necessary to design a controller that is able to force the PV systems to continuously pursuing and rapidly extracting the maximum power from PV arrays under climatic condition changes [18].

Numerous MPPT techniques have been proposed in the literature; nevertheless, most of those techniques have certain drawbacks such as loss of tracking direction, low tracking speed and large oscillations. MPPT techniques that overcome those problems suffer from computational burden and increase the implementation costs [9].

For this reason, the first objective among the control schemes objectives in this dissertation focuses on the design of modified MPPT techniques that provide high performance tracking under atmospheric condition changes and simple to be implemented practically.

On the other hand, the produced PV power should be injected by using a second conversion stage (DC-AC converter) into the grid with minimum total harmonic distortions THDi% in grid currents under all atmospheric level conditions. This control step aims to achieve a good DC-

link regulation, and high powers control performance, which can offer fast transient response, accurate power control and low THDi%.

Besides to employ the two-level inverter as a second conversion stage, different NPC multilevel inverters employed for the same reason due to inject a high quantity of produced power into the grid. The multilevel NPC inverters suffer from the unbalancing capacitor potential of DC-Link voltage, complexity of design and hard implementation of the control scheme [28].

The most conventional control schemes used for the second stage, employ cascaded linear PI regulators and pulse width or space vector modulation stage (PWM/SVM). The advantage provided by using the conventional control scheme based on PWM/SVM is to guarantee the operation at fixed switching frequency [23]. However, the switching frequency operation at high and medium power rang should be lower in order to minimize switching losses. Due to this condition, the conventional control schemes suffer from several drawbacks such as:

- Inaccurate power control, in addition to significant lower order harmonics which degrade the quality of grid current [23].
- The slow regulation of PI regulators and low-bandwidth modulation stage causes a slow transient response [23].
- The grid voltage harmonics and control delay degrade the performance [23].

Moreover, the design of conventional control schemes is complicated in case of employing multilevel inverter in grid-connected systems because one must include DC-link capacitor voltages balancing into consideration [28-29].

Nowadays, Finite-control set model predictive control (FCS-MPC) is widely engaged in power electronics converters control due to its simplicity in experimental implementation and control design [30-32]. FCS-MPC remove the PI controllers and modulation stage. Moreover, it offers the ability to include nonlinearities and constraints in the design of the controller. In PV system applications, FCS-MPC has been emerged for different PV systems such as: stand-alone systems [33], grid-connected PV systems [34-35]. As presented in [30-35], whatever the purposes which the FCS-MPC has been applied for them, a high performance control is achieved in comparison to the conventional methods. From that, FCS-MPC is considered as a best choice to control the second stage. Although, this technique suffers from two essential problems which are variable inherent switching frequency in addition to computational burden especially in case of high-level inverters.

The last objective is to exploit the effectiveness of FCS-MPC and overcome their problems in order to design an effective controller for the second conversion stage that provide high performance control under several atmospheric conditions.

1.4 DISSERTATION ORGANIZATION

This dissertation is planned into six chapters. The work performed in each chapter is summarized as follows:

Chapter-2:

This chapter reviews the most widely employed control techniques for dual-stage grid-connected PV system. Where, maximum power point algorithms for photovoltaic systems are presented in the first part of this chapter. While, a short overview about DC-link voltage regulation techniques and control techniques of three-phase grid-connected systems are described in the second and third parts of this chapter respectively.

Chapter-3:

An improved control strategy based on fixed switching predictive control strategy for three phase dual-stage grid-connected PV system is proposed in this chapter. A variable incremental current step size of an MPPT current oriented loop based on fixed switching predictive current control is proposed and employed to control the first stage. While, a modified VOC based on predictive control strategy is introduced to control the second stage. The efficiency of the proposed control strategy is tested under sudden irradiation and reactive power changes demanded by the grid operator through numerical simulations and real-time HIL implementations.

Chapter-4:

In this chapter, high-level NPC inverters are employed in grid-connected PV system in order to inject the high produced PV power into the grid with high grid current quality.

Moreover, a simple and effective model predictive control (MPC) algorithm is proposed for grid-connected PV system using high-level NPC inverter (six-level) that permits to inject the active power generated by the PV system, the reactive power demanded by the grid operator and assure the balance of DC-link capacitor voltages.

Then, an optimized model predictive control (O-MPC) is proposed in order to achieve the same performance control provided by the first MPC algorithm with a significant reduction in computational burden.

The effectiveness of the proposed MPC and O-MPC are tested and compared through numerical simulations and real-time HIL implementations.

Chapter-5:

Chapter five proposes simple and effective controllers for large-scale PV system using NPC multilevel based on finite control set model predictive control (FCS-MPC) strategy.

The studied system is composed of two conversion stages, the first stage contains four PV arrays, each one connected to an individual DC-DC converter (boost converter). In the second stage, a five level NPC inverter tied to the grid is employed. Each DC-Link capacitor input of the NPC inverter is connected to the output of the DC-DC boost converter.

A voltage oriented maximum power point tracking (VO-MPPT) performed by FCS-MPCC is applied for each boost converter to draw the maximum power point from each PV array. In addition, an FCS-MPC controller is proposed to control the centralized five-level NPC inverter connected to the grid.

The proposed control scheme is evaluated versus the conventional control scheme based on PI regulators through Matlab/Simulink and Simpower packages simulations.

Chapter-6:

The thesis general conclusion and the author’s contributions are summarized in this chapter. In addition, possible extensions to the research presented in this thesis are suggested.

Chapter 2

Review of Control Techniques for Dual-Stage Grid-Connected PV System

2.1 INTRODUCTION

Grid connected PV systems have been used to inject the produced power from the PV arrays into the public grid [10-12]. The present challenge of these systems is to extract the maximum power from the PV arrays and deliver it to the grid with high grid current quality under climatic changes. As detailed in chapter 1, dual- stage grid-connected PV system topology offers an important advantage. This one eases the MPP tracking as well as boosts the DC-link voltage value above the grid peak voltage value whatever the produced PV power [10]. During the last decades, many research works have proposed several control schemes, which can be employed for dual-stage grid-connected PV system topology in order to increase its conversion efficiency [10-12]. These controls schemes are divided into three control steps, maximum power point tracking (MPPT), DC-link regulation and control of power injected into the grid.

In this chapter, a review of the most widely employed control techniques for dual-stage grid-connected PV system is presented. Maximum power point algorithms for photovoltaic systems is presented and compared in the first part of this chapter. While, short overviews about DC-link voltage regulation techniques and control techniques of three-phase grid-connected systems are described respectively in the second and third part of this chapter.

2.2 MAXIMUM POWER POINT TRACKING

PV arrays still do not provide a maximum efficiency, since their characteristics are highly nonlinear and are affected by climatic conditions. The random changes of these conditions

reduce the PV array output power [18]. Therefore, it is necessary to design a controller that is able to force the PV systems to continuously pursuing and rapidly extracting the maximum power from PV arrays under climatic condition changes [18]. This controller is namely the maximum power point tracking (MPPT) controller that is employed in the first conversion stage (DC-DC converter). In this section, the most used MPPT algorithms are described and compared. This overview includes perturb and observe (P&O) algorithm, incremental conductance (INC) algorithm, advanced MPPT algorithm based on artificial intelligence, Current-oriented MPPT, Voltage-oriented MPPT.

2.2.1 PERTURB AND OBSERVE (P&O) ALGORITHM

This algorithm is designed depending on PV array behaviours. Where, voltage-current-power curve are scanned in order to find maximum power point (MPP). To be nearer to the MPP, if the operating power point is on the left side of the MPP, the algorithm moves it to the right by increasing the power converter duty cycle of the first conversion stage (DC-DC converter), and vice versa when the operating point is on the right side. Figure 3.2 (a) presents the basic flowchart of the P&O algorithm [36-39]. This MPPT algorithm is simple, easy to be implemented practically, and its cost is low. However, it suffers from slow and inaccurate convergence to the MPP under sudden irradiation change, as well as large power oscillation at steady state operation, which causes system power losses.

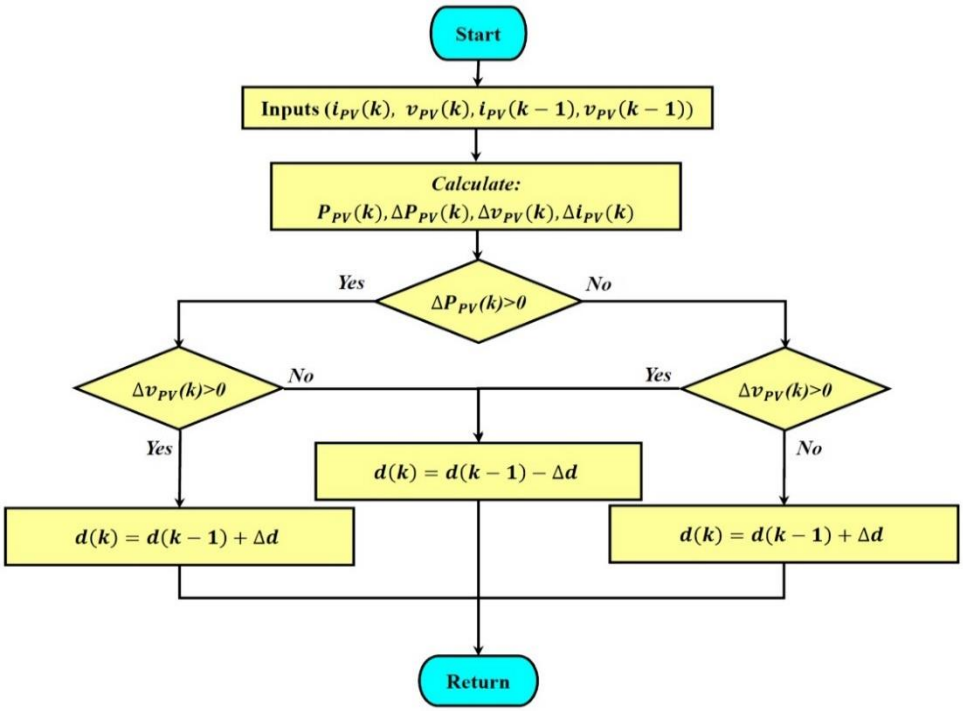

Figure 2.1: Flowchart of the P&O algorithm.

2.2.2 INCREMENTAL CONDUCTANCE (INC) ALGORITHM

Also, the incremental conductance algorithm (INC) as P&O algorithm is also designed depending on the PV array behaviours. The identification of the instantaneous position to the MPP is determined based on the slope of the PV power curve; zero at the MPP, positive on the right-hand side of the MPP and negative on the left-hand side of the MPP. The basic equations of this algorithm are given as follows [40-41]:

$$\frac{dp_{pv}}{dv_{pv}} = 0 \qquad \text{at MPP} \tag{2.1}$$

$$\frac{dp_{pv}}{dv_{pv}} < 0 \qquad \text{at left of MPP} \tag{2.2}$$

$$\frac{dp_{pv}}{dv_{pv}} > 0 \qquad \text{at right of MPP} \tag{2.3}$$

Since

$$\frac{dp_{pv}}{dv_{pv}} = \frac{d(v_{pv} * i_{pv})}{dv_{pv}} = \frac{di_{pv}}{dv_{pv}} v_{pv} + i_{pv} \tag{2.4}$$

Equation (2.4) can be expressed as:

$$\frac{di_{pv}}{dv_{pv}} < \frac{i_{pv}}{v_{pv}} \qquad \text{at left of the MPP} \tag{2.5}$$

$$\frac{di_{pv}}{dv_{pv}} > \frac{i_{pv}}{v_{pv}} \qquad \text{at right of the MPP} \tag{2.6}$$

$$\frac{di_{pv}}{dv_{pv}} = \frac{i_{pv}}{v_{pv}} \qquad \text{at the MPP} \tag{2.7}$$

The goal is to adjust the power converter duty cycle to reach the MPP by comparison of the instantaneous conductance (I/V) with incremental conductance (ΔI/ΔV) [40-41]. The basic flowchart of the INC algorithm is illustrated in Figure 3.2(a).

The MPP is difficult to be obtained by Equation 2.7 in practical implementation due to the noise. In addition, The INC algorithm has the same advantages and disadvantages as the P&O algorithm.

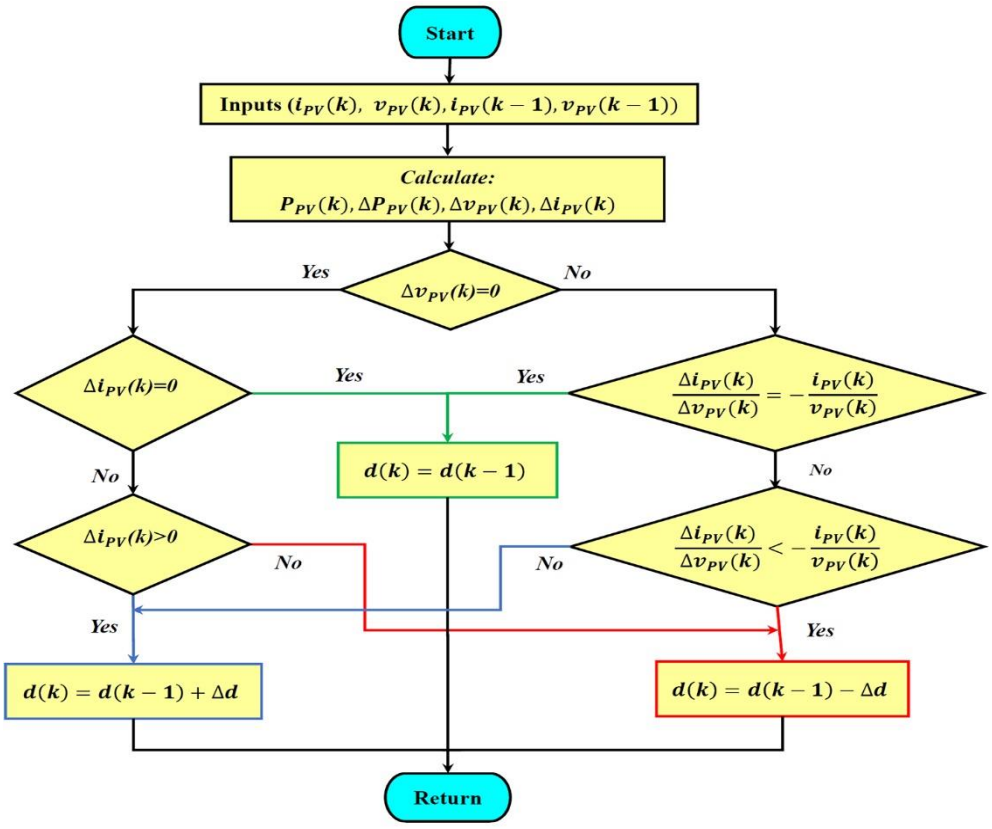

Figure 2.2: Flowchart of the INC algorithm.

2.2.3 ADVANCED MPPT ALGORITHM BASED ON ARTIFICIAL INTELLIGENCE

To overcome the drawbacks of P&O and INC algorithms, several recent research works have been investigated to introduce the artificial intelligence (AI) such as fuzzy logic control (FLC) [42-43] and neural networks (NN) [44-45], neuro-fuzzy networks (NFIS) [46-47], genetic algorithm (GA) [48-49], particle swarm optimization (PSO) [50-51]. The IA-MPPT methods offer high performance operation in terms of stability and response time. However, the implementation of these MPPTs is limited in real time because it requires a high computational burden and large memory.

2.2.4 VOLTAGE- ORIENTED MPPT

The Voltage-oriented MPPT method consists of MPPT voltage-based algorithm (V-MPPT) in cascade with voltage controller as illustrated in Figure 2.3. the objective of V-MPPT is to deliver the reference voltage that represents the MPP voltage. While, the voltage controller aims to enforce the output PV voltage to track the reference voltage generated by the V-MPPT [52-53].

The P&O and INC algorithms presented in Figure 2.4 and 2.5 are widely employed as V-MPPT. Besides, the voltage regulator is performed usually by a simple PI controller [53]. Nevertheless, the application of PI controller provides some drawbacks which affects MPP tracking such as: long response time, large overshoot and significant voltage ripples during steady-state operation [54-55]. For these reasons, sliding mode control (SMC) [54-55], and backstepping control [56] have been investigated in order to design a voltage controller characterized by high control operations.

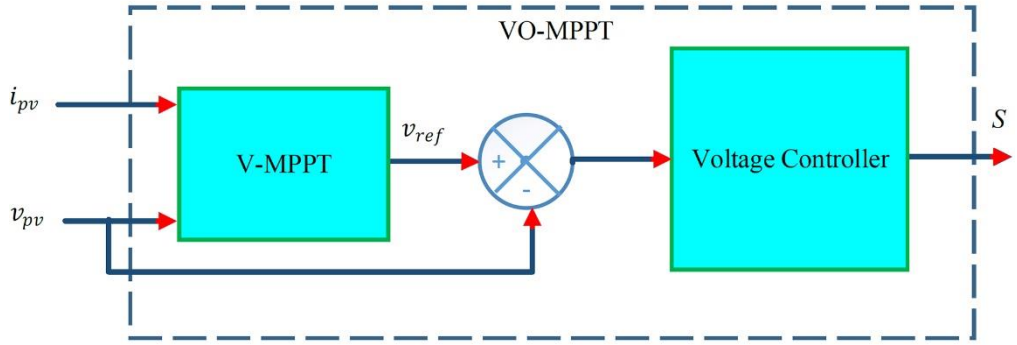

Figure 2.3: Diagram of voltage-oriented MPPT method.

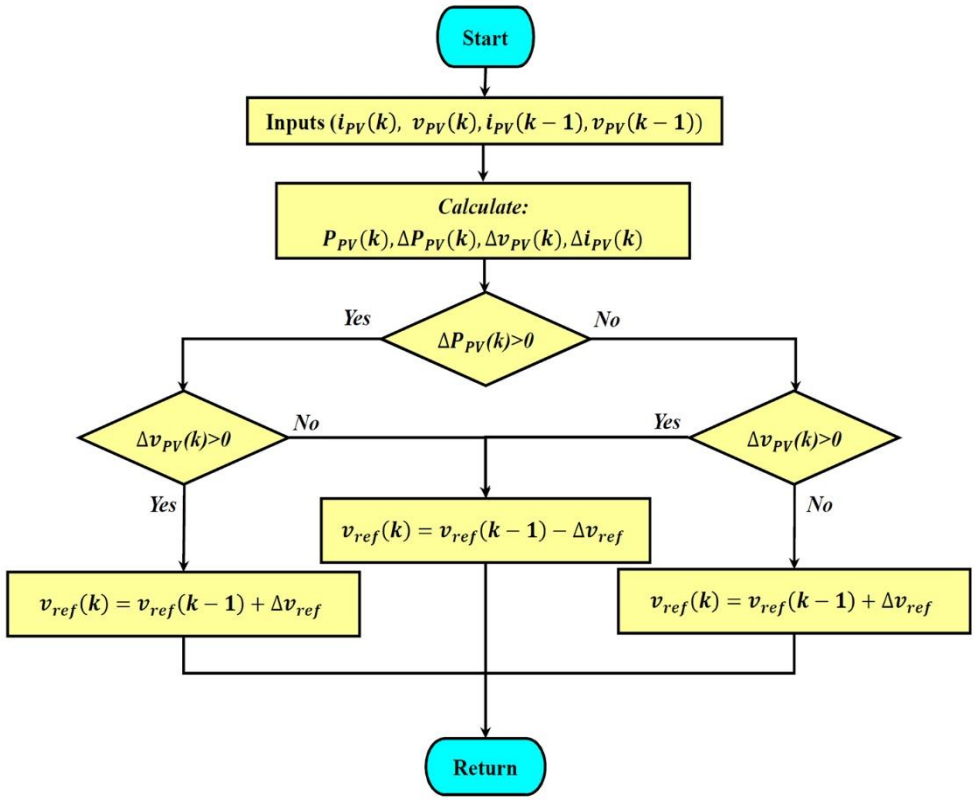

Figure 2.4: Flowchart of the V-P&O algorithm.

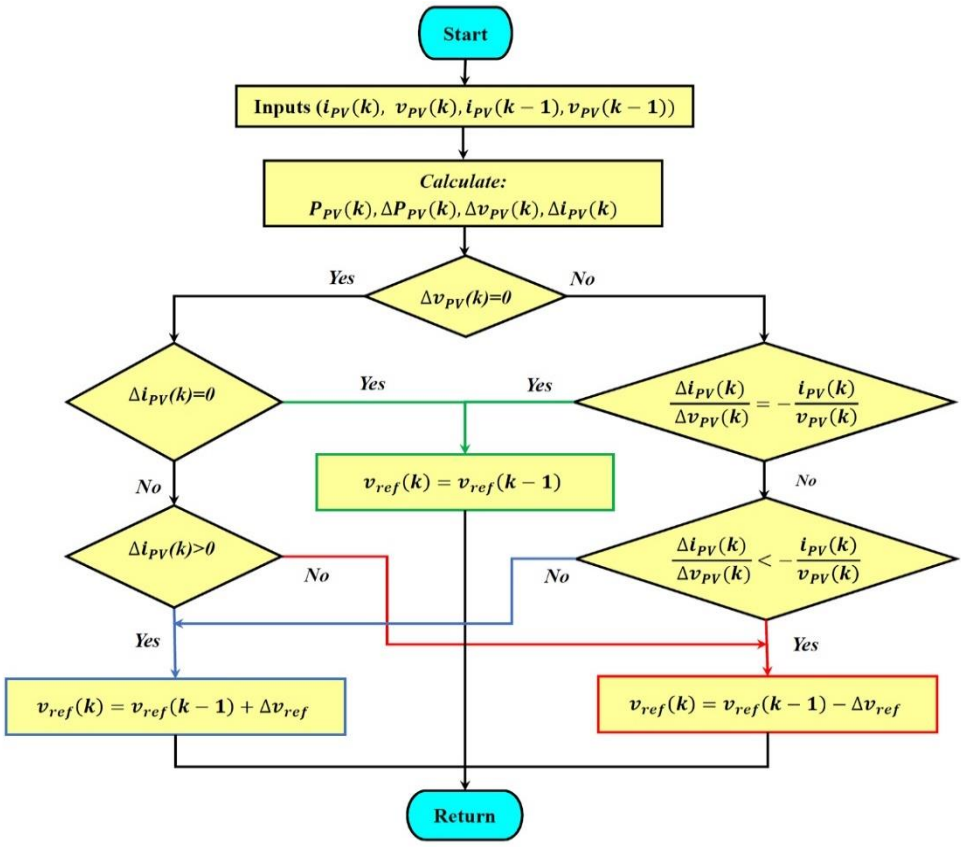

Figure 2.5: Flowchart of the V-INC algorithm.

Because PV voltage corresponding the MPP changes slightly under sudden irradiation changes, VO-MPPT provides a fast MPP tracking. But it has low accuracy tracking. Moreover, the efficiency of this method depends on the voltage controller concept [55].

2.2.5 CURRENT-ORIENTED MPPT

Figure 2.6 presents the basic concept of current- oriented MPPT. This MPPT involves MPPT current-based algorithm (C-MPPT) in cascade with current controller. The C-MPPT aims to generate the reference current that represents the MPP current, while the current controller aims to enforce the output PV current to track the reference current delivered by the C-MPPT [57-60].

Generally, the P&O and INC algorithms presented in Figure 2.7 and 2.8 are the most employed for this reason. The PI controller [57], the predictive current controller [58-59] and sliding mode current controller (SMCC) [60] are among the most useful techniques as current controller in this method. Predictive current controller besides to Sliding mode current controller has significant advantages such as robustness and implementation simplicity. Also, it has a good performance operation (fast response and very low current ripple) compared to PI

controller.

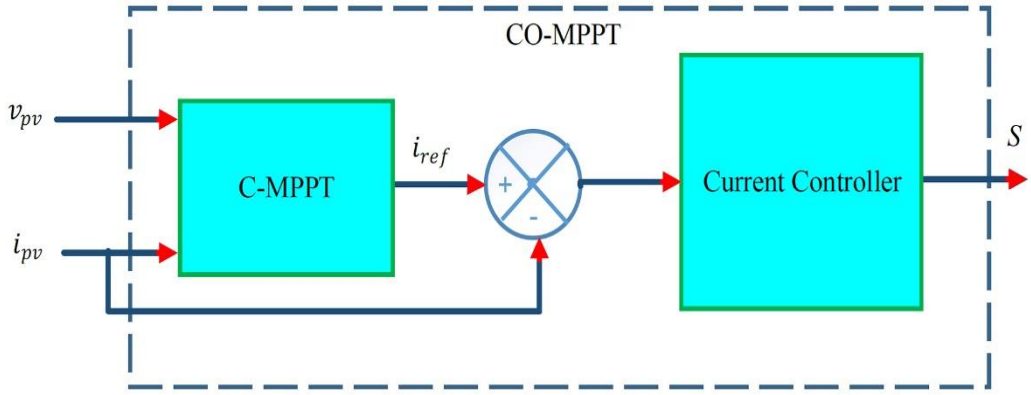

Figure 2.6: Diagram of Current-oriented MPPT method.

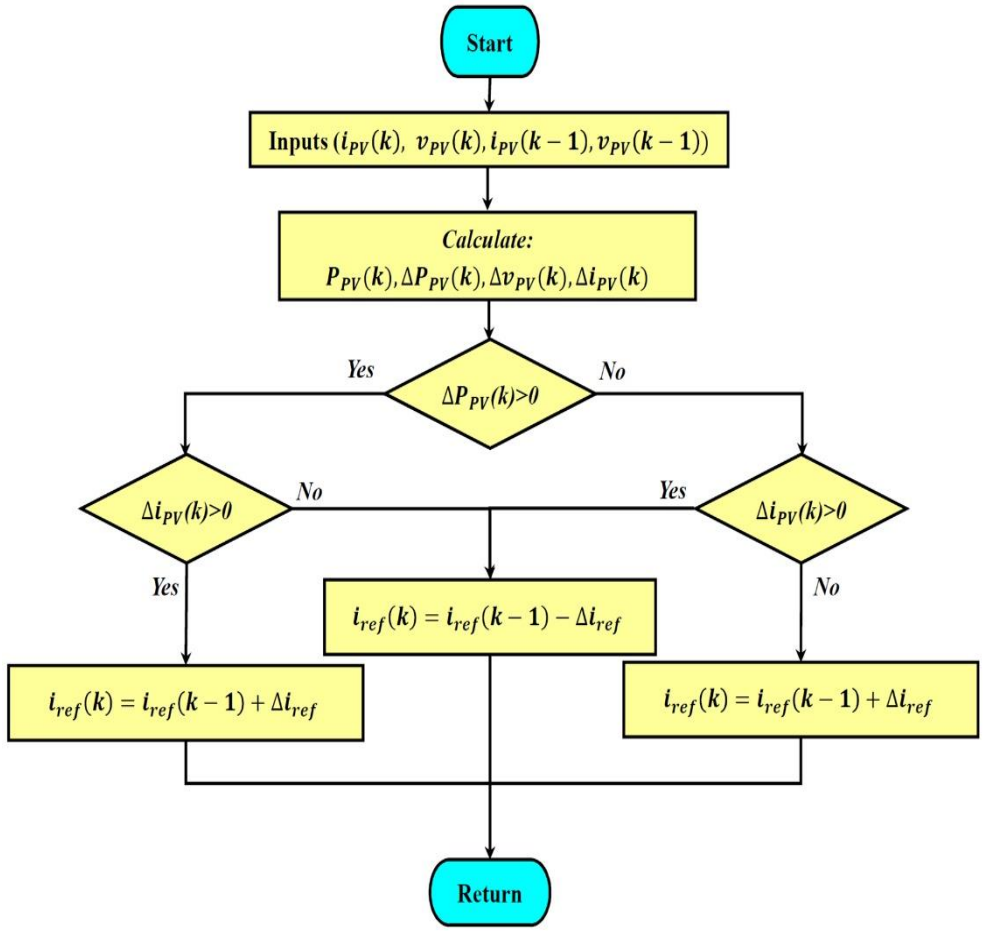

Figure 2.7: Flowchart of the C-P&O algorithm.

The CO-MPPT provides an accurate MPP tracking as well as a satisfactory oscillation reduction around the MPP, owing to the linear relation between the PV array current and solar irradiation. Nevertheless, it has a slow response time under sudden irradiation changes.

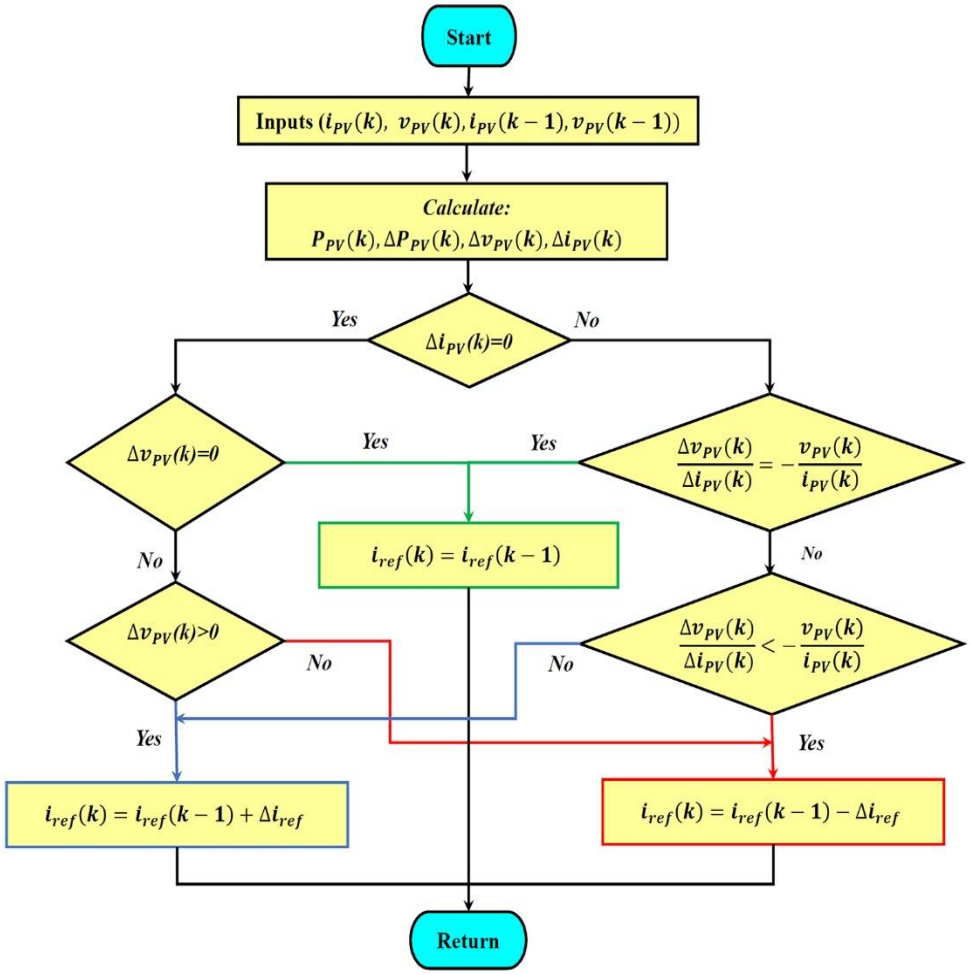

Figure 2.8: Flowchart of the C-INC algorithm.

Table 2.1 MPPT techniques comparison.

	P&O [36-39]	**INC** [40-41]	**AI-MPPT** [42-51]	**VO-MPPT** [52-53]	**CO-MPPT** [57-60]
Tracking speed time	Low	Low	High	High	Low
Tracking accuracy	Bad	Bad	Good	Bad	Very-good
Power oscillation	Large	Large	Very-small	Small	Small
Implementation complexity	Lower	Lower	Very-Higher	Lower	Lower
Power efficiency	Low	Low	High	Medium	Medium

2.2.6 COMPARISON OF MPPT TECHNIQUES

Regarding the research results offered in the literature, a comparison between the previous MPPT techniques is summarized in Table 2.1. This comparison is carried out in terms of tracking speed time, tracking accuracy, power oscillation, implementation complexity and power efficiency.

2.3 DC-LINK CONTROL

The first conversion stage extracts the PV power from the PV arrays to feed DC-link. The objective at this level is to regulate the DC-link voltage to the set reference value and estimate the amplitude of grid currents. To ensure a proper power injection control, the value of DC-link voltage reference must be choose higher than the grid peak voltage. The block diagram of DC-link voltage control is depicted in Figure 2.9. A simple PI regulator is mostly used in the industrial applications [61-62]. However, it has long time response, large overshoot and significant voltage ripples during steady-state operation. Several controllers that overcome these problems are presented in this section.

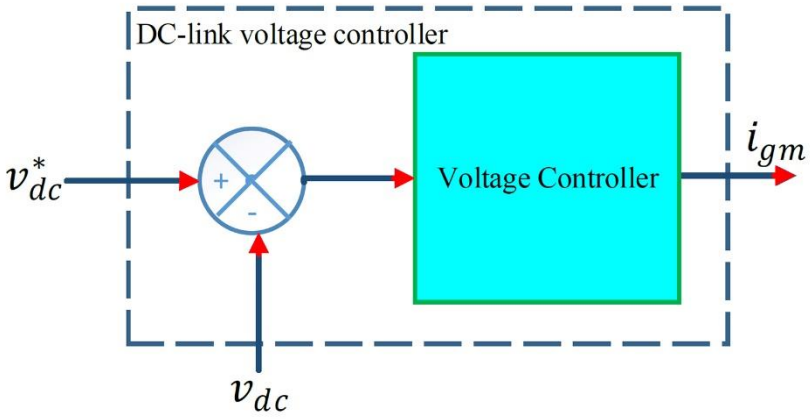

Figure 2.9: Diagram of DC-link voltage controller.

2.3.1 DC-LINK CONTROLLERS BASED ON ARTIFICIAL INTELLIGENCE

Several research works have employed the artificial intelligence (AI) such as fuzzy logic control (FLC) [63] and, neuro-fuzzy networks (NFIS) [64], and particle swarm optimization (PSO) [65] to design an effective DC-link controller. These types of controllers overcome the drawbacks presented by PI regulator. But, the implementation of these controllers requires a high computational burden and large capacity of the memory. For this reason, the application of these controllers is limited especially in the complicated systems.

2.3.2 DC-LINK CONTROLLER WITH FEED FORWARD TERM

The block diagram of this controller is illustrated in Figure 2.10. The grid current consists of two terms, the first term is the contribution current by the PV array while the second one is the current losses [36, 66].

$$i_{gm}^{*} = i_{PVg} - i_{loss} \tag{2.8}$$

The contribution current by the PV array is given as

$$i_{PVg} = \frac{2P_{pv}}{3V_m} \tag{2.9}$$

Whereas, the difference between the measured V_{dc} and the reference V_{dc}^{*} is passed through a simple PI regulator in order to estimate the loss current [36, 66].

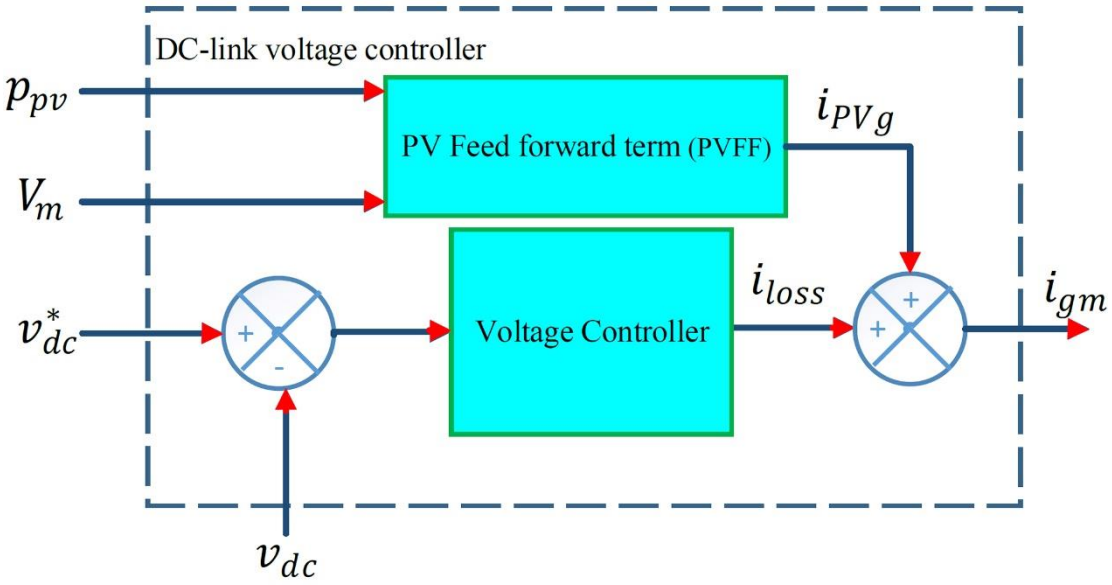

Figure 2.10: Diagram of DC-link voltage controller with feed forward term.

This controller provides a fast response time and low voltage ripple in steady-state operation under irradiation changes. Moreover, the hardware implementation of this type of controller is easy which makes it a best choice for the complicated systems.

2.3.3 OTHER DC-LINK VOLTAGE CONTROLLERS

Recently, other control theories have been introduced to design new DC-link voltage controllers such as sliding mode theory [67] and integral sliding mode theory [68]. These controllers provide high performance operations under irradiation changes. Also, the hardware implementation of this type of controllers is easy. For these reasons, the application of these control theories is considered as an ongoing research topic.

2.4 OVERVIEW OF GRID CURRENT CONTROL TECHNIQUES

This section discusses the control issues employed for grid tied voltage source converter (VSI) in PV systems. Different control structures such as direct power control (DPC), voltage oriented control (VOC) in stationary frame and synchronous frame, and model predictive control are presented and discussed. Moreover, the description of these control structures is summarized in order to perform a brief comparison.

2.4.1 DIRECT POWER CONTROL BASED ON SWITCHING TABLE (DPC)

The objective of the DPC scheme is to regulate the grid powers to their references and to achieve low total harmonics distortions. The active power reference is estimated from DC-link voltage controller, while the reactive power reference is given by the grid operator. The functionality of this control schemes depends on the selection of switching state that minimize the error between the measured powers and their references. This selection is carried out using a predefined switching table. As indicated in Table. 2.2, The switching table is designed by dividing the plane α-β into twelve sectors S_x as shown in Figure 2.11 using the angular position of the vector of grid voltage obtained from the PLL. Also, from the error S_d and S_q between the references and the measured values of the active and reactive powers, obtained through two comparators with hysteresis band [69]. The scheme of DPC based on switching table is presented in Figure 2.12.

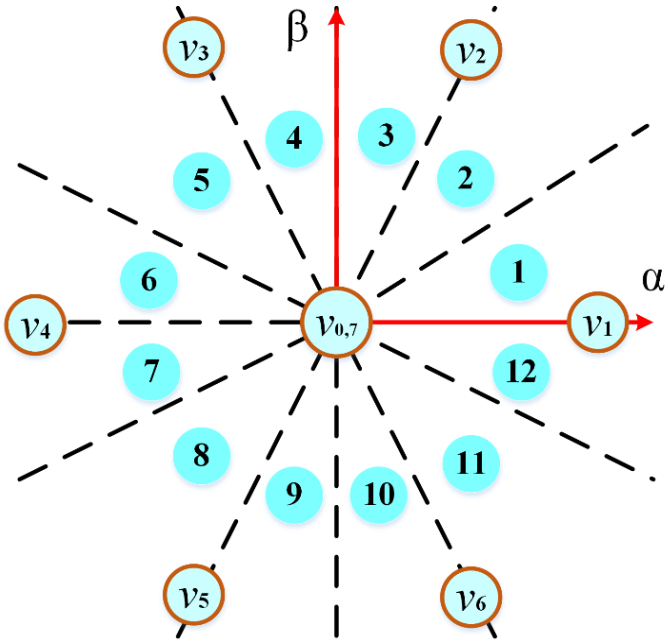

Figure 2.11: Number of sectors with voltage vectors generated by VSI.

Table 2.2 Conventional switching table of DPC.

S_d	S_q	S_1	S_2	S_3	S_4	S_5	S_6	S_7	S_8	S_9	S_{10}	S_{11}	S_{12}
1	0	v_6	v_7	v_1	v_0	v_2	v_7	v_3	v_0	v_4	v_7	v_5	v_0
	1	v_7	v_7	v_0	v_0	v_7	v_7	v_0	v_0	v_7	v_7	v_0	v_0
0	0	v_6	v_1	v_1	v_2	v_2	v_3	v_3	v_4	v_4	v_5	v_5	v_6
	1	v_1	v_2	v_2	v_3	v_3	v_4	v_4	v_5	v_5	v_6	v_6	v_1

$v_0(0\ 0\ 0), v_1(1\ 0\ 0), v_2(1\ 1\ 0), v_3(0\ 1\ 0), v_4(0\ 1\ 1), v_5(0\ 0\ 1), v_6(1\ 0\ 1), v_0(1\ 1\ 1)$

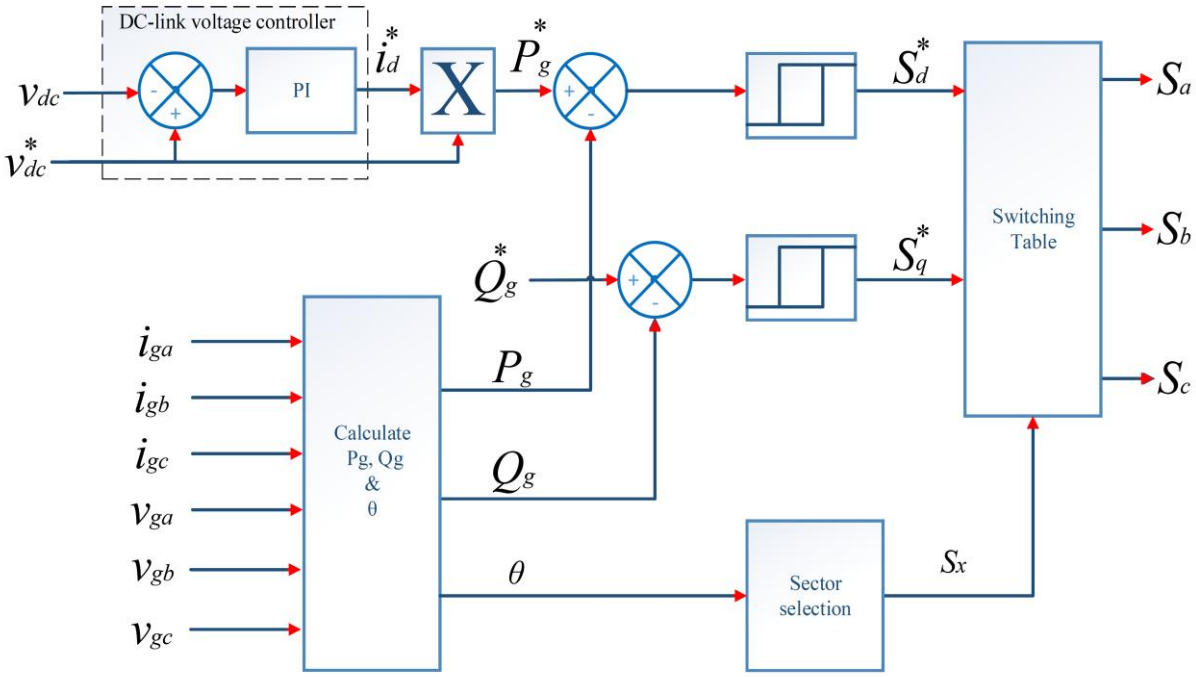

Figure 2.12: Direct power control (DPC) scheme.

The DPC scheme is easy to be implemented practically. But, it has slow response time and significant lower order harmonics. Furthermore, it operates with variable switching frequency.

2.4.2 STATIONARY FRAME VOC

The scheme of stationary frame is presented in Figure 2.13. The objective of this control scheme is to achieve a sinusoidal form of grid currents with low total harmonics distortions. In this scheme, the DC-link voltage controller estimates the peak of grid current reference *igm*.

While, the PLL is still used for adapting the frequency of the resonant controllers and extracting the first harmonic of the grid voltages used for calculating the unitary waveforms. The current i_{gm} is multiplied by grid unitary waveforms in order to obtain three phase grid current references and transformed it to αβ frame. Also, the measured grid currents are transferred to stationary frame and compared with their reference's values. Then, two PI regulators are used to generate the reference voltage that will be given to the modulation stage [70].

The stationary frame VOC scheme guarantees the operation at fixed switching frequency. Also, it is easy to be implemented practically. But, it has slow response time and significant lower order harmonics [30].

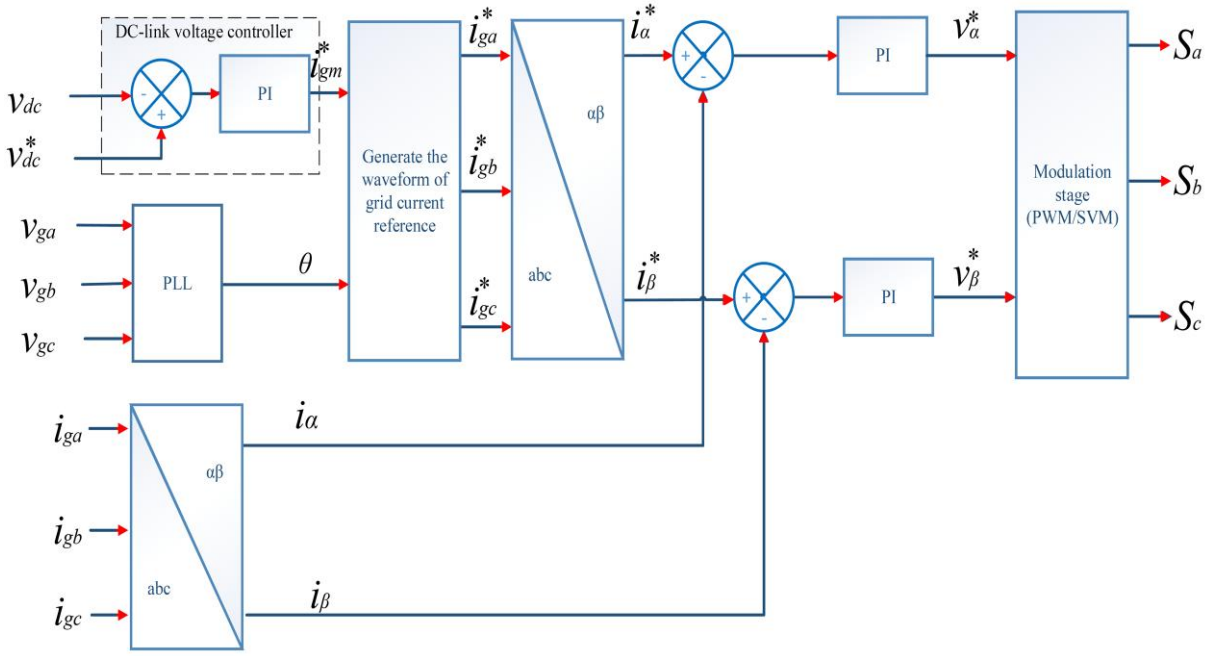

Figure 2.13: Stationary frame VOC scheme.

2.4.3 SYNCHRONOUS FRAME VOC

The scheme shown in Figure 2.14 represents the synchronous frame VOC. This control scheme aims to regulate the grid current i_d-i_q over their references. The reference current i*d* is estimated by DC-link voltage controller while the i_q reference current is estimated from the reactive power requested by the grid operator.

The measured grid currents are transformed from natural frame (abc) to rotating frame and their values i_d-i_q are compared with their reference's values. Then, PI-based controllers generate the reference *d* and *q* components of the reference voltage that will be given to the modulation stage after transfer it to αβ frame [70].

Also, this control scheme as the stationary frame VOC scheme guarantees the operation at fixed switching frequency and easy to be implemented practically. However, it has slow response time, large current fluctuation and significant lower order harmonics [28].

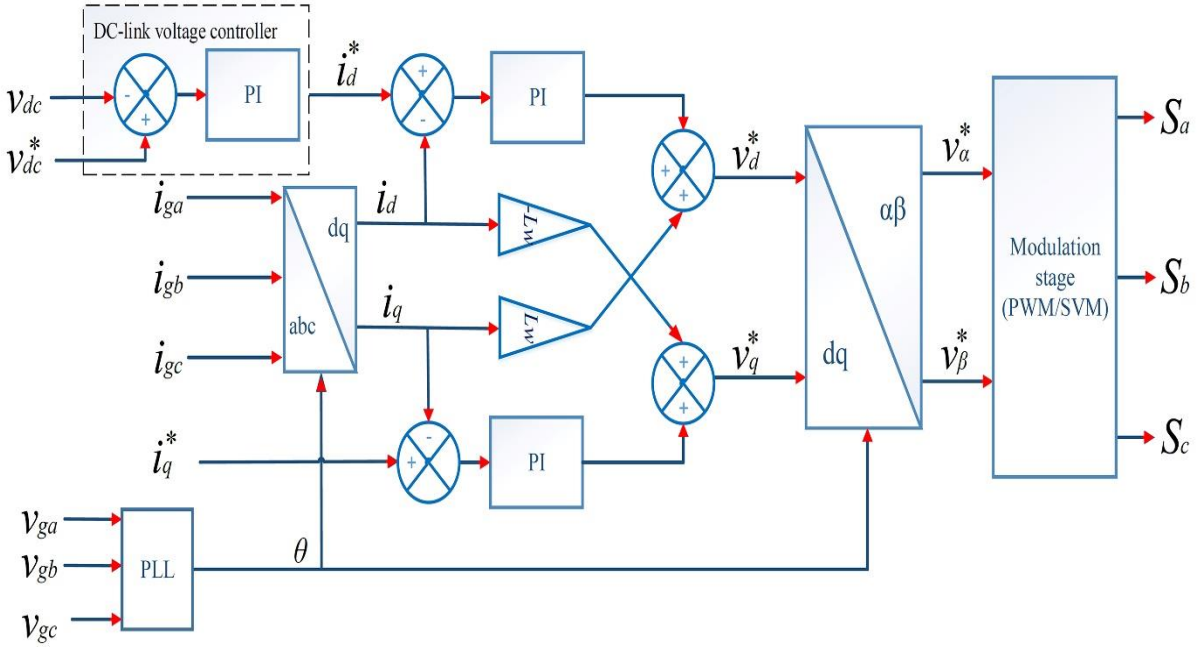

Figure 2.14: Synchronous Frame VOC scheme.

2.4.4 FINITE CONTROL SET MODEL PREDICTIVE CONTROL FOR VOLTAGE SOURCE CONVERTER TIED TO THE GRID

In recent research, the finite-control set model predictive control (FCS-MPC) has been applied in many power electronics applications [30-32]. This due to the power electronic converter that contains finite number of switching states, for example eight switching states are available for two levels VSI. In grid connected systems, FCS-MPC method has been employed for different control purposes such as synchronous grid current control [30], d-q rotating frame grid current control [30] and power control [32]. From the references and measured variables and by using the discrete time model of VSI tied to the network, the functionality of FCS-MPC is based on prediction of the future behavior of state variables for all possible switching states and compare them using a cost function. The optimal switching that minimizes the cost function is selected and applied for the VSI during the next sampling time. The scheme and flowchart presented respectively in Figure 2.15 and 16 summarize the functionality of FCS-MPC. Compared to the classical control techniques, FCS-MPC eliminates the need for linear PI regulators and modulation stage. Furthermore, it provides high performance operation. The main features and challenges of the FCS-MPC are summarized as follows [28]:

Main Features of FCS-MPC:

- The concept of FCS-MPC is simple and easy to understand
- Uses the inherent discrete nature of the VSI connected to the grid which makes it easy to be implemented using the industry standard digital control platforms.
- The ability to add nonlinearities and constraints in the design of the controller
- Optimizations are greatly simplified due to finite number of switching states generated by VSI.

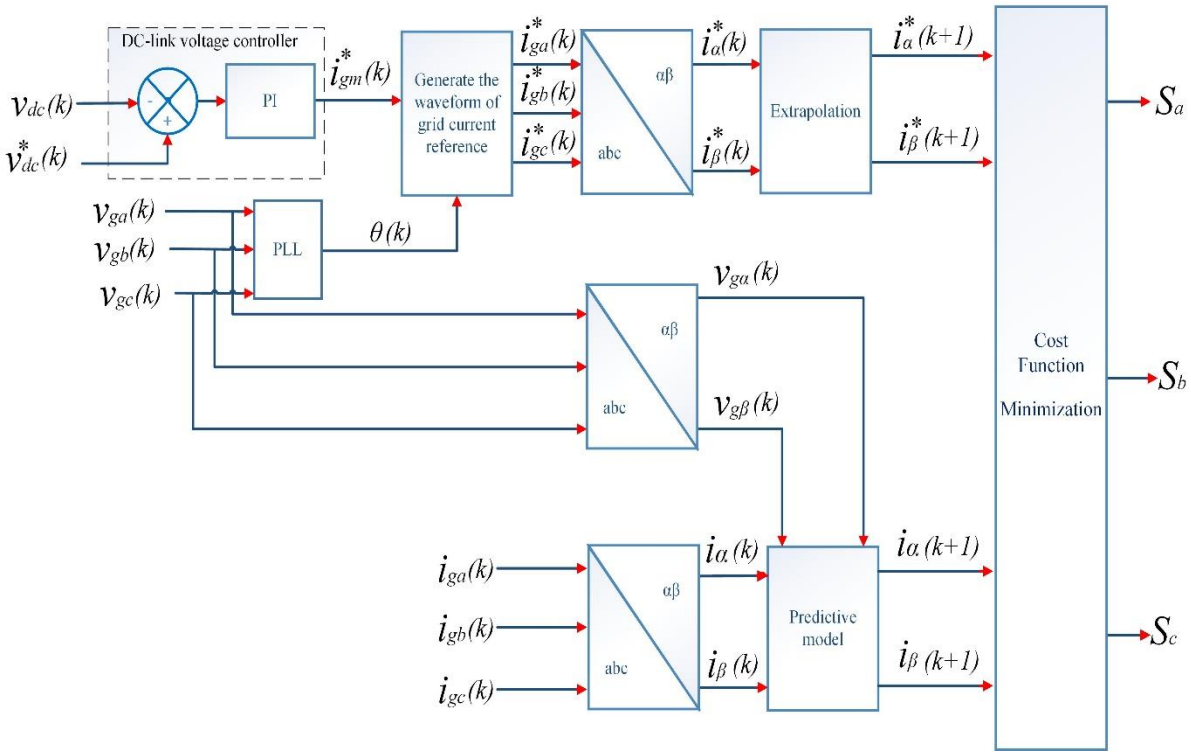

Figure 2.15: Finite control-set model predictive control (FCS-MPC) scheme.

Drawbacks of FCS-MPC:

- Needs a high computational burden
- Operates with the variable switching frequency
- Estimation of weighting factor values is not analytical or numerical
- Degradation of control performance if the system model and prediction horizon is not formulated properly.

The first challenge is investigated carefully in this dissertation. While, a solution to reduce the computational burden has been developed to promote the FCS-MPC strategy as the next generation high performance control tool for multilevel VSI.

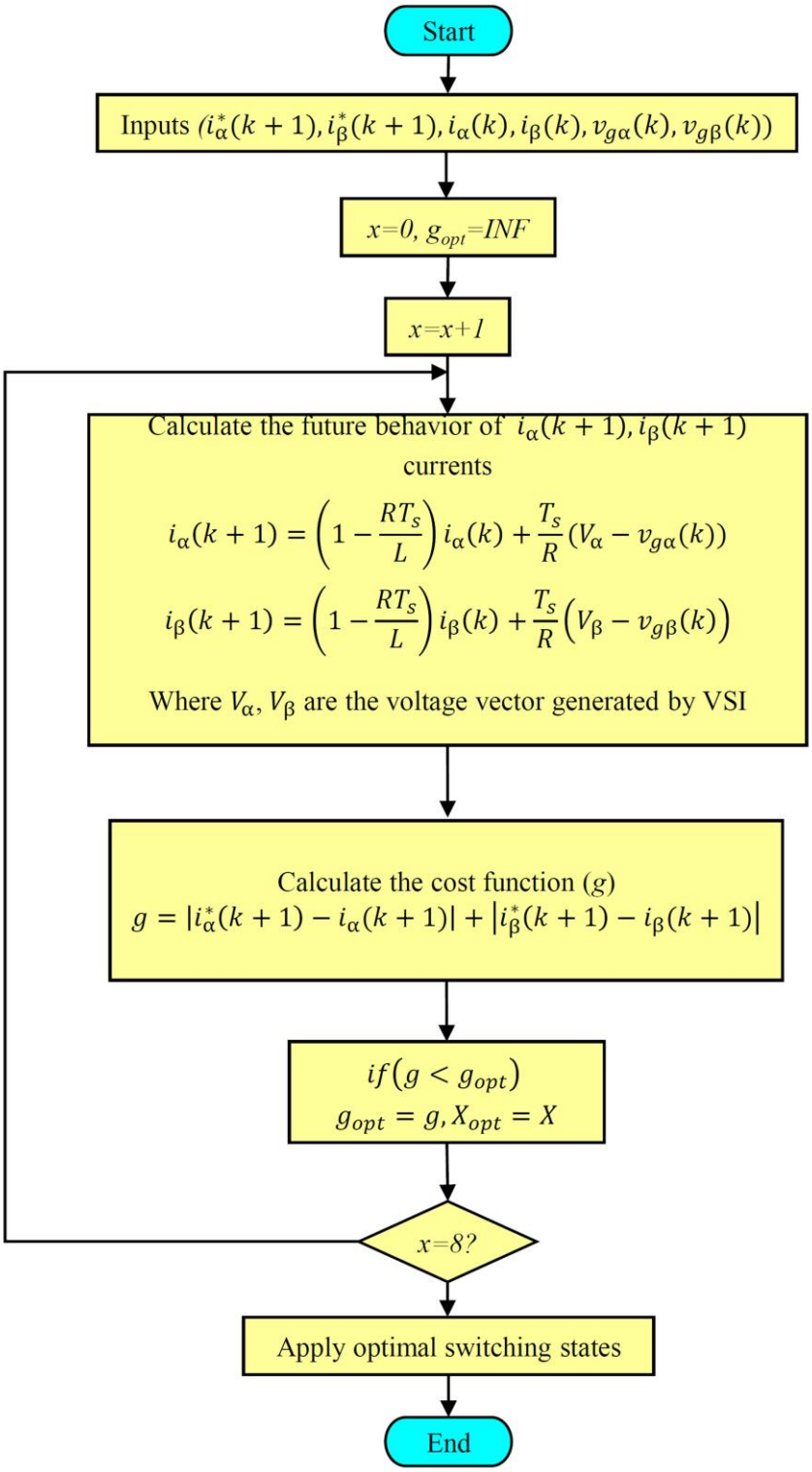

Figure 2.16 Flowchart of finite control set model predictive control (FCS-MPC).

2.4.5 COMPARISON OF FCS-MPC WITH CONVENTIONAL CONTROL SCHEMES

In this section, a comparison between FCS-MPC strategy and the conventional strategies is performed based on the research results offered in the literature. This comparison is

summarized in Table 2.3 tacking into account several criteria of comparison. The analysis recommends that the FCS-MPC strategy is an intuitive and powerful tool to control the grid tied VSI systems compared to the other conventional methods. Nevertheless, FCS-MPC strategy has some drawbacks such as variable switching frequency and high computational burden.

Table 2.3 Comparison between conventional control schemes and FCS-MPC.

Description	**linear control based on PI/modulator** [70]	**DPC based on switching table** [69]	**FCS-MPC** [30-32]
Control diagram	Fig. 2.14	Fig. 2.12	Fig. 2.15
Model	-Linear load model for PI -Inverter model for SVM	-	- Discrete-time model of the complete system
Controller design	PI adjustment (root locus) + Modulator design	Design of lookup table	Cost function definition
Nature of controller	Linear	Nonlinear	Nonlinear
Implementation platform	Analog or digital	Digital	Digital
Modulation	PWM/SVM/SHE	Not required	Not required
Switching frequency	Fixed	Variable	Variable (but controllable)
Multivariable	Coupled	Coupled	Decoupled
Constraints inclusion	Not possible	Not possible	easy to include
Complexity of concept	High with SVM	Simple and intuitive	Simple and intuitive
Steady-state performance	Good in *dq* frame	Bad	Good in *abc*, *αβ* and *dq* frames
Transient performance	Moderate	Moderate	Excellent
Computational burden	High with SVM	low	High
Robustness of controller	Poor	Poor	Excellent
Stability of controller	Moderate	Moderate	Excellent

2.5 CONCLUSION

A review of the most widely employed control techniques for dual-stage grid-connected PV system is presented in this chapter. Several maximum power point algorithms for photovoltaic systems are presented and compared in the first part of this chapter. The advantages and disadvantages related to different MPPT algorithms in terms of response time, tracking accuracy, power oscillations, and computational burden are discussed. Furthermore, the state-of-the-art of the DC-link voltage controllers are reviewed and compared regarding quality of the performance operation, easy design and implementation simplicity. Also, control schemes of three-phase VSI grid-connected systems are described in the third part of this chapter. The analysis presented in this chapter favors the voltage oriented MPPT, current oriented MPPT and the FCS-MPC strategy as the next generation control tool to achieve high performance operation for the grid-connected PV systems

Chapter 3

Improved Control of Three Phase Dual-Stage Grid Connected PV System Based on a Predictive Control Strategy

3.1 INTRODUCTION

The conventional control strategies of dual-stage grid-connected PV system suffer from several drawbacks such as: bad MPPT tracking, inaccurate grid power control, low grid current quality, hard implementation practically and variable switching frequency as detailed in the previous chapter. Therefore, an improved control strategy based on fixed switching predictive control strategy for three-phase dual-stage grid-connected PV system is proposed in this chapter. A variable incremental current step size of an MPPT current oriented loop based on fixed switching predictive current control is proposed and employed to control the first stage in order to improve the performance in terms of MPP tracking accuracy, dynamic response speed and oscillation reduction at the MPP. While, the second contribution proposed in this chapter is about the control of second stage. A predictive control strategy is introduced with space vector modulation (SVM) to modify voltage oriented control (VOC) strategy. The proposed PS-VOC aims to eliminate the PI regulators drawbacks as well as the control delay in order to generate the produced PV power and the reactive power demanded by the grid operator into the grid with high grid current quality.

The efficiency of the proposed control strategy is tested under irradiation and reactive power changes demanded by the grid operator through numerical simulations and real-time HIL implementations.

3.2 PROPOSED CONTROL STRATEGY

As shown in Figure 3.1, the global system is controlled by three controllers:

A) VS-INC/PCC controller whose role is to track the MPP quickly and accurately.

B) PI controller to regulate the DC-link voltage.

C) PS-VOC controller for i_d-i_q grid currents.

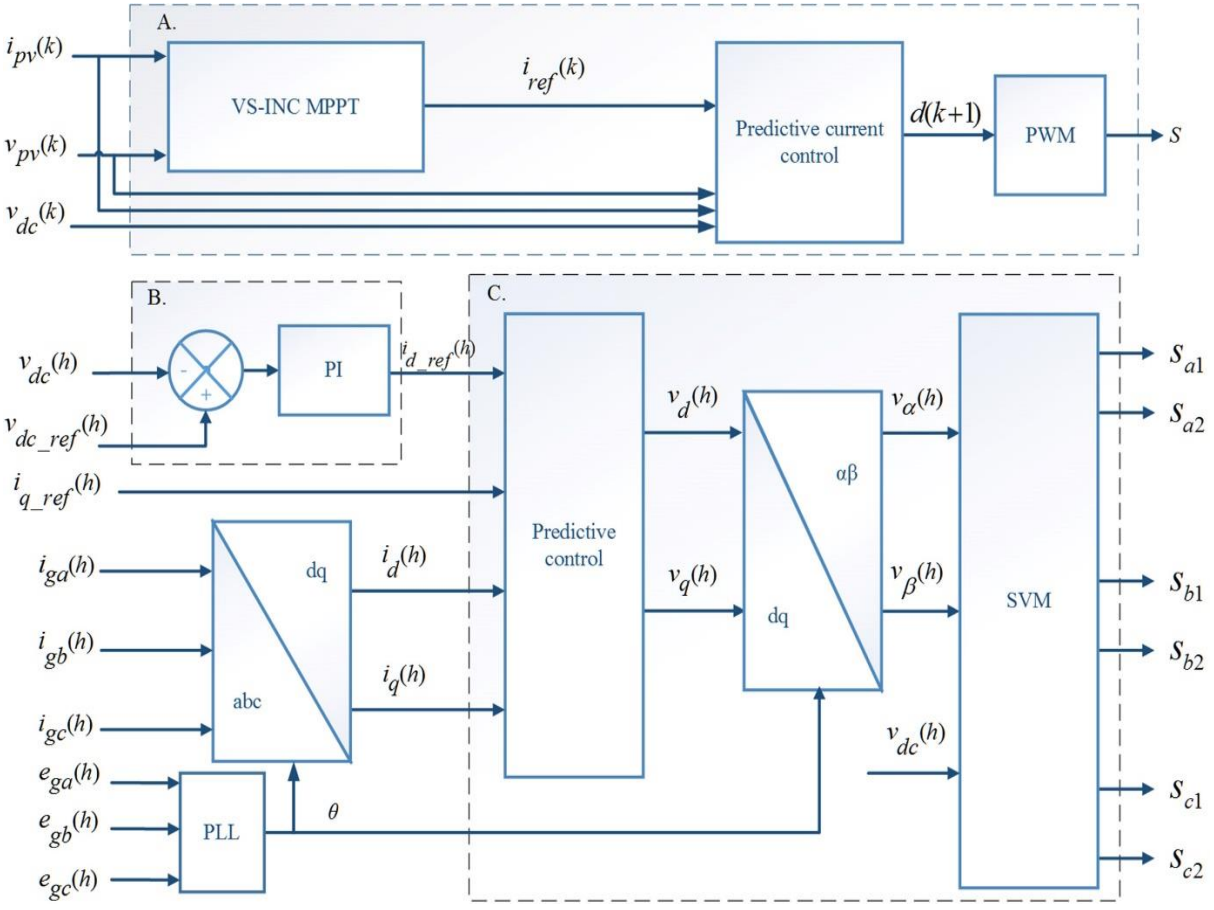

Figure 3.1: Proposed control strategy (A) proposed MPPT controller (B) DC-link voltage controller (C) proposed PS-VOC controller.

3.2.1 PROPOSED MPPT TECHNIQUE

Under irradiation changes, the extreme current *Impp* must be tracked quickly with less ripple to reach the maximum power *Pmpp*. In this paper, an MPPT method based on the

combination of both conventional current incremental algorithm [58] and variable step size algorithm [71, 72] is considered.

A. Variable Current Step Size Incremental Algorithm

The current incremental algorithm as the conventional method is based on the slope of the PV power curve [3]. It identifies the instantaneous position value of the maximum power point; zero at the MPP, negative on the left-hand side of the MPP and positive on the right-hand side of the MPP; i_{ref} increases when the slope is positive and decreases when it is negative.

The basic equations of this method are as follows

$$\frac{dp_{pv}}{di_{pv}} = 0 \tag{3.1}$$

Equation (3.1) can be expressed as

$$\frac{dp_{pv}}{di_{pv}} = \frac{d(v_{pv} * i_{pv})}{di_{pv}} = \frac{dv_{pv}}{di_{pv}} i_{pv} + v_{pv} \tag{3.2}$$

$$\frac{dv_{pv}}{di_{pv}} > -\frac{v_{pv}}{i_{pv}} \qquad \text{at right of the MPP} \tag{3.3}$$

$$\frac{dv_{pv}}{di_{pv}} < -\frac{v_{pv}}{i_{pv}} \qquad \text{at left of the MPP} \tag{3.4}$$

$$\frac{dv_{pv}}{di_{pv}} = -\frac{v_{pv}}{i_{pv}} \qquad \text{at the MPP} \tag{3.5}$$

$$M = \left| \frac{\Delta p_{pv}}{\Delta v_{pv}} \right| \tag{3.6}$$

The proposed MPPT scheme is employed with an algorithm of variable current step size, which is added to the current INC in order to obtain an enhancement in terms of response time and oscillation at the MPP. A small positive quantity e is considered in order to separate the dynamic and steady states tracking operation. In addition, the calculation of the ratio M is given by Equation 3.6; when M is bigger than the chosen positive value e, the step Δi_{ref} takes a big value as well as the MPP will be reached quickly. Thus, when it is smaller than e, Δi_{ref} will take a small value and consequently, the power oscillation at the MPP will be reduced.

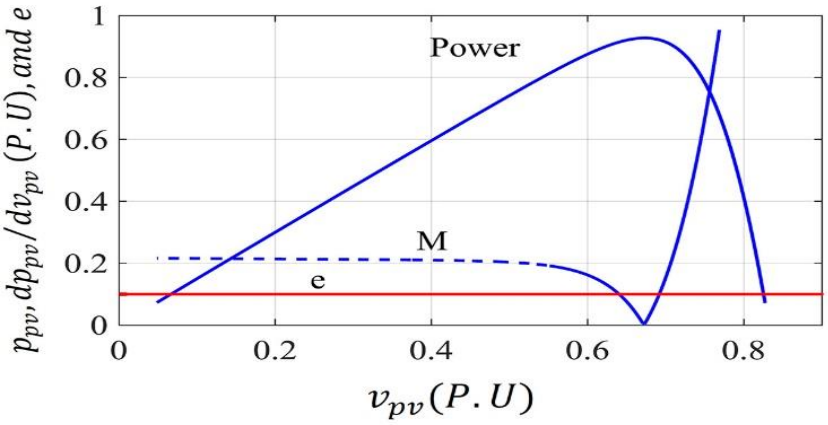

Figure 3.2: Basic idea of VS-INC current algorithm on P-V curve.

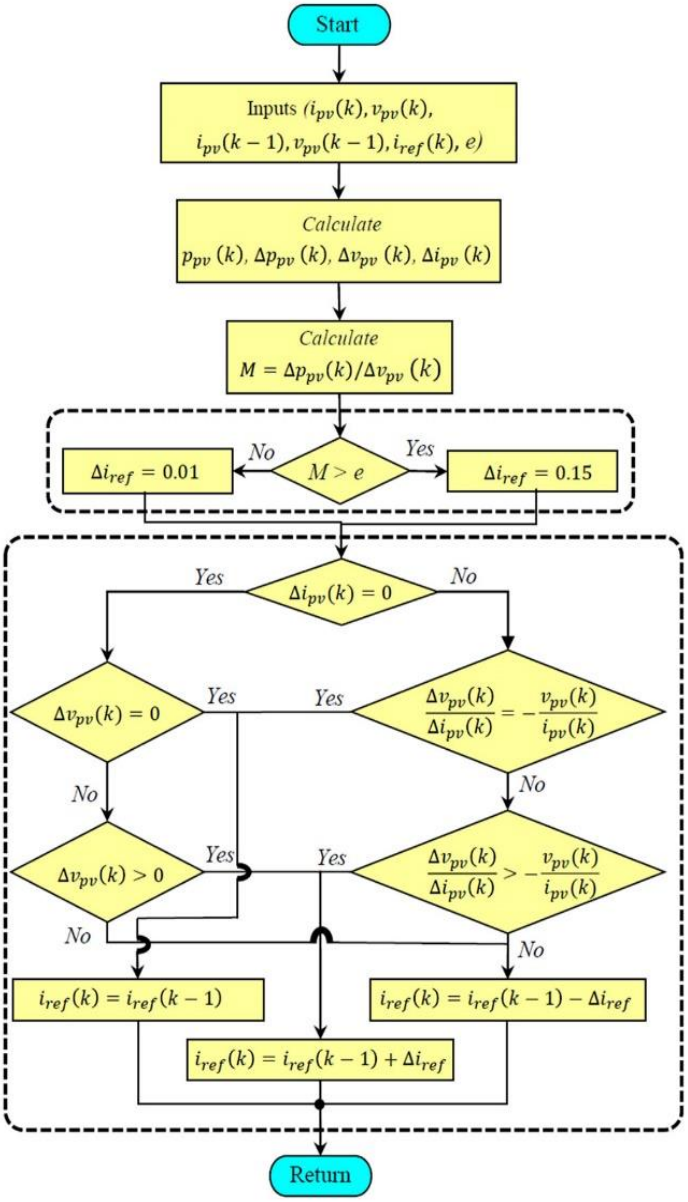

Figure 3.3: Flowchart of the VS-INC current MPPT.

From Figure 3.2, it is clear that the ratio *M* takes large positive value in case where the PV power point is far left or far right from the MPP. In contrast, when PV power is close to the MPP, *M* takes very small positive value. For this reason, the value *e* is chosen as small positive value in order to separate the steady and dynamic states tracking. Figure 3.3 represents the flowchart of the proposed current MPPT algorithm.

B. Fixed switching predictive current control

The role of the predictive current controller is to enforce i_{pv} to track i_{ref} delivered by the MPPT unit via control of the DC-DC boost converter using predicted duty cycle. The determination of the predicted duty cycle is based on exact knowledge of DC-DC boost converter model [73]. Figure 3.4 illustrates the equivalent circuit of DC-DC boost converter considering ON and OFF switching states.

When the switch is ON (Figure 3.4 (a)), the boost converter equations can be described as follows

$$\begin{cases} L\dfrac{di_{pv}(t)}{dt} = v_{pv}(t) \\ C\dfrac{dv_{dc}(t)}{dt} = -i_{inv}(t) \end{cases} \tag{3.7}$$

When the switch is OFF (Figure 3.4 (b)), the boost converter equations yield

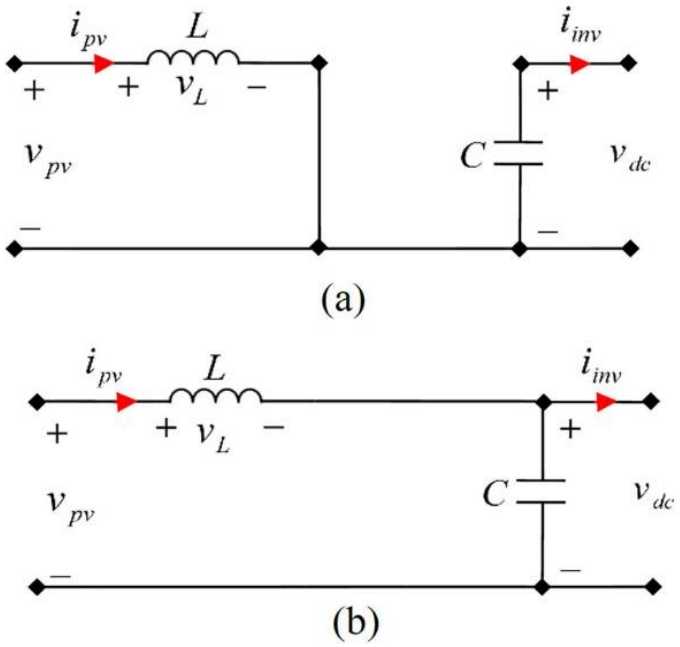

Figure 3.4: DC-DC equivalent circuit.

$$\begin{cases} L\dfrac{di_{pv}(t)}{dt} = [v_{pv}(t) - v_{dc}(t)] \\ C\dfrac{dv_{dc}(t)}{dt} = [i_{pv}(t) - i_{inv}(t)] \end{cases} \tag{3.8}$$

The averaged system of the Equations 3.7 and 3.8 over a switching period Tp is obtained by multiplying Equation 3.7 and 3.8 by the duty cycle *d(t)* and *1-d(t)* respectively [74].

$$\begin{cases} L\dfrac{di_{pv}(t)}{dt} = v_{pv}(t) - v_{dc}(t) + v_{dc}(t)d(t) \\ C\dfrac{dv_{dc}(t)}{dt} = i_{pv}(t) - i_{inv}(t) - i_{pv}(t)d(t) \end{cases} \tag{3.9}$$

By applying Euler's discretization rule and considering the switching period Tp the discrete time system of Equation 3.9 is given as follows [73]

$$\begin{cases} i_{pv}(k+1) = i_{pv}(k) + \dfrac{T_p}{L}[v_{pv}(k) + (d(k)-1)v_{dc}(k)] \\ v_{dc}(k+1) = v_{dc}(k) + \dfrac{T_p}{C}[(1-d(k))i_{pv}(k) - i_{inv}(k)] \end{cases} \tag{3.10}$$

In order to obtain duty cycle at instant k+1, Equation 3.10 is extended for one switching period and can be rewritten as

$$i_{pv}(k+2) = i_{pv}(k+1) + \frac{T_p}{L}[v_{pv}(k+1) + (d(k+1)-1)v_{dc}(k+1)] \tag{3.11}$$

To solve Equation 3.11, we assume that the current i_{pv} is regulated at its reference i_{ref} delivered by MPPT unit [35] which means

$$i_{pv}(k+2) = i_{ref}(k+2) \tag{3.12}$$

And for sufficiently small sampling period Tp , it can be assumed that $i_{ref}(k+2)=i_{ref}(k)$ and no extrapolation is needed.

Assumed that v_{pv} and v_{dc} do not change considerably during one switching period and, thus $v_{pv}(k+1)$ and $v_{dc}(k+1)$ can be estimated as

$$\begin{cases} v_{pv}(k+1) = v_{pv}(k) \\ v_{dc}(k+1) = v_{dc}(k) \end{cases} \tag{3.13}$$

From Equations 3.11, 3.12 and 3.13, the predicted duty cycle for the next sampling period can be derived as [35]

$$d(k+1) = \frac{\frac{L}{T_p}[i_{ref}(k) - i_{pv}(k+1)] - v_{pv}(k)}{v_{dc}(k)} + 1 \tag{3.14}$$

The predicted duty cycle obtained from Equation 3.14 is compared with a sawtooth waveform signal to generate a modulated PWM signal (*S*) to control the DC-DC boost converter.

3.2.2 PROPOSED PS-VOC CONTROL

In this section, rotating frame *d-q* grid currents control for the two-level inverter is performed through PS-VOC control strategy. As shown in Figure 3.1, this control strategy is based on the calculation of the reference voltage vector which is applied during the next sampling time through SVM modulation in order to minimize the error between the predicted currents $i_d(h+1)$, $i_q(h+1)$ and their respective references $i_{d\_ref}(h+1)$, $i_{q\_ref}(h+1)$. From $i_{d\_ref}(h)$ estimated by DC-link PI controller and $i_{q\_ref}(h)$ estimated according to reactive power demanded by the grid operator

$$i_{q\_ref}(h) = \frac{Q_{ref}(h)}{e_{gd}(h) * 1.5} \tag{3.15}$$

where, e_{gd} is the direct component of grid voltage in d-q frame.

One can easily assume that $i_{d\_ref}(h+1)=i_{d\_ref}(h)$ *and* $i_{q\_qref}(h+1)=i_{q\_ref}(h)$ and no extrapolation is needed due to sufficiently small sampling period.

To apply predictive control strategy, the grid-tied inverter model is necessary to calculate the voltage vector reference corresponding to the predicted currents. The required mathematical model in natural frame (abc) is described by [75, 76]

$$\frac{di_g(t)}{dt} = \frac{1}{L_g}[V - e_g(t) - R_g i_g(t)] \tag{3.16}$$

where *V*, e_g and i_g are voltage vectors generated by the inverter, grid voltages and grid currents respectively.

From Equation 3.16, the grid tied inverter model in rotating frame *d-q* can be expressed as follows [28]

$$\begin{cases} \dfrac{di_d(t)}{dt} - \omega_g i_q(t) = \dfrac{1}{L_g}[-R_g i_d(t) - e_d(t) + V_d] \\ \dfrac{di_q(t)}{dt} + \omega_g i_d(t) = \dfrac{1}{L_g}[-R_g i_q(t) - e_q(t) + V_q] \end{cases} \tag{3.17}$$

where ω_g is the grid angular frequency.

Euler forward method is used to approximate the derivatives in Equation 3.17 in order to obtain the discrete time model,

$$\begin{cases} \dfrac{di_d(t)}{dt} = \dfrac{i_d(h+1) - i_d(h)}{T_m} \\ \dfrac{di_q(t)}{dt} = \dfrac{i_q(h+1) - i_q(h)}{T_m} \end{cases} \tag{3.18}$$

where T_m is the sampling period.

The discrete time model of Equation 3.17 can be described as

$$\begin{cases} i_d(h+1) = \dfrac{T_m}{L_g}[-R_g i_d(h) - e_d(h) + V_d] + T_m \omega_g i_q(h) + i_d(h) \\ i_q(h+1) = \dfrac{T_m}{L_g}[-R_g i_q(h) - e_q(h) + V_q] - T_m \omega_g i_d(h) + i_q(h) \end{cases} \tag{3.19}$$

To calculate the reference voltage vector (V_d , V_q) that can be given to SVM modulator, the predicted i_d-i_q synchronous frame currents should track their respective references i_{d_ref} -i_{q_ref} during the next sampling time, which means

$$\begin{cases} i_d(h+1) = i_{d\_ref}(h) \\ i_q(h+1) = i_{q\_ref}(h) \end{cases} \tag{3.20}$$

By substituting Equation 3.20 in 3.19, the reference voltage vector can be expressed as [35]

$$\begin{cases} V_d = \dfrac{L_g}{T_m}(i_{d\_ref}(h) - i_d(h)) + R_g i_d(h) + e_d(h) - \omega_g L_g i_q(h) \\ V_q = \dfrac{L_g}{T_m}(i_{q\_ref}(h) - i_q(h)) + R_g i_q(h) + e_q(h) + \omega_g L_g i_d(h) \end{cases} \tag{3.21}$$

The obtained reference voltage vector (V_d, V_q) by Equation 3.21 is transferred to αβ frame and applied during the next sampling time through SVM modulation.

Figure 3.5 summarized the functionality of the proposed PS-VOC.

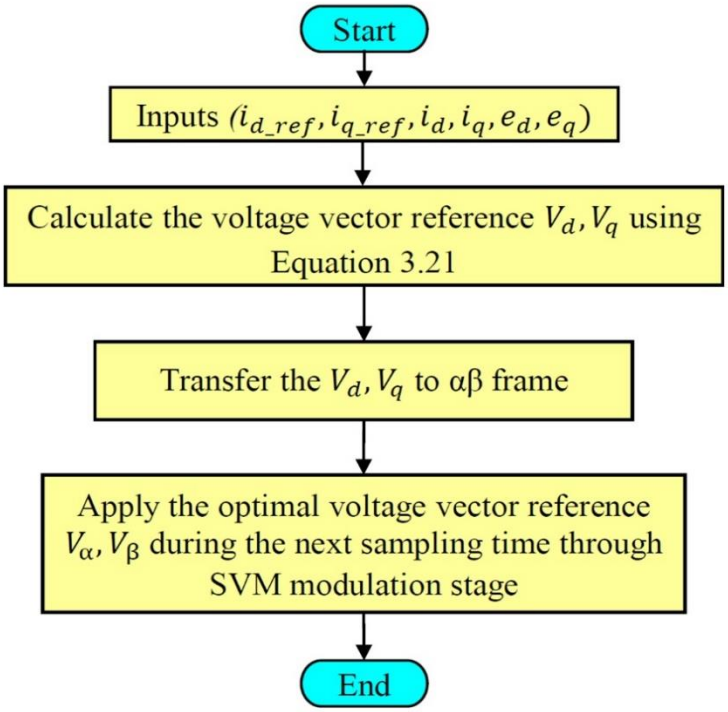

Figure 3.5: Flowchart of the Proposed PS-VOC.

3.3 SIMULATION RESULTS

In order to evaluate the performance of the proposed control scheme illustrated in Figure 3.1, extensive simulations with the specifications depicted in Table 3.1 are performed for the three-phase dual-stage grid-connected PV system using MATLAB/Simulink and Simpower packages. The core of the VS-INC, PCC and PS-VOC algorithms are implemented using embedded MATLAB functions as program lines. Moreover, the power converters are built by Simpower system toolbox components.

This section is divided into two parts. In the first part, the objective is to compare the proposed MPPT (VS-INC/PCC) with both INC/PCC and conventional INC in terms of MPP tracking speed, accuracy and power oscillations under solar irradiation changes. In the second part, the objective is to test the effectiveness of the proposed PS-VOC control technique regarding i_d-i_q grid current regulation and grid current quality under irradiation changes and also reactive power demanded by the grid operator changes.

TABLE 3.1: System global parameters.

PV Siemens SM110 electrical parameters	**Value**
Maximum power (*Pmpp*)	110 *W*
Open circuit voltage (*Voc*)	43.5 *V*
Short circuit current (*Isc*)	3.45 *A*
Voltage at Pmax	*35 V*
Current at Pmax	*3.15 A*
Number of cells connected in parallel (*Np*)	1
Number of cells connected in series (*Ns*)	72
Number of modules connected in series (*Nss*)	2
Number of modules connected in parallel (*Npp*)	2
Boost converter electrical parameters	**Value**
Resistor *R*	50 Ω
Inductor *L*	40 *mH*
Capacitor *C*	1100 *μF*
Grid electrical parameters	**Value**
Grid inductance *Lg*	10 mH
Grid resistance *Rg*	0.1 Ω
Grid Voltage e_g	50 V
Grid frequency *Fg*	50 Hz
Simulation parameters	**Value**
MPPT sampling time *Ts*	1 *ms*
SVM sampling period *Tm*	5 *ms*
PWM switching period *Tp*	5 *ms*

3.3.1 VS-INC/PCC VERSUS INC/PCC AND CONVENTIONAL INC COMPARISONS

Under irradiation changes represented in Figure 3.6 (a), the proposed VS-INC/PCC MPPT method, INC/PCC, and conventional INC are tested by numerical simulation. Initially, the irradiance level is set to 500 W/m^2. Then, at 0.1 s, a sudden irradiation change from 500 to 700 W/m^2 occurs. With VS-INC/PCC method MPP is reached after 7 ms, while with INC/PCC it takes 18 ms. As the conventional method reaches the MPP during 34 ms with tracking direction drift. Then the irradiation level is decreased slowly from 700 to 400 W/m^2 during a time interval of 0.2 s. The proposed method exhibits better accuracy tracking than both INC/PCC and conventional INC as shown in Figure 3.6. Finally, a sudden irradiation changes from 400 to 1000 W/m^2 occurs at 0.5 s, the improved MPPT shows also a faster tracking than both INC/PCC and conventional MPPT, where the proposed MPPT takes only 25 ms to reach the MPP while the INC/PCC needs 56 ms and conventional MPPT needs 100 ms as shown in Figure 3.6 (d). On other side, the proposed MPPT shows a high performance in term of power oscillation compared to INC/PCC and conventional methods as depicted in Figure 3.7, where the oscillation widths around MPPs, by using the proposed method, under different steady irradiations levels (500, 700, 400 and 1000 W/m²) are [209.2- 209.7], [301.6- 302], [163.4- 163.8], and [439.8- 440] respectively. In counterpart, the widths of power oscillation widths by using the INC/PCC method are [208.5- 209.7], [300.5- 302], [162.2- 163.8], [440- 439.4] respectively, and when the conventional one they are [206- 209.7], [299- 302], [161- 163.8], [437.2- 440] respectively.

Table 3.2 summarized the comparison between the proposed VS-INC/PCC MPPT method, INC/PCC, and conventional INC in terms of MPPT tracking speed, accuracy and power oscillations.

As shown in simulations results, the MPPT algorithms based on predictive current control respond to the change in irradiation quickly and accurately than the conventional algorithm, due to the linear relationship between the irradiance and the PV current [77]. This linear relationship demonstrates that it's a beneficial factor toward the MPP rapidly and accurately. Furthermore, the developed variable step size current Incremental conductance algorithm makes the proposed MPPT scheme quicker and more accurate with a significant power oscillations reduction compared to both conventional algorithms. Where, it provides high Δi_{ref} during sudden irradiations and a small Δi_{ref} for fixed or slow irradiation changes as shown in Figure 3.8. On the other hand, the INC/PCC provides a fixed Δi_{ref} under all irradiation changes.

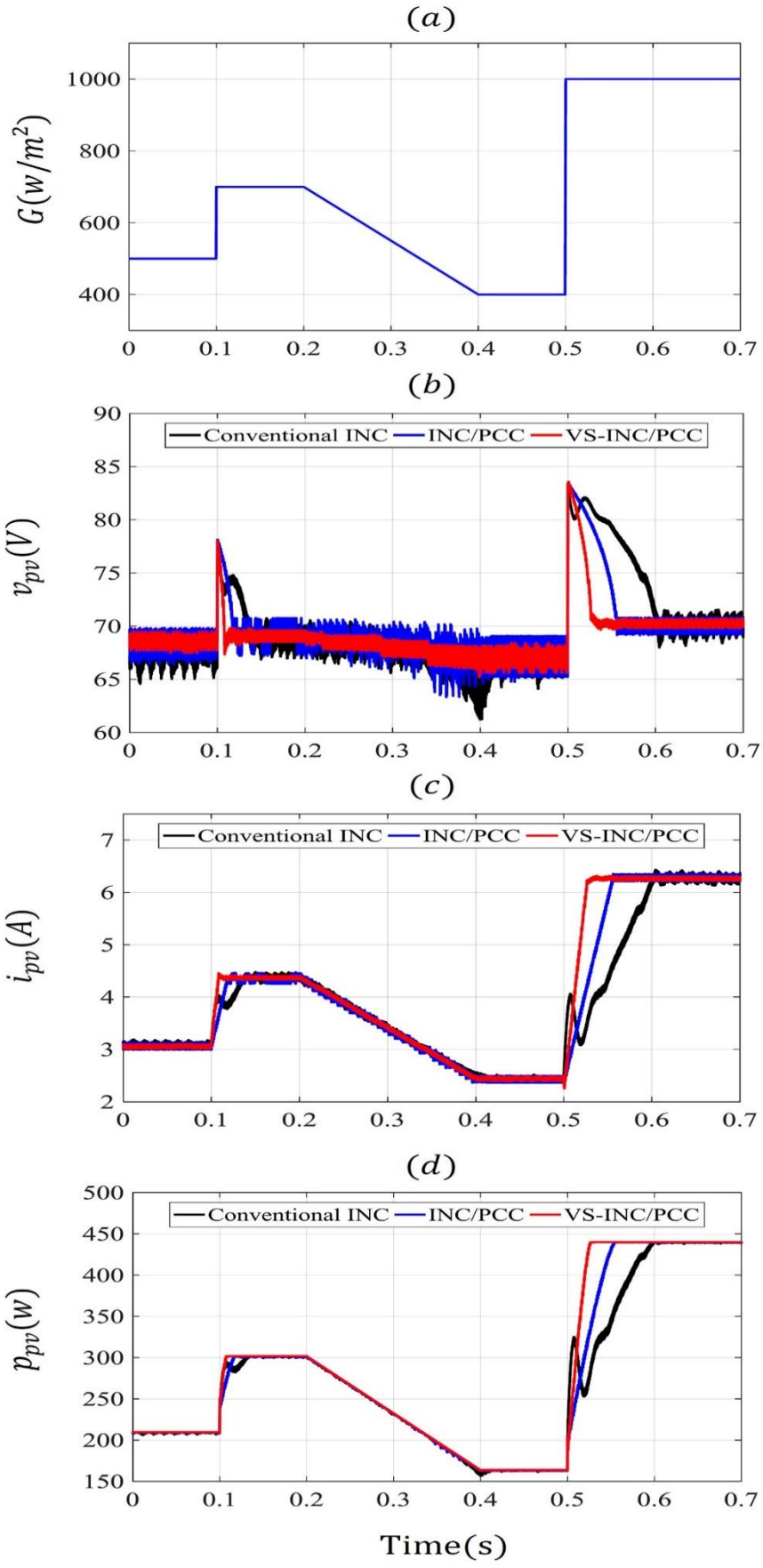

Figure 3.6: Performance of INC, INC/PCC and proposed MPPT under irradiation changes.

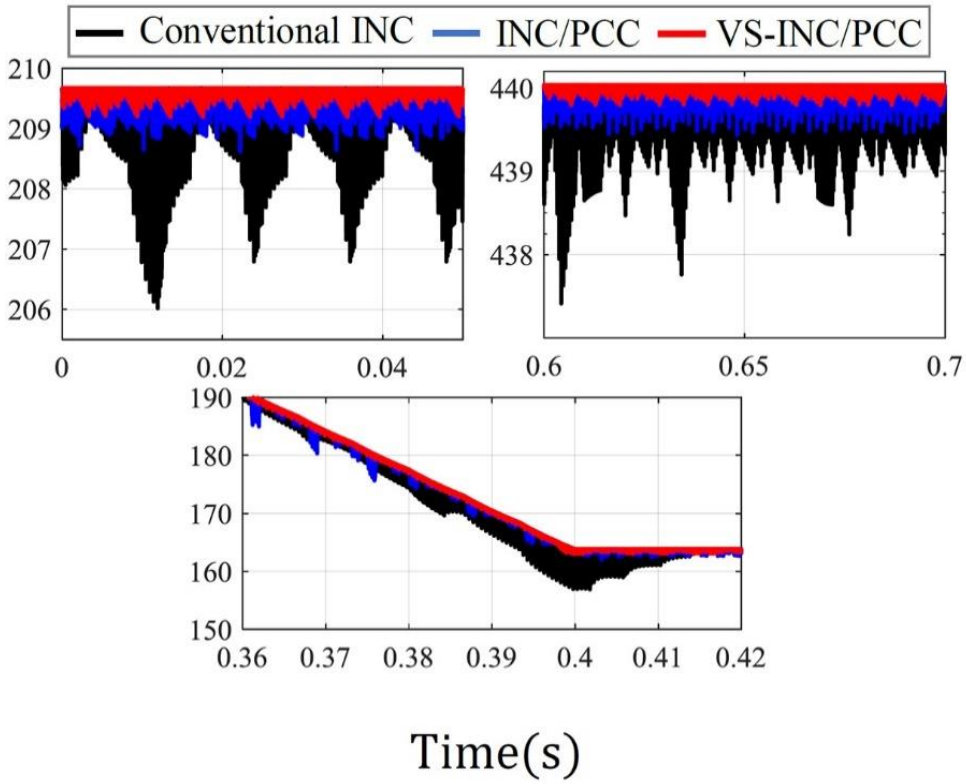

Figure 3.7: Zoom of PV power output.

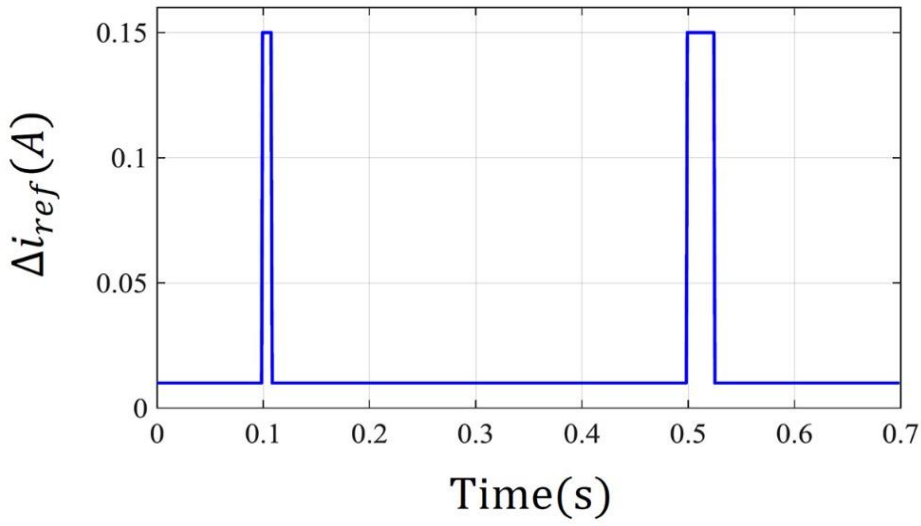

Figure 3.8: Behavior of proposed VS-INC.

TABLE 3.2: Summary of MPPT simulation results.

Technique	Step change in irradiance 500→700 W/m²		Linear change in irradiance 700→400W/m²	Step change in irradiance 400→1000W/m²	
	Tracking speed time (*ms*)	Power oscillation (*W*)	Tracking accuracy	Tracking speed time (*ms*)	Power oscillation (*W*)
Conventional INC	34	3	Bad (power deviation)	100	2.8
INC/PCC	18	1.5	Good	56	0.6
VS-INC/PCC	7	Less than 0.4	Very Good	25	Less than 0.2

3.3.2 PERFORMANCE OF PS-VOC UNDER IRRADIATION CHANGES

This section deals with test of the global system performance under different irradiation changes and presents the efficiency of the applied method in terms of *d-q* currents control and grid current THD.

Firstly, as illustrated in Figure 3.9 (a), for a fixed irradiation condition at 500 W/m² during the interval [0, 0.1s], the PV array output is oscillating around the MPP and v_{dc} is completely maintained to its reference. Hence, i_d and i_q are regulated according to their references by means of the proposed method (PS-VOC), as observed in Figure 3.9 (c, d). Furthermore, the grid currents are balanced and sinusoidal.

Afterward, the sudden irradiation changes from 500 to 700 W/m² at instant 0.1s leads to an increase in the PV power output and a small deviation in v_{dc} from its reference as shown in Figure 3.9 (a, b). Despite that, i_d and i_q remain tracking their references, whereas the grid currents are increased and kept sinusoidal due to the capability of the proposed method. Then, under the slow irradiation change from 700 to 400 W/m² during the time interval 0.2 to 0.4s, the PV power decreases slowly. Also, v_{dc} is a bit far from its reference as illustrated in Figure 3.9 (b). Meanwhile, i_d_i_q currents track their references and grid currents are decreasing with a sinusoidal form.

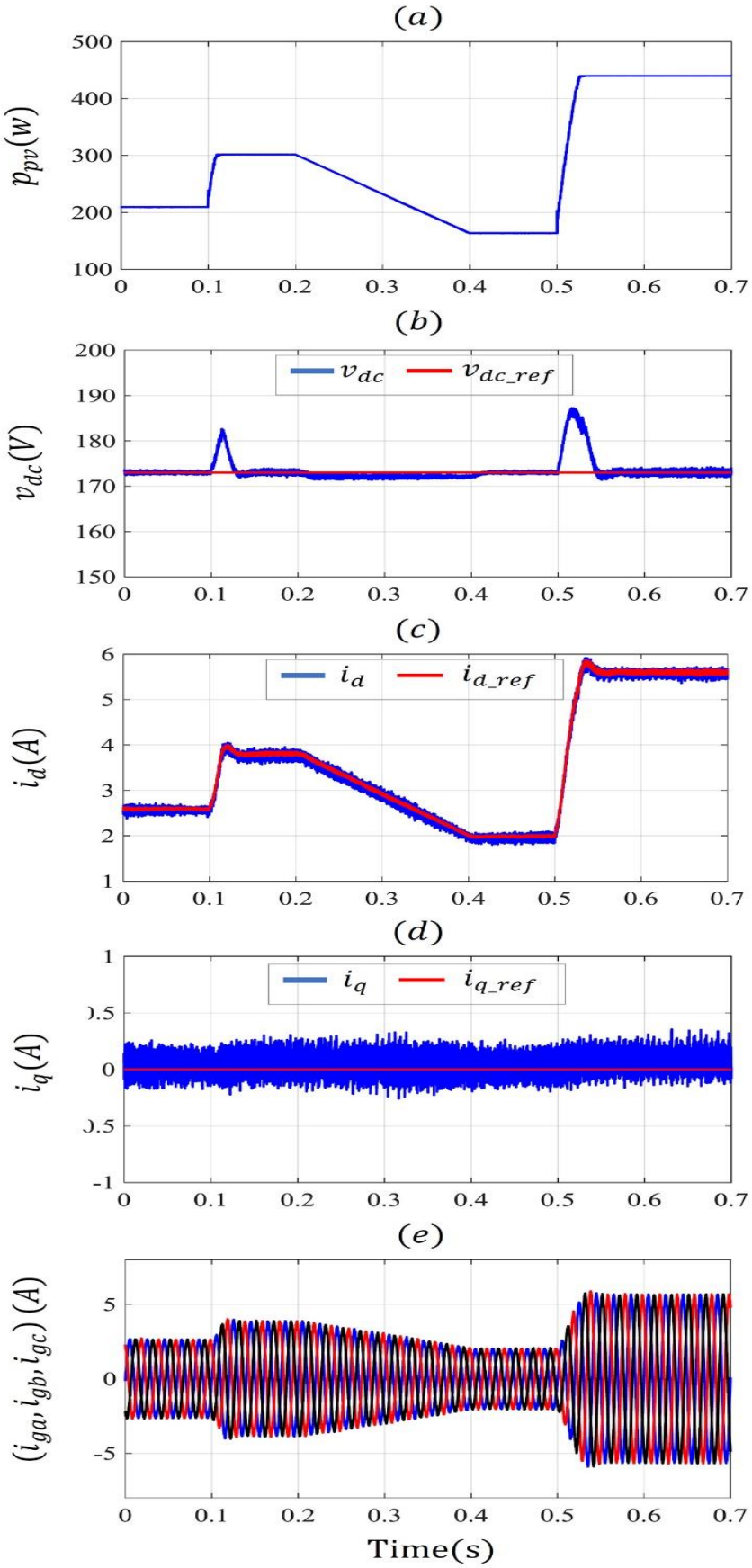

Figure 3.9: Performance of global system under irradiation changes.

Finally, a large sudden change in irradiation occurs at instant 0.5 s. The PV power output is rapidly increased, which leads to a large deviation of v_{dc} from its reference, as shown in Figure 3.9(b) even though, i_d and i_q remain tracking their references whereas the grid currents remain sinusoidal. This is due to the efficiency of the proposed method.

As presented in Table 3.3, the proposed method (VOC based on predictive strategy through SVM) provides high grid current quality under all irradiation change level cases according to the international standards (IEEE-519, THDi< 5%).

TABLE 3.3: Obtained THD under different irradiation levels.

Irradiation levels G(W/m²)	500	700	400	1000
Proposed PS-VOC THDi%	3.56	2.66	4.08	1.51

3.3.3 PERFORMANCE OF PS-VOC UNDER REACTIVE POWER REFERENCE CHANGES

In this section, the performance of the proposed PS-VOC is examined under reactive power reference changes and fixed PV power output at 440 W.

As shown in Figure 3.10, the reactive power reference is set to zero during 0.2s, hence, the i_{q_ref} is also set to zero. The DC-link voltage is completely maintained to its reference, when the i_d-i_q currents track their references and the grid currents are sinusoidal.

Next, at instant 0.2 s, a sudden increase from 0 to 300 VAR is occurred in the reactive power reference while, the i_q reference is estimated to be 4 A. The proposed PS-VOC method shows a rapid i_q tracking to its reference (2.7 ms). Besides, the grid currents increase swiftly due to the increase in grid apparent power S_g where the grid current amplitude is proportional to S_g. It is also observed that the angle between the grid currents and grid voltage is changed as depicted in Figure 3.11(a).

Then, at instant 0.4 s, a sudden decrease from 300 to 0 VAR in the reactive power reference occurs while, i_{q_ref} is set to 0A. The ability of the proposed PS-VOC shows a quick tracking of i_q to its reference (4 ms). Also, grid currents amplitude increase is observed due to the increase of apparent power Sg. While the grid currents and voltages become in phase as illustrated in Figure 3.11(b).

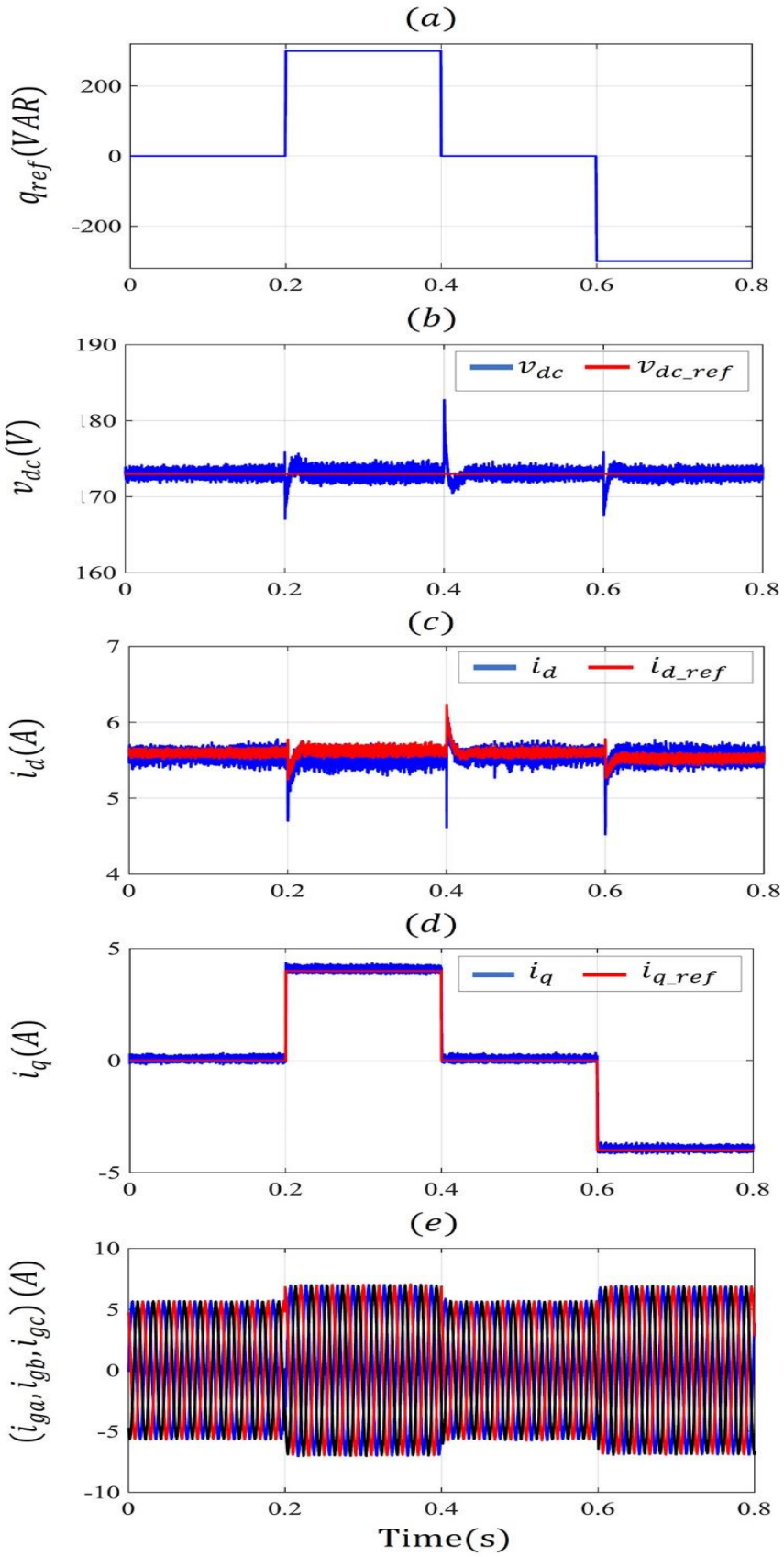

Figure 3.10: Performance of global system under reactive power grid operator demand changes.

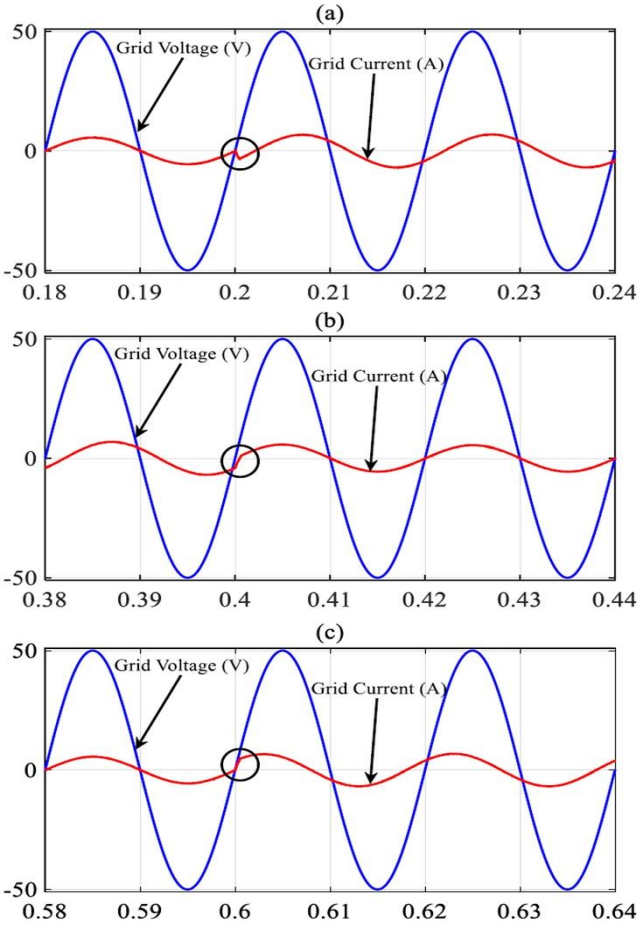

Figure 3.11: Grid current and voltage angle change under reactive power change.

Finally, at instant 0.6 s another sudden decrease from 0 to -300 VAR occurs again in the reactive power reference while i_{q_ref} is estimated to be -4 A. The proposed VOC method enforces i_q to reach its reference in only 3.7 ms. Also, the grid currents are rapidly increased due to the increase in grid apparent power S_g. Where, the grid current amplitude is proportional to S_g and the angle between the grid currents and voltages is changed as depicted in Figure 3.11(c). The proposed method (VOC based on predictive strategy trough SVM) provides high grid current quality under all reactive power reference level changes according to the international standards (IEEE-519, THDi< 5%), as presented in Table 3.4.

TABLE 3.4: Obtained THD under different reactive power reference levels.

Reactive power reference Q_{ref} (VAR)	0	300	-300
Proposed PS-VOC THDi%	1.51	1.45	1.30

3.4 REAL-TIME HIL IMPLEMENTATION

To confirm the efficiency of the proposed control scheme established in the previous section, real-time HIL implementation experiments have been carried out with the same parameters used in simulations. As illustrated in Figure 3.12, the HIL system includes two essential components which are real-time simulator and an independent control-processing unit (CPU). The objective of real-time simulator is to simulate the three-phase dual-stage grid-connected PV system while, the CPU is to run the proposed control scheme. The communication between two essential components is guaranteed by a communication channel [77].

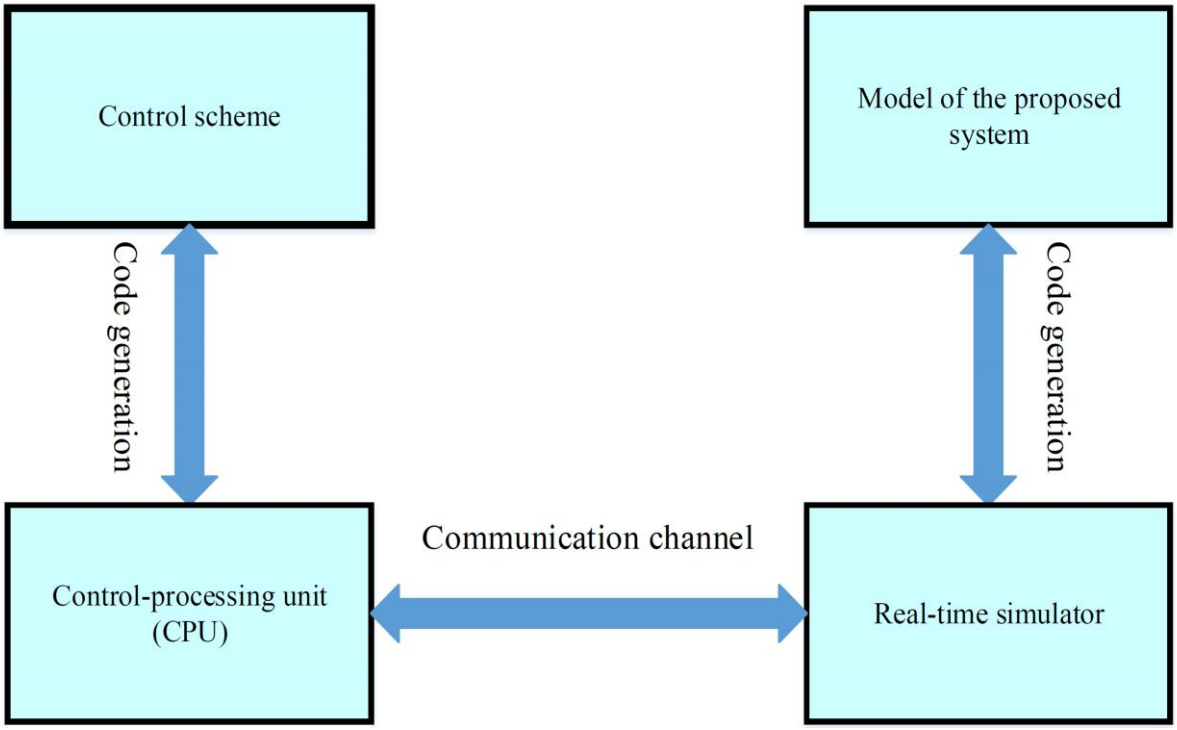

Figure 3.12: Diagram of hardware in the loop system (HIL).

At the start of every sampling time, the CPU obtains the actual PV voltage and current, DC-link voltage, grid currents, grid voltages from the real-time simulator through a communication channel. Then, the CPU calculates the optimal control actions for the two conversion stages based on these actual state variables, and transmit it to the real-time simulator to be employed during the next sampling time. 500 MHz Instek oscilloscope is used to record the real time HIL results.

As the simulation section, the proposed MPPT (VS-INC/PCC) is compared with both

INC/PCC and conventional INC in terms of MPP tracking speed, accuracy and power oscillations under solar irradiation changes. Moreover, the proposed PS-VOC control technique is tested under irradiation changes and also reactive power demanded by the grid operator changes regarding i_d-i_q grid current regulation and grid current quality.

The real time HIL implementation results for the three MPPT methods is carried out under the periodically irradiation conditions variation represented as : fixed at 500 W/m² then a sudden irradiation change from 500 to 1000 W/m^2, after slowly irradiation change from 1000 to 500 W/m^2.

The measured waveforms of the PV system employing the three studied methods are shown in Figures 3.13, 3.14 and 3.15. It is clear that high dynamic performance is obtained from the proposed MPPT control compare to the INC/PCC and the conventional INC. Moreover, the proposed MPPT presents a high accuracy tracking with less power oscillation. On the other side, the conventional INC shows a large power oscillation, in addition, it illustrated some deviation in the tracking operation of MPP during the linear decrease of irradiance level, and the INC/PCC provided a high accuracy tracking but with large oscillation as depicted in Figures 3.13, 3.14 and 3.15.

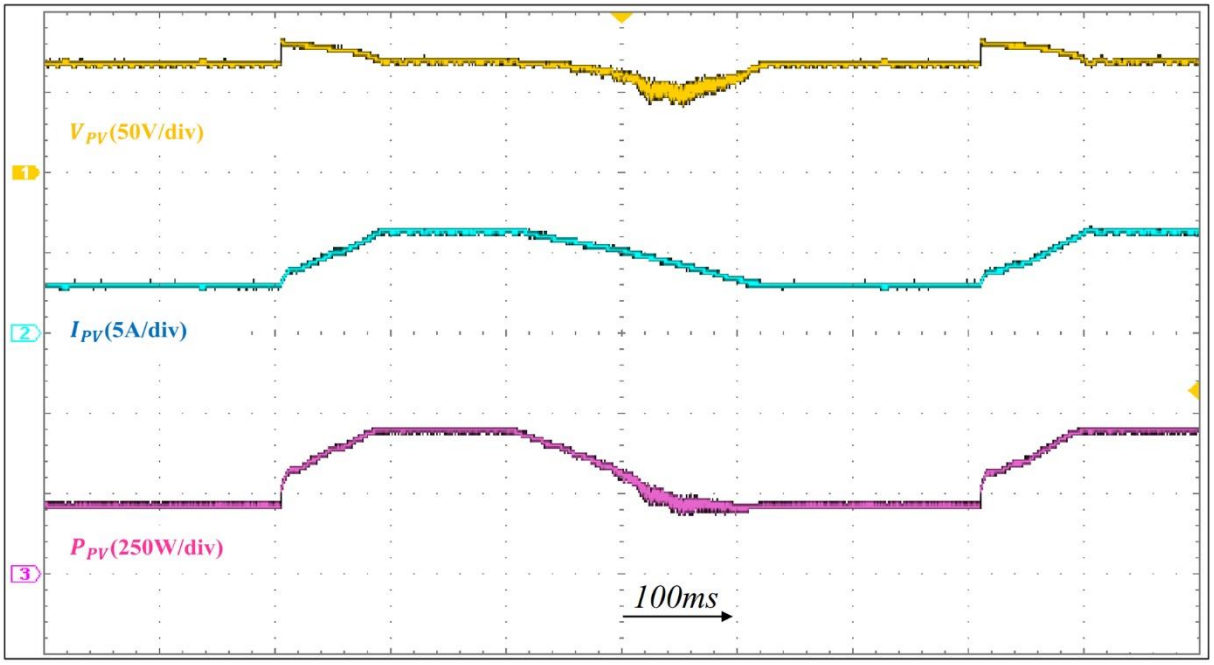

Figure 3.13: Performance of conventional INC MPPT under irradiation changes.

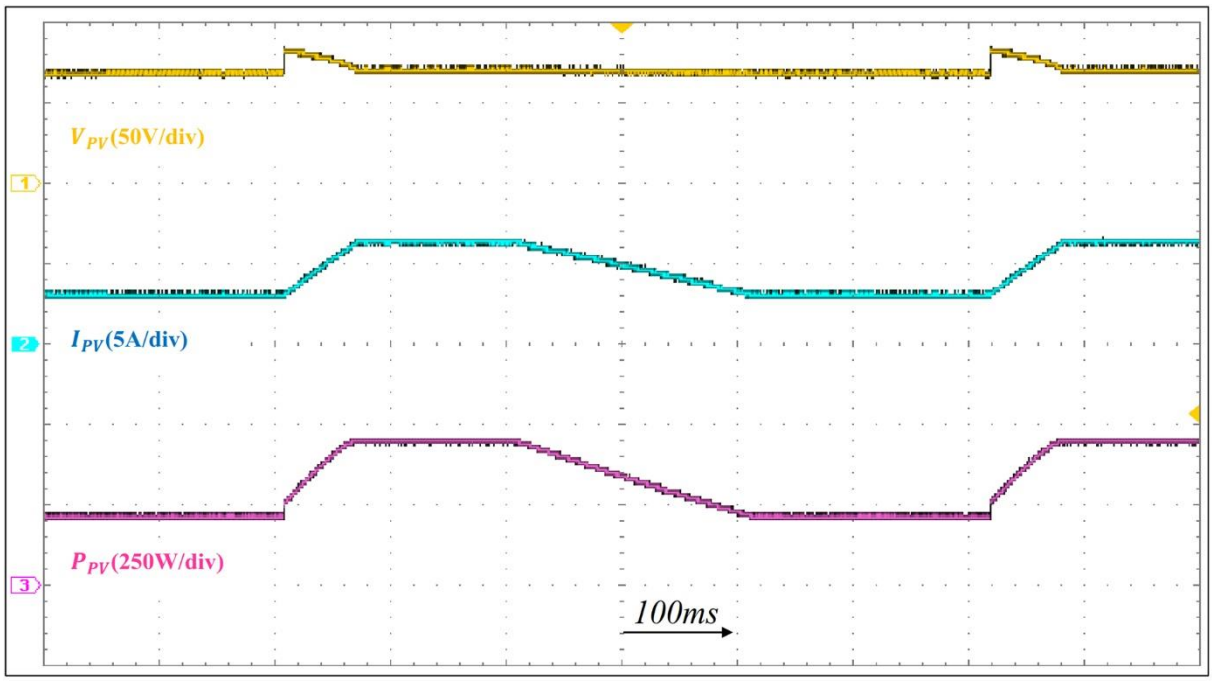

Figure 3.14: Performance INC/PCC MPPT under irradiation changes.

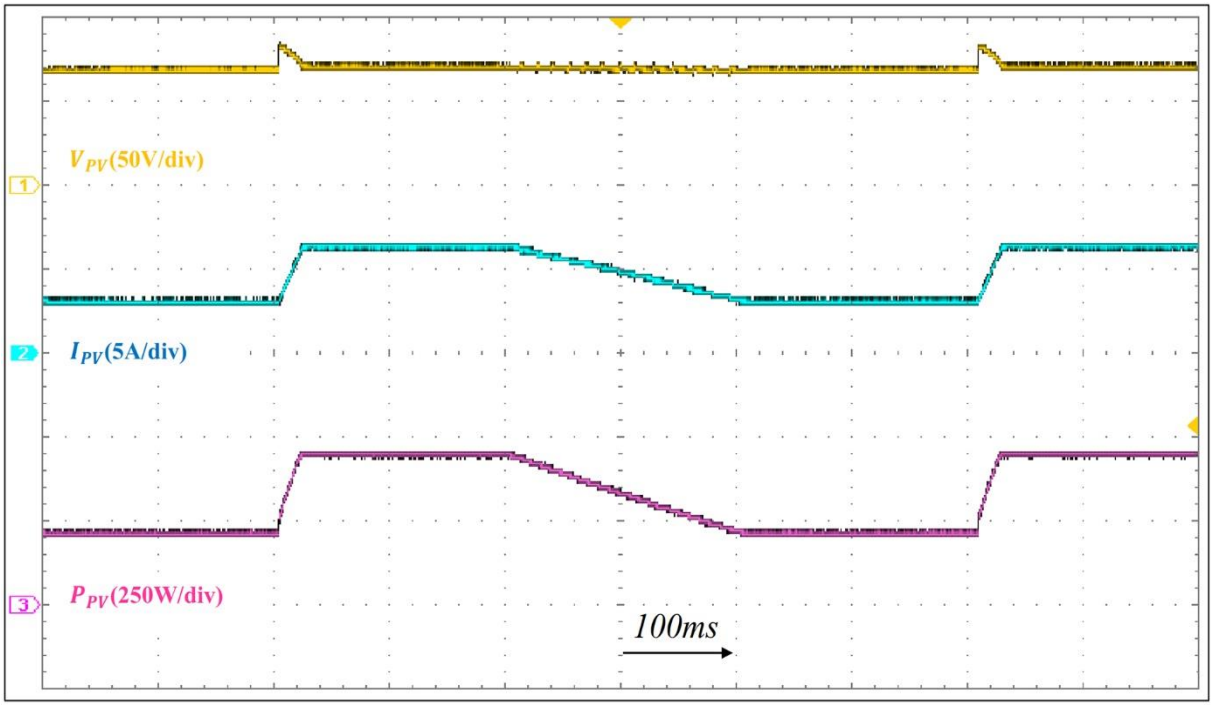

Figure 3.15: Performance of proposed MPPT under irradiation changes.

Also, the evaluation of the proposed PS-VOC under irradiation changes is performed under the same periodically profile of irradiation conditions variation. The real time HIL implementation results for the global system are shown in Figure 3.16.

The DC-link voltage is well regulated by using a simple PI regulator. Also, the proposed PS-

VOC assure a well regulation of i_d and i_q currents as shown in Figure 3.16. Moreover, the amplitudes of the grid currents increased or decreased according to the irradiance change and keeping their balanced as shown in Figures. 3.17 and 3.18.

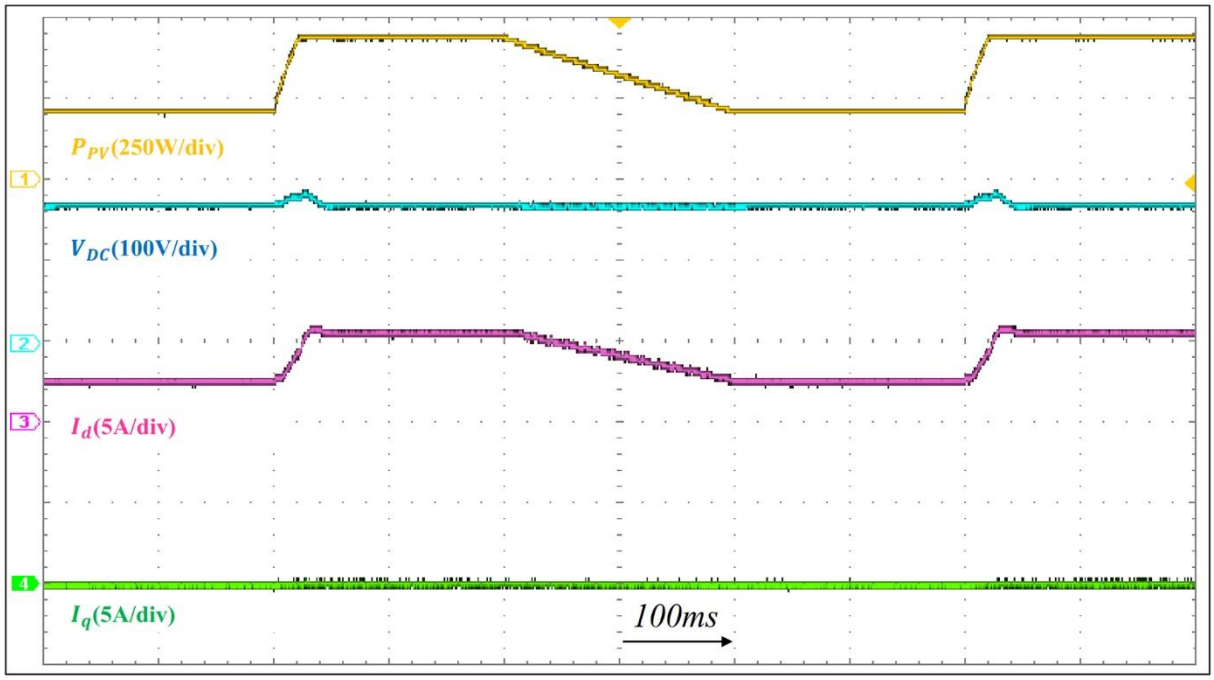

Figure 3.16: Performance of global system under irradiation changes.

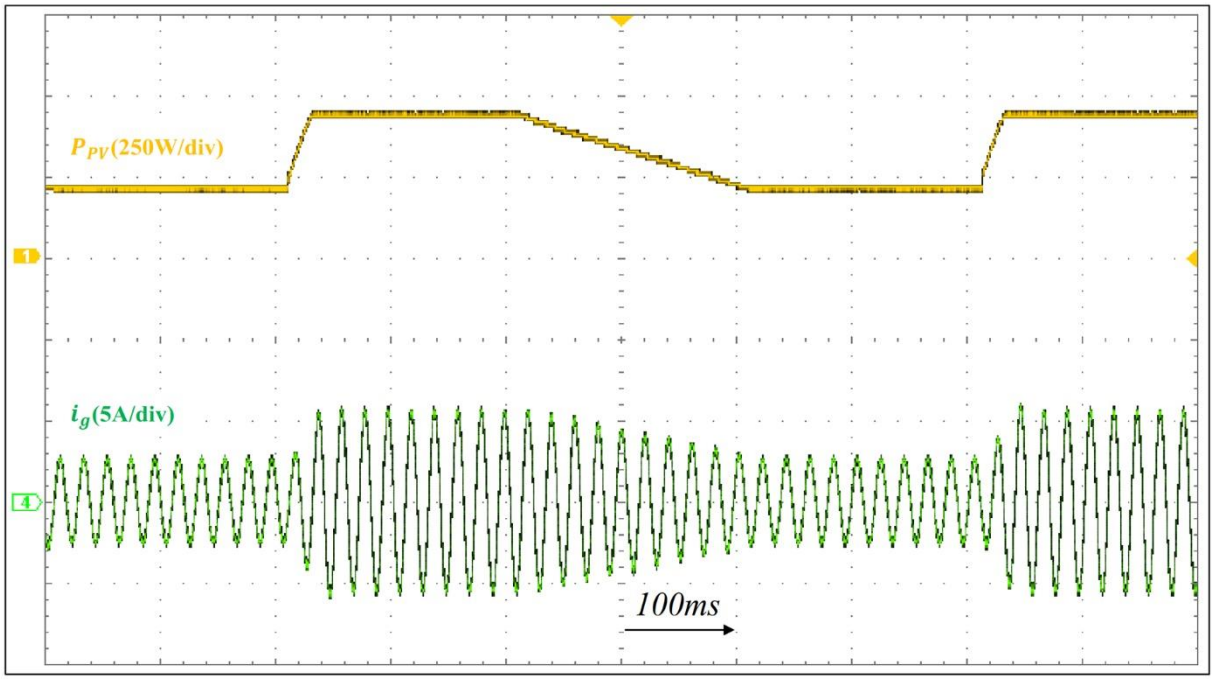

Figure 3.17: Performance of global system under irradiation changes.

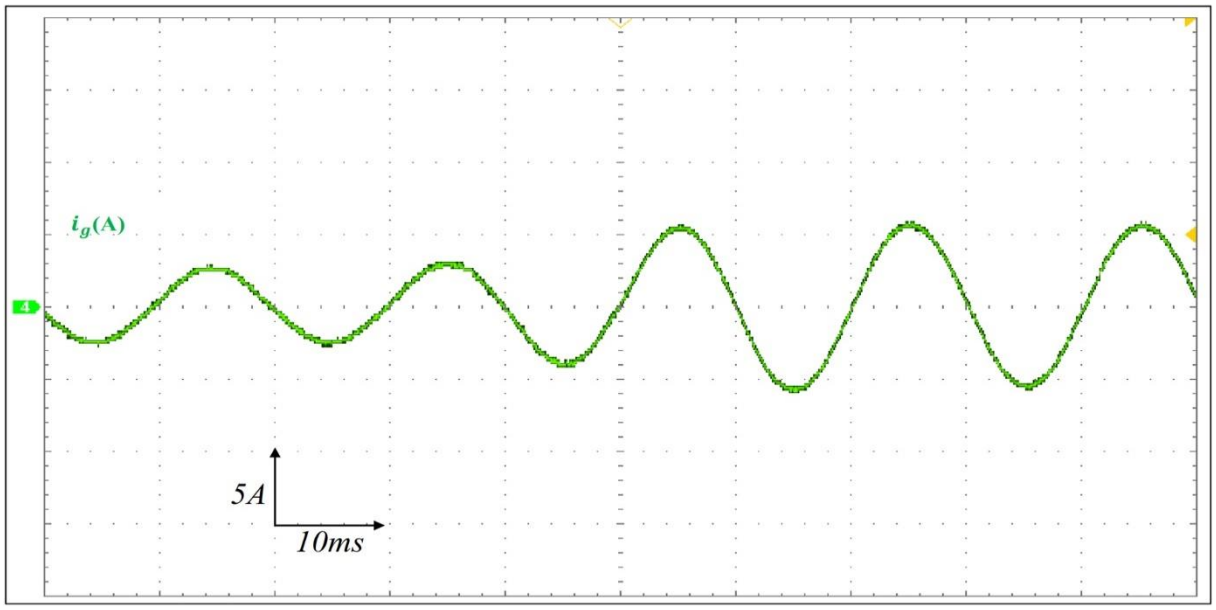

Figure 3.18: Zoom of grid current under irradiation changes.

Several step changes in reactive power reference are performed in order to evaluate the proposed PS-VOC from 0 Var to 300 Var, from 300 Var to 0 Var, from 0 Var to -300 Var and from -300 Var to 0 Var while the active power reference is remained at 440 W.

As presented in Figure 3.19, the DC-link voltage, i_d and i_q currents are well regulated. Moreover, the grid currents are change their phase and increased or decreased while keeping their balanced as shown in Figures 3.20 and 3.21.

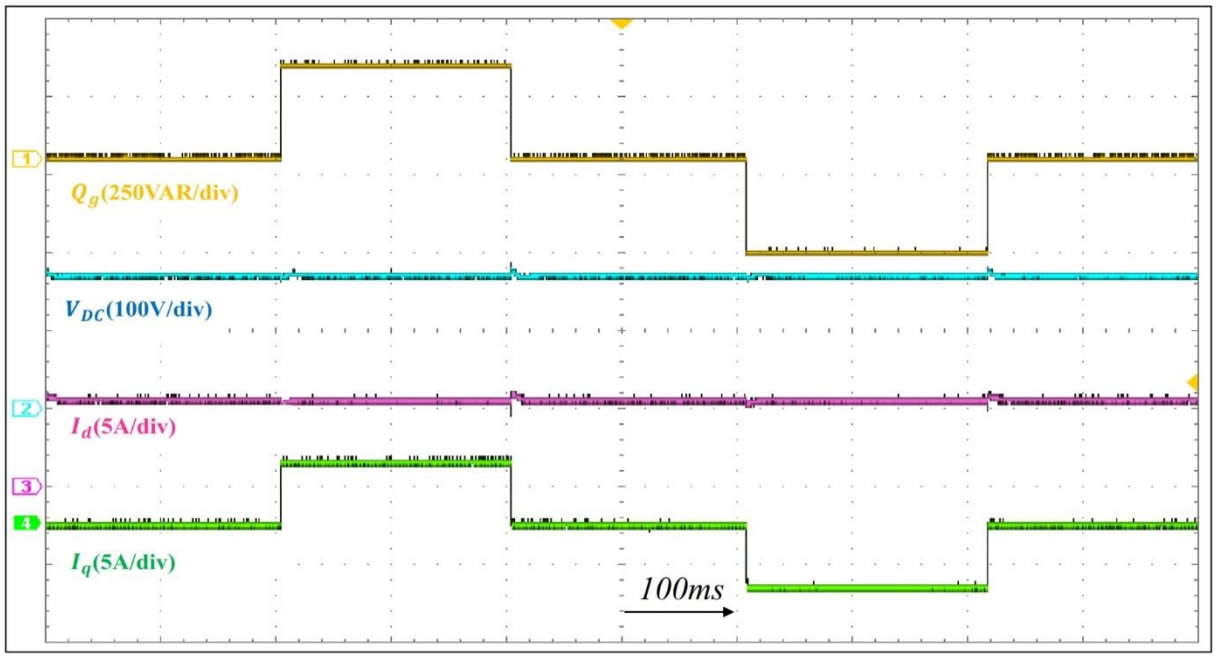

Figure 3.19: Performance of global system under reactive power reference changes.

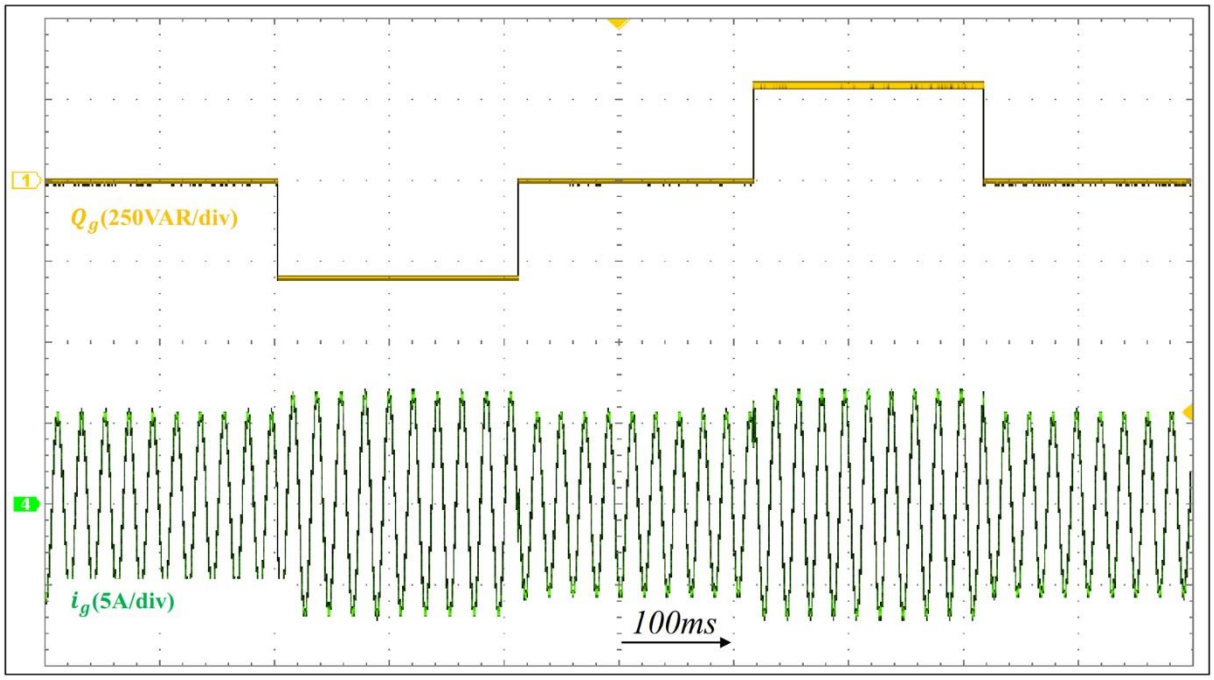

Figure 3.20: Grid current behavior under reactive power reference changes.

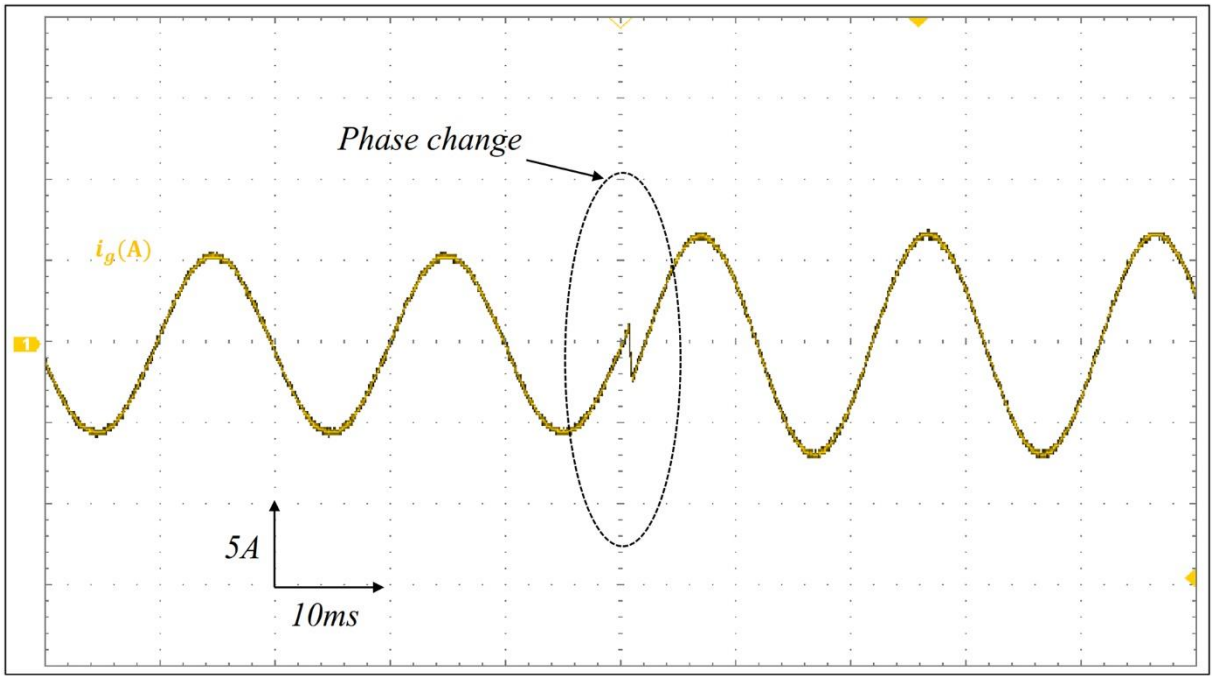

Figure 3.21: Zoom of grid current with angle change under reactive power change.

The grid currents THDi% obtained by employing the proposed PS-VOC algorithm under all irradiation and reactive power reference levels is summarized in Table 3.5. According to the international standards (IEEE-519, THD < 5%), it's clear that the proposed PS-VOC provide high grid current quality which confirms the effectiveness of the proposed algorithm.

TABLE 3.5: Obtained THD under different reactive power reference levels.

Irradiation and reactive power reference Level	500 W/m^2 & 0 Var	1000 W/m^2 & 0 Var	1000 W/m^2 & 300 Var	1000 W/m^2 & -300 Var
Proposed PS-VOC THDi %	4.14	2.03	1.89	1.77

3.5 CONCLUSION

In this chapter, an improved control scheme based on predictive control strategy for three phase dual-stage grid tied photovoltaic (PV) system was presented. A predictive current control technique, VS-INC/PCC, is proposed and applied to the first stage in order to track the MPP quickly and accurately. Whereas, VOC based on predictive control strategy through SVM, PS-VOC, was employed to control the second stage in order to inject the generated PV power in addition to the reactive power demanded by the grid operator with high grid currents quality. The simulation and real time HIL implementation results clearly show a significant enhancement by applying the proposed MPPT method in comparison with the conventional INC and INC through PCC methods in terms of accuracy tracking, response time and stability around the maximum power point under irradiation changes. Moreover, the proposed PS-VOC control of grid tied two-level inverter presents high grid currents quality in accordance with international standards (IEEE-519) for any irradiation and reactive power level

Chapter 4

Control of Grid-Tied PV System using Multilevel NPC Inverter Based on FCS-MPC

4.1 INTRODUCTION

Nowadays, many research works have contributed to develop new topologies besides control strategies employed in grid-connected systems by using numerous voltage source inverters (VSIs) [78-81]. The use of two-level inverter in grid PV systems has many disadvantages such as large ripple, large switching frequency, high values of grid-side filter, large stress on semiconductor switches and rich harmonic content of the output voltage and current. In order to overcome the drawbacks of two-level inverter, researchers tend to use the multilevel inverters such as neutral point clamped multilevel inverters (NPC) and cascaded H-bridge multilevel inverters [78, 79], that provide high control performance in terms of powers control and grid currents quality. The NPC inverters are the most commonly studied and employed topologies for high-power grid-tied inverter systems [27]. Where, they use the semiconductor switches connected in series, then permitting the operation with larger DC voltages. However, the major drawbacks of such inverters are the DC-link capacitor voltage unbalance and control design complexity [27].

In this chapter, high-level NPC inverters are employed in grid-connected PV system in order to inject the high produced PV power into the grid with high grid currents quality. Moreover, a simple and effective model predictive control (MPC) algorithm is proposed for grid-connected PV system using high-level NPC inverter (six-level) that permits to inject the active power generated by the PV system, the reactive power demanded by the grid operator

and assure the balance of DC-link capacitor voltages. Then, an optimized model predictive control (O-MPC) is proposed in order to achieve the same performance control provided by the first MPC algorithm with a significant reduction in computational burden. The effectiveness of the proposed MPC and O-MPC are tested under sudden irradiation and reactive power changes demanded by the grid operator through numerical simulations and real-time HIL implementations.

4.2 State of the art of grid-connected PV system using Multilevel inverter controllers

Numerous control techniques based on the instantaneous active and reactive powers, have been developed and widely explored in the literature for grid-connected high-level NPC inverters. These control techniques can be divided in two categories:

- Power control methods without modulation stage such as: direct power control (DPC) [80, 81] and Virtual flux oriented DPC (VF-DPC) [82] based on switching table. The design of the switching table will be complex for high-level inverter cases (3 levels and more). Furthermore, these methods do not provide high power control performance.

- Power control methods with modulation stage such as: voltage-based direct power control (V-DPC) [83, 84]. To apply these techniques, PI controller is necessary in the internal current loop in addition to modulation stage such as pulse width modulation (PWM) or space-vector modulation (SVM) [88, 28]. To design the modulation stage for high-level inverters, the DC-link capacitor voltages control must be included, which makes these methods more complicated. Moreover, PI controller drawbacks and control delay will deteriorate the performance.

In recent research works, the finite-control set model predictive control (FCS-MPC) has been intensively investigated in power converters control [31]. FCS-MPC has been applied for grid-connected PV systems using high-level inverter for different control purposes such as: grid current control [85-88], d-q rotating frame grid current control [28] and power control [89-91]. It is considered as a good and simple control strategy, where it is easy to include the DC-link capacitor voltages balancing in the objective control. Furthermore, it provides high control performance in comparison with conventional methods [85-91]. However, this technique suffers from the computational burden because it generates the control of multilevel NPC inverter switches after evaluation of the predicted value for all vectors; it causes the

computational burden especially in high-level inverters (more than 5 levels) [94]. Besides the common control problems, this one limits the utilization of high-level inverters. In [92], the authors proposed a model predictive torque control for induction motor using three level NPC inverter. The proposed strategy reduces the number of voltage vectors for prediction by 48% compared to the conventional model; in addition, this model is available only for simple grid current control (αβ stationary). Hence, it is not allowed to inject the reactive power as per of the grid operator demand due to the change in angle between grid voltage and current. In [93], the authors have proposed a modified MPC for cascaded H-bridge inverter that considerably reduces the amount of calculations without affecting the system performance. They eliminate the redundant vectors in addition to create an algorithm which selects the adjacent vectors to the last applied vector for prediction. In contrast to the NPC topology, the studied topology in [93], does not suffer from DC-link capacitor voltages unbalance problem, which allowed to eliminate the need of redundant vectors. Therefore, this model is not designed to treat the DC-link capacitor voltages unbalance. In addition, it is not allowed to inject the reactive power as per of the grid operator demand.

4.3 OVERALL SYSTEM CONFIGURATION

According to Figure 4.1, the considered system consists of PV array, DC-DC converter (boost), six-level NPC inverter, and R, L filter tied to the grid.

The PV arrays generate the power depending on solar radiations. The boost converter is used to track the MPP and deliver it continuously to the DC-link. The six-level NPC inverter injects the power coming from the boost converter into the grid, taking into account reactive power demanded by the grid operator.

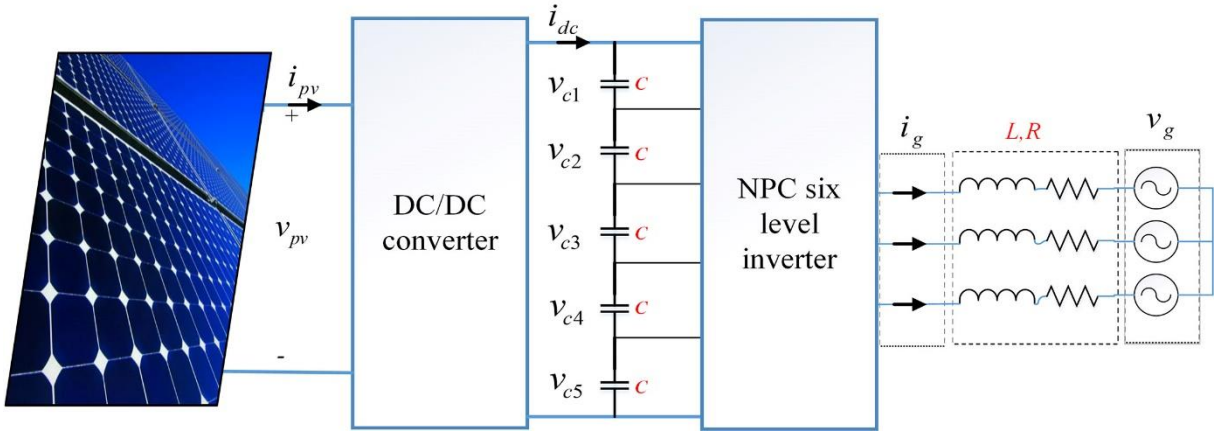

Figure 4.1: Proposed PV system configuration.

4.4 OVERALL SYSTEM CONTROL

As discussed in chapter 3, the overall system is controlled by an MPPT technique, DC-link regulator and grid-connected multilevel NPC inverter control strategy.

4.4.1 MPPT TECHNIQUE AND DC-LINK REGULATOR

In this chapter, we focus only on the development of grid-tied multilevel inverter control strategies. Therefore, the MPPT technique and the DC-link regulator are performed by conventional control schemes which are:

A) A voltage-oriented MPPT based on PI controller used in [53], is employed to track the maximum power point delivered by the PV arrays under irradiation changes.

B) A simple PI (with parameters K_i= -3.5, K_p = -0.5) is used to regulate the DC-link voltage and to generate the active power reference.

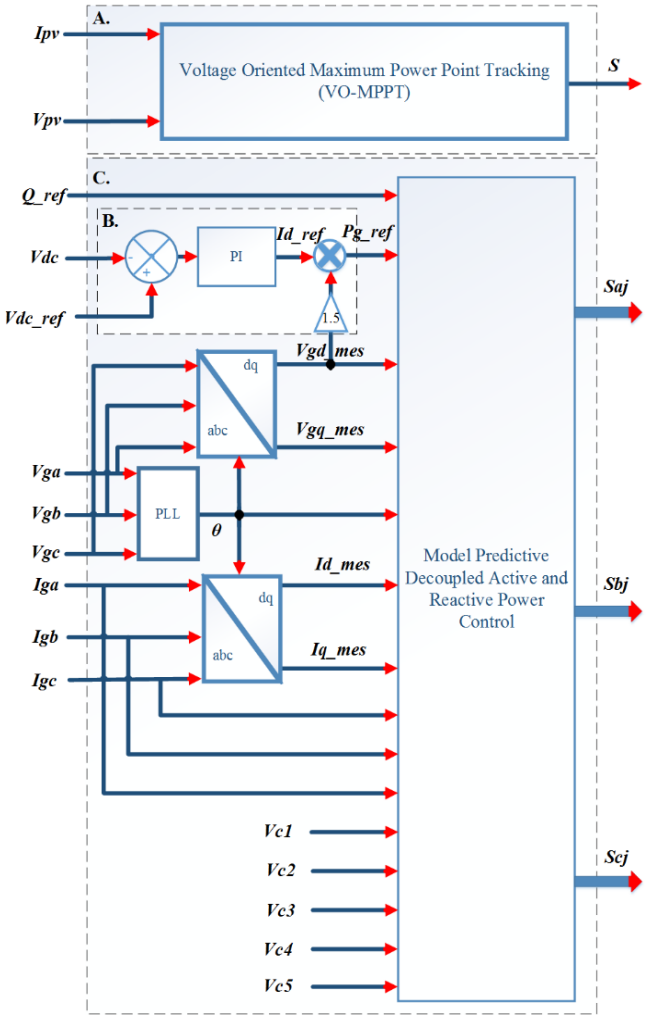

Figure 4.2: Global system control employing MPC.

4.4.2 GRID-CONNECTED MULTILEVEL INVERTER CONTROL STRATEGY

Two decoupled active and reactive power MPC strategies (MPC and O-MPC) are applied for grid-connected PV system using six-level diode-clamped inverter.

The first one is designed based on classical MPC theory whilst, the second one is optimized MPC which reduces by 57% the number of voltage vectors for prediction compared to the conventional model. The global control scheme employing MPC and O-MPC are illustrated in Figures 4.2 and 4.3 respectively. The designs of the two MPC methods are based on the discrete time model of grid-connected six-level diode-clamped inverter.

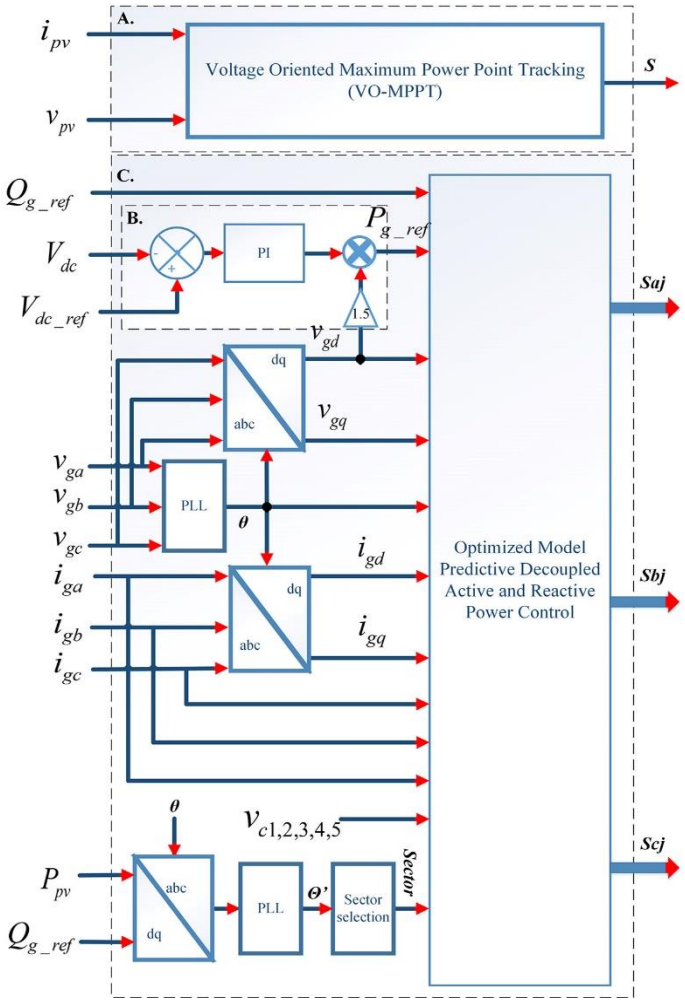

Figure 4.3: Global system control employing O-MPC.

4.5 MODELING OF GRID-CONNECTED SIX-LEVEL NPC INVERTER

A high-level NPC inverter (six-level) is employed to inject the produced PV power, in addition to reactive power following the grid operator demand with high control performance.

The six-level NPC inverter generates six voltage levels. These levels are achieved according to the switching states summarized in Table 4.1. The three phase six-level NPC inverter has a total of 216 possible switching states which produces 91 different voltage vectors, as shown in Figure 4.4. We observe that most switching states are redundant, generating the same voltage vector. However, they have different effects on the balance of the DC-link capacitor voltages [94].

TABLE 4.1: Switching states for one phase of six-level NPC inverter *(p=a, b, c)*.

Voltage levels	**Switching state**									
	S_{p1}	S_{p2}	S_{p3}	S_{p4}	S_{p5}	S_{p6}	S_{p7}	S_{p8}	S_{p9}	S_{p10}
1) V_{dc}	1	1	1	1	1	0	0	0	0	0
2) $0.8V_{dc}$	0	1	1	1	1	1	0	0	0	0
3) $0.6V_{dc}$	0	0	1	1	1	1	1	0	0	0
4) $0.4V_{dc}$	0	0	0	1	1	1	1	1	0	0
5) $0.2V_{dc}$	0	0	0	0	1	1	1	1	1	0
6) 0	0	0	0	0	0	1	1	1	1	1

According to Figure 4.4, the mathematical model of grid currents in natural frame (*abc*) can be expressed as [75]

$$\frac{di_g(t)}{dt} = \frac{1}{L}[V - v_g - Ri_g] \tag{4.1}$$

where i_g is the grid current, V the voltage vector generated by the NPC inverter, v_g the grid voltage and R, L are the filter components.

To achieve the control of active power delivered by PV system and reactive power demanded by grid operator, the above expression should be converted to synchronous frame as follows [32]

$$\begin{cases} \dfrac{di_{gd}(t)}{dt} - w_g i_{gq}(t) = \dfrac{1}{L}[-Ri_{gd}(t) - v_{gd}(t) + V_d] \\ \dfrac{di_{gq}(t)}{dt} + w_g i_{gd}(t) = \dfrac{1}{L}[-Ri_{gq}(t) - v_{gq}(t) + V_q] \end{cases} \tag{4.2}$$

where V_d and V_q represent the voltage vector components in d-q frame, which can be obtained by transformation of voltage vector from stationary to rotating frame. While w_g is the grid angular frequency.

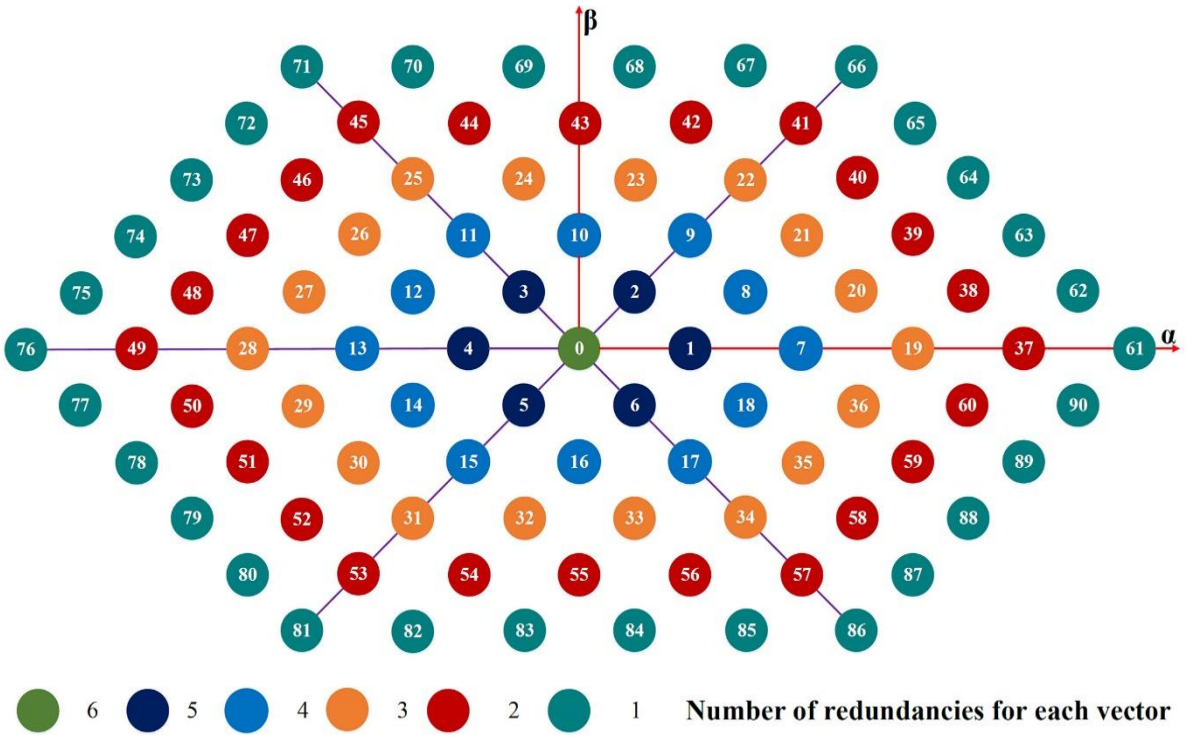

Figure 4.4: Voltage vectors for six-level NPC inverter in αβ stationary.

The DC-link capacitor voltages v_{cx} model can be described in terms of the DC-link capacitor currents i_{cx} by the following equation [28, 32]

$$\frac{dv_{cx}}{dt} = \frac{1}{C} i_{cx}, \qquad x = 1,2,3,4,5 \tag{4.3}$$

where C is the capacitor value.

As illustrated in Figure 4.5, the capacitor currents can be derived in terms of the net DC current i_{dc} and the input inverter currents i_{sx} as follows

$$\begin{cases} i_{c1} = i_{dc} - i_{s1} \\ i_{c2} = i_{dc} + i_{c1} - i_{s2} \\ i_{c3} = i_{dc} + i_{c2} - i_{s3} \\ i_{c4} = i_{dc} + i_{c3} - i_{s4} \\ i_{c5} = i_{dc} + i_{c4} - i_{s5} \end{cases} \tag{4.4}$$

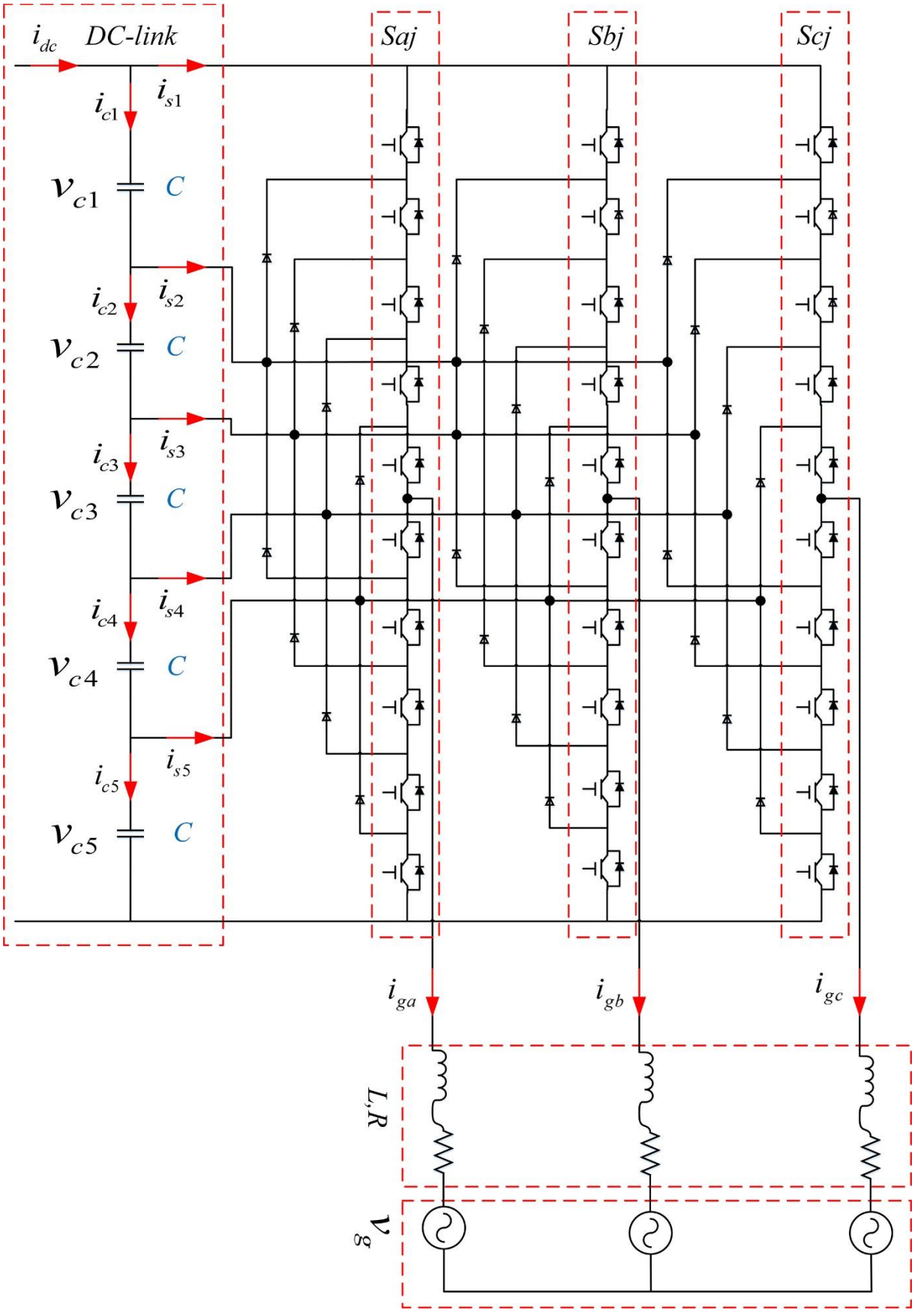

Figure 4. 5: Topology of grid-tied six-level NPC inverter.

The i_{dc} becomes null under equal energy capacitors condition, then Equation 4.4 can be rewritten as [94]

$$\begin{cases} i_{c1} = -i_{s1} \\ i_{c2} = i_{c1} - i_{s2} \\ i_{c3} = i_{c2} - i_{s3} \\ i_{c4} = i_{c3} - i_{s4} \\ i_{c5} = i_{c4} - i_{s5} \end{cases} \tag{4.5}$$

From the measured grid currents (i_{ag}, i_{bg}, and i_{cg}), the inverter input currents can be estimated as

$$\begin{cases} i_{s1} = \sum_{p=a,b,c} (S_x = 1) i_{pg} \\ i_{s2} = \sum_{p=a,b,c} (S_x = 2) i_{pg} \\ i_{s3} = \sum_{p=a,b,c} (S_x = 3) i_{pg} \\ i_{s4} = \sum_{p=a,b,c} (S_x = 4) i_{pg} \\ i_{s5} = \sum_{p=a,b,c} (S_x = 5) i_{pg} \end{cases} \tag{4.6}$$

4.6 DECOUPLED ACTIVE AND REACTIVE POWER STRATEGY FOR GRID-CONNECTED SIX-LEVEL NPC INVERTER

Depending on the classic model predictive control (MPC) proposed in [31, 76], a decoupled active and reactive power control strategy based on finite set model predictive control is proposed and applied to PV system using six level NPC inverter. The aims of the proposed control scheme are:

- Enforce the P_g to track the P_{g_ref} delivered by the DC-link voltage control.
- Enforce the Q_g to track the Q_{g_ref} demanded by the grid operator.
- Assure the balance of five DC-link capacitor voltages.

Those goals are included in the cost function which is defined as:

$$g = \left|P_{g\_ref} - P_g(k+1)\right| + \left|Q_{g\_ref} - Q_g(k+1)\right| + \lambda\left\{\sum_{j=1}^{4}\left|Vc_j(k+1) - Vc_{j+1}(k+1)\right| + \sum_{j=1}^{3}\left|Vc_j(k+1) - Vc_{j+2}(k+1)\right| + \sum_{j=1}^{2}\left|Vc_j(k+1) - Vc_{j+3}(k+1)\right| + \left|Vc_1(k+1) - Vc_5(k+1)\right|\right\} \quad (4.7)$$

where P_{g_ref} is the active power reference delivered by DC-link regulator, Q_{g_ref} is the reactive power reference demanded by the grid operator, λ is the weight factor of the DC-link capacitor voltages balance. The $P_g(k+1)$,Q_g $(k+1)$,$V_j(k+1)$ are the future behavior of active power, reactive power and DC-link capacitor voltages which demonstrated their calculation bellow.

The future behavior of active and reactive powers $P_g(k+1)$, Q_g $(k+1)$ is calculated based on the discretization of mathematical model of six-level NPC inverter tied to the grid through RL filter given in Equation 4.1. By using the Euler forward method [32], the future current $i_{gd}(k+1)$, $i_{gq}(k+1)$ can be expressed as follows

$$\begin{cases} i_{gd}(k+1) = \dfrac{T_s}{L}[-Ri_{gd}(k) - v_{gd}(k) + V_d(k)] + T_s w_g i_{gq}(k) - i_{gd}(k) \\ i_{gq}(k+1) = \dfrac{T_s}{L}[-Ri_{gq}(k) - v_{gq}(k) + V_q(k)] - T_s w_g i_{gd}(k) - i_{gq}(k) \end{cases} \quad (4.8)$$

By using Equation 4.8, the future behavior of active and reactive powers can be written as

$$\begin{cases} Pg(k+1) = 1.5 v_{gd}(k) i_{gd}(k+1) \\ Qg(k+1) = 1.5 v_{gd}(k) i_{gq}(k+1) \end{cases} \quad (4.9)$$

Using again the Euler forward method in Equation 4.3, the future behavior of DC-link capacitor voltages are given as [28, 32]

$$v_{cx}(k+1) = v_{cx}(k) + \frac{T_s}{C} i_{cx}(k) \quad (4.10)$$

From the measured grid currents and voltages in addition to the five DC-link capacitor voltages, the future behaviors of active power, reactive power and DC-link capacitor voltages are calculated for all 216 possible switching states. Then, a cost function g is evaluated for all switching states. The switching state that minimizes the cost function is selected for applying during the next sampling time. The flowchart presented in Figure 4.6 summarizes the operation of the proposed method.

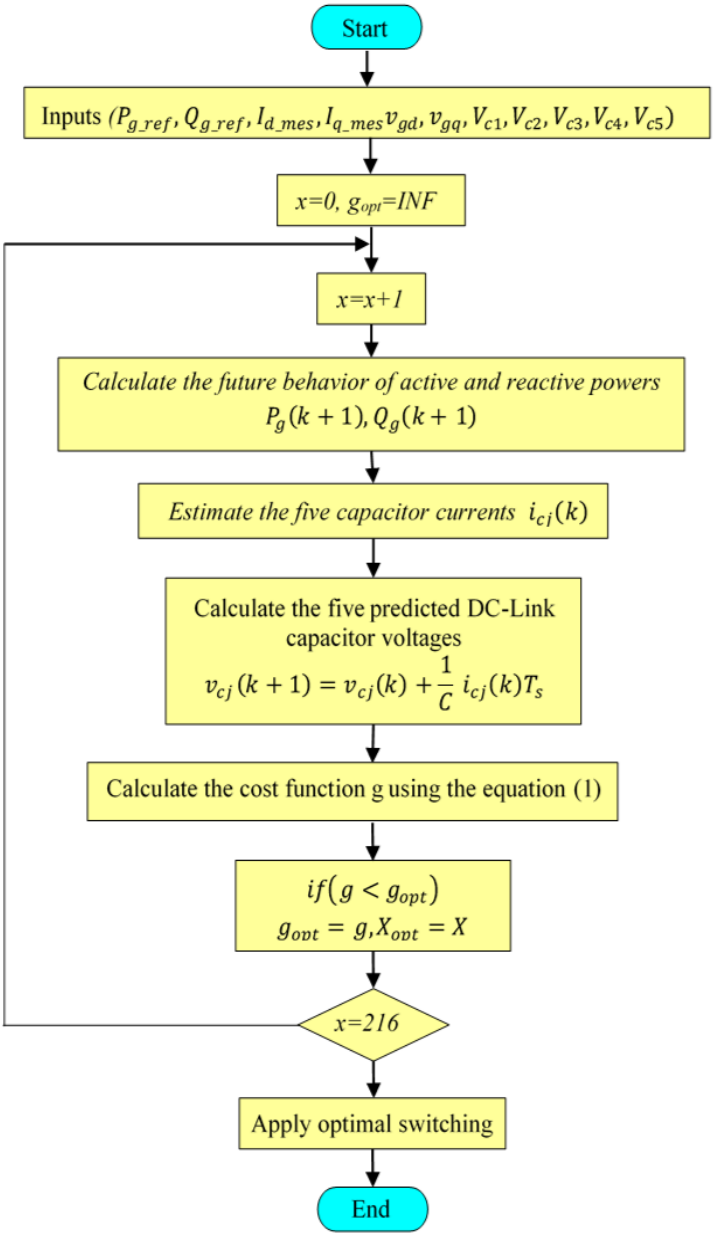

Figure 4.6: Flowchart of the model predictive control (MPC).

4.7 O-MPC DECOUPLED ACTIVE AND REACTIVE POWER STRATEGY FOR GRID-CONNECTED SIX-LEVEL NPC INVERTER

The O-MPC decoupled active and reactive power strategy is improved comparatively to MPC algorithm presented in the previous section. Where, the conventional MPC uses all the possible switching states of the inverter (216 switching possible states) for the prediction and evaluates them using a cost function. In the other hand, the proposed O-MPC uses only 94 switching possible states.

TABLE 4.2: Group of vectors for each sector.

Θ	Sector	Vectors
[0° - 60°[	1	0,1,2,7,8,9,19,20,21,22,37,38,39,40,41,61,62,63,64,65,66,6,18,36,60,90, 17,3,10,23,42,67,11
[60° - 120°[	2	0,2,3,9,10,11,22,23,24,25,41,42,43,44,45,66,67,68,69,70,71,1,8,21,40,65, 7,4,12,26,46,72,13
[120° - 180°[	3	0,3,4,11,12,13,25,26,27,28,45,46,47,48,49,71,72,73,74,75,76,2,10,24,44, 70,9,5,14,29,50,77,15
[180° - 240°[	4	0,4,5,13,14,15,28,29,30,31,49,50,51,52,53,76,77,78,79,80,81,3,12,27,48, 75,11,6,16,32,54,82,17
[240° - 300°[	5	0,5,6,15,16,17,31,32,33,34,53,54,55,56,57,81,82,83,84,85,86,4,14,30,52, 80,13,1,18,35,58,87,7
[300° - 360°[	6	0,6,1,17,18,7,34,35,36,19,57,58,59,60,37,86,87,88,89,90,61,5,16,33,56, 85,15,2,8,20,38,62,9

The O-MPC reduces the number of switching states for prediction by classifying all voltage vectors in 6 groups. Each vectors group reflects a specific sector, as presented in Table 4.2. Each group of voltage vectors must include: all the voltage vectors of the actual sector in addition to, the voltage vectors which are adjacent to the actual sector in order to confirm the achievement of control objective; whatever the change in external conditions. Every selected voltage vector should be represented by all its switching states due to the fact that, each switching state has a different effect on DC-link capacitor voltages. Regarding the previous selection conditions, the minimum number of switching state which can be selected for each sector is 94 switching states. The actual sector is selected through an optimal theta Θ' as detailed in Table 4.2. The calculation of the optimal angle Θ' is performed depending on the active and reactive power references, where the optimal Θ' equals grid angle θ in case of zero reactive reference, and different in the opposite case. From the measured grid currents and voltages in addition to the five DC-link capacitor voltages, the future behaviors of active power, reactive power and DC-link capacitor voltages are calculated for 94 switching states of the present sector. Then, a cost function *g* is evaluated. The switching state that minimizes the cost function

is selected to be applied during the next sampling time. The flowchart presented in Figure 4.7 summarizes the operation of the O-MPC.

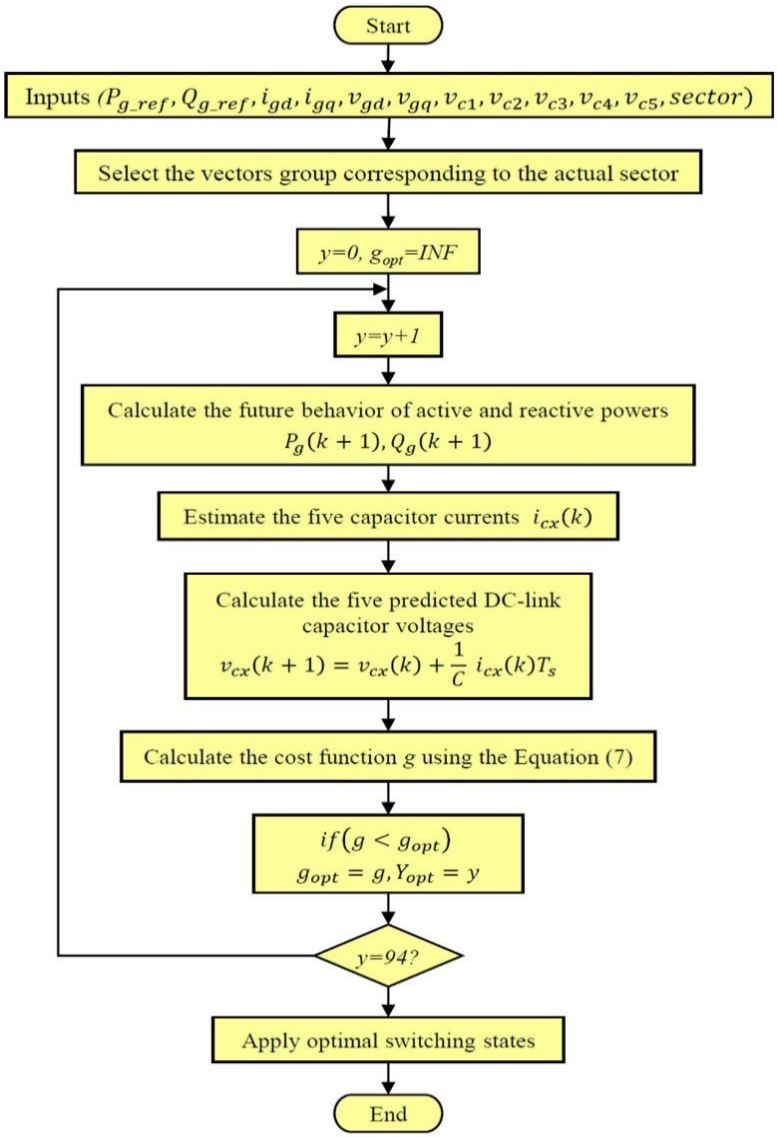

Figure 4.7: Flowchart of the optimized model predictive control (O-MPC).

4.8 RESULTS ANALYSIS

In this section, a comparison between the proposed MPC and O-MPC algorithms in grid-tied six-level NPC inverter for PV applications is performed through simulations by using Matlab/Simulink and Simpower packages. The core of the MPC, O-MPC algorithms and VO-MPPT are implemented in an embedded MATLAB function as program lines. Furthermore, the power converters are built using Simpower system toolbox components. The O-MPC algorithm is tested under step changes in irradiation and reactive power reference, in addition to different

steady state levels with the parameters detailed in Table 4.3, in order to evaluate its performance compared to MPC algorithm.

Firstly, the proposed MPC and O-MPC algorithms are tested under two sudden irradiation changes as presented in Figure 4.8(a). It is seen clearly that the PV system reaches quickly the new MPP in both cases. In addition, these changes lead to undershoot or overshoot and a small rise time in V_{dc} over its reference as shown in Figures 4.8(c) and 4.9(c). Despite that, the two MPC algorithms assure a good powers control and perfect DC-link capacitor voltages balance. Whereas, the grid currents keep their sinusoidal form. Next, the O-MPC and MPC algorithms are tested under two step changes in the reactive power reference as presented in Figures 4.8(f) and 4.9(f). The PV power output remains constant under these changes due to constant solar irradiation.

TABLE 4.3: System global parameters.

PV Siemens SM110 electrical parameters	**Value**
Maximum power (*Pmpp*)	120 *W*
Open circuit voltage (*Voc*)	42.1 *V*
Short circuit current (*Isc*)	3.87 *A*
Voltage at Pmax	33.7 *V*
Current at Pmax	3.56 *A*
Number of cells connected in parallel (*Np*)	1
Number of cells connected in series (*Ns*)	72
Number of modules connected in series (*Nss*)	36
Number of modules connected in parallel *(Npp*)	36
Boost converter electrical parameters	**Value**
Input Capacitor C_{in}	550 μF
Inductor L_b	1 *mH*
DC-link Capacitors value C_b	2200 μF
Grid electrical parameters	**Value**
Grid inductance *L*	4 *mH*
Grid resistance *R*	*0.1* Ω
Grid Peak Voltage v_g	250 *V*
Grid frequency f_g	50 *Hz*
Simulation Parameters	**Value**
MPPT sampling Time *Ts_MPPT*	1 *ms*
Predictive sampling Time *Ts*_Predictive	0.1 *ms*

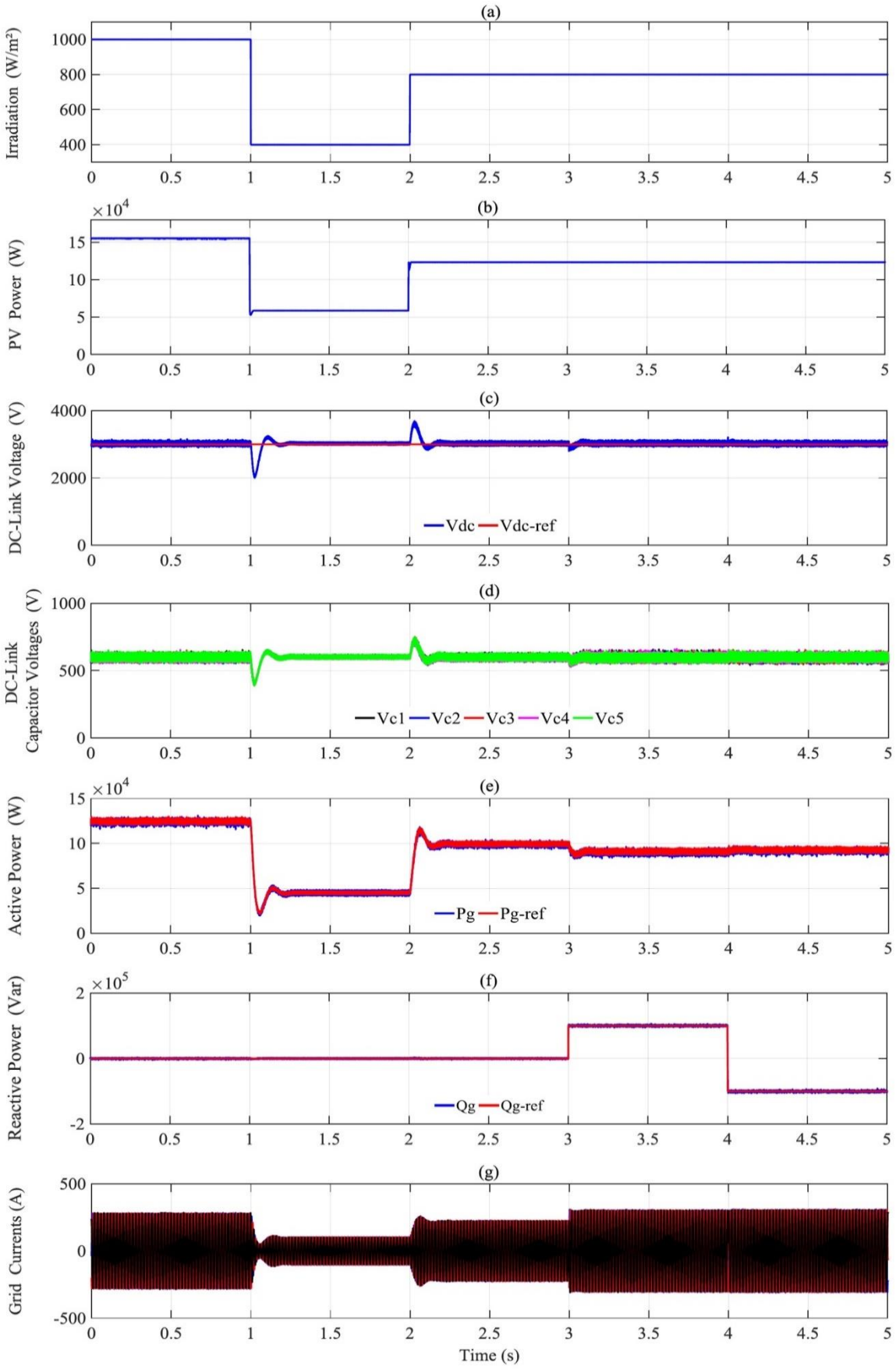

Figure 4.8: Simulation results with MPC algorithm.

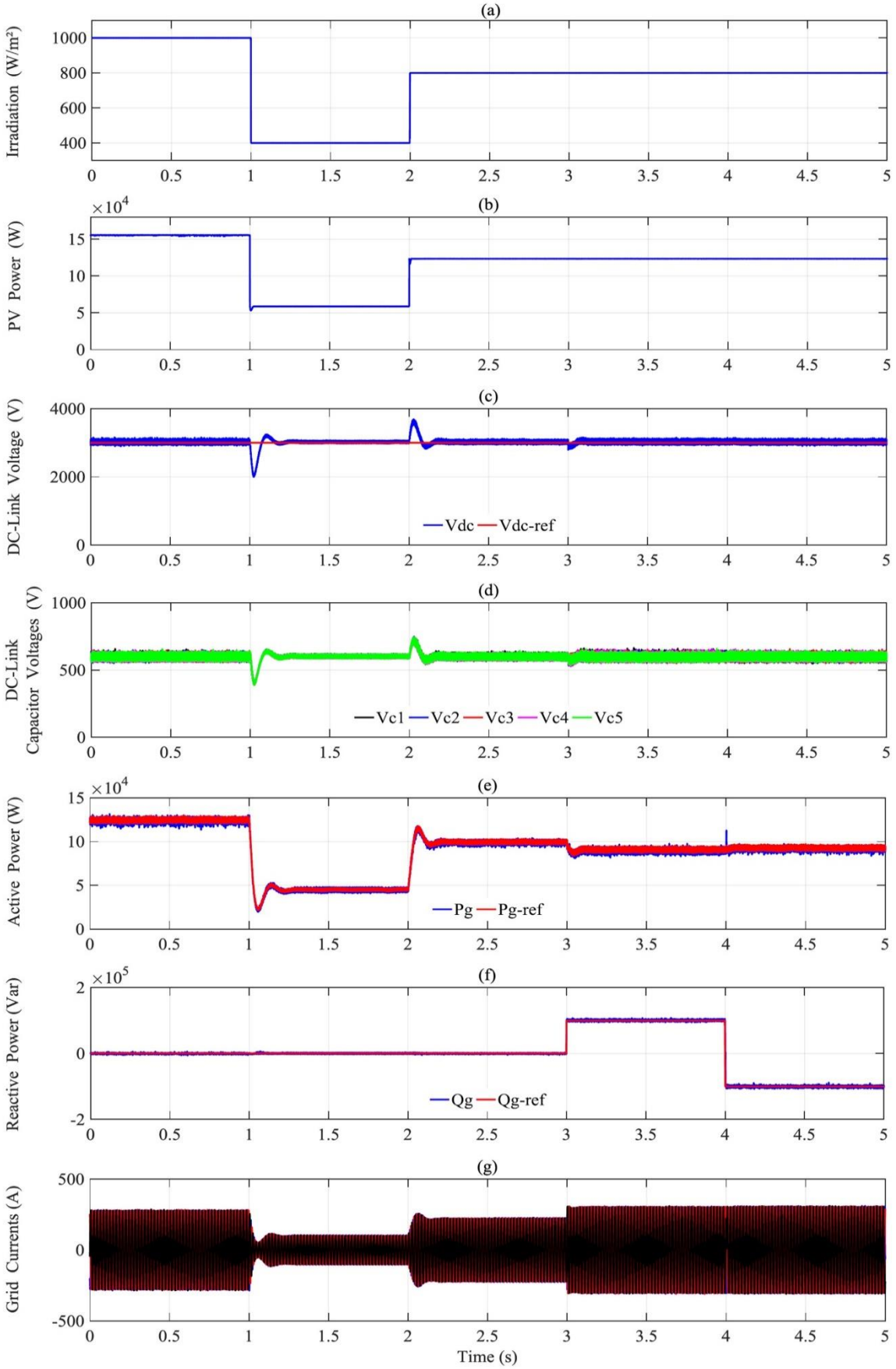

Figure 4.9: Simulation results with O-MPC algorithm.

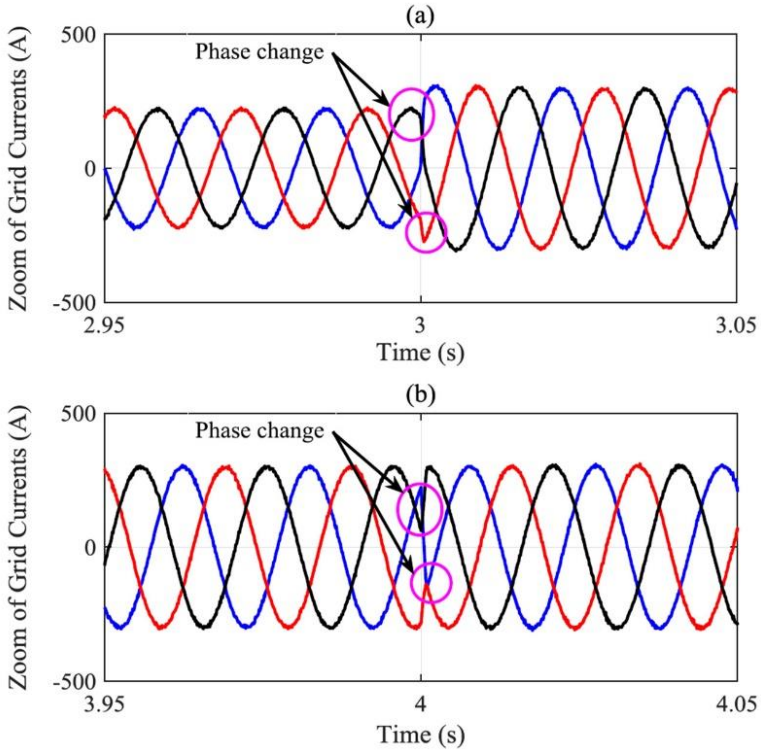

Figure 4.10: Zoom of grid currents under reactive power reference change with MPC algorithm.

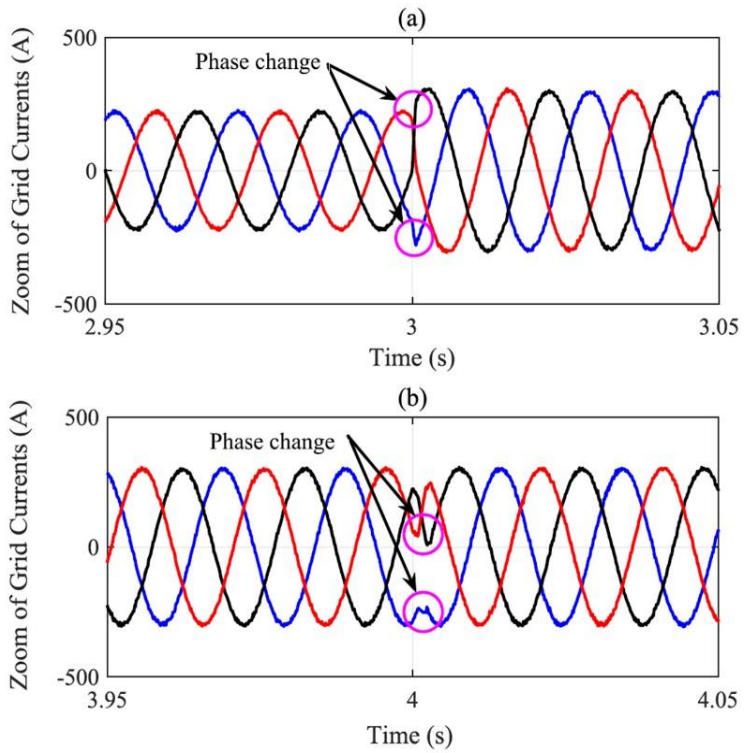

Figure 4.11: Zoom of grid currents under reactive power reference change with O-MPC algorithm.

The first step change in reactive power reference from 0 Var to 0.15 Mvar occurs at 3s, this change leads to a small undershoot in V_{dc} over its reference as shown in Figures 4.8(c) and 4.9(c). The O-MPC works like the MPC algorithm despite the phase change in grid currents which occurs when the reactive power is injected into the grid as depicted in Figures 4.10(a), 4.11(a). We note that the two MPC algorithms provide a high-power control and perfect DC-link capacitor voltages balance. Moreover, the grid currents increase rapidly due to the increase in grid apparent power S_g, where the grid current amplitude is proportional to S_g.

Afterward, at instant 4 *s*, the second step change in the reactive power reference occurs from 0.15 Mvar to -0.15 Mvar. This large change has no effect on the DC-link voltage and balance of the five DC-link capacitor voltages according to the two MPC algorithms. However, the O-MPC suffers from a small overshoot of the measured active power over its reference and a small delay to detect the new current phase as showed in Figure 4.11(b) which leads to track the reactive power reference during 3 *ms* using the O-MPC, whereas only 1.5 *ms* using the MPC algorithm.

Finally, from Figures 4.8 and 4.9 the O-MPC provides high performance during five steady state operating conditions as the MPC algorithm. Where, the active and reactive powers are completely regulated to their references as presented in Figures 4.9(f)-(g). Moreover, as shown in Figures 4.9(c)-(h), the five DC-link capacitor voltages are in perfect balance and the grid currents are balanced and sinusoidal.

According to Table 4.4, the MPC algorithm provides a high grid current quality under all solar irradiation and reactive power reference levels according to the international standards (IEEE-519, THD < 5%). Whereas, the O-MPC provides almost the same grid current quality as the MPC algorithm, which confirms the effectiveness of the two MPC algorithms.

TABLE 4.4: THD under different irradiation reactive power reference levels.

Irradiation Level	1000 W/m²	400 W/m²	800 W/m²	0.1 Mvar	-0.1 Mvar
THDi% **Proposed O-MPC**	1.04	3.15	1.26	0.94	1.09
THDi% **Proposed MPC**	0.99	3.26	1.29	0.98	1.01

4.9 REAL TIME HIL IMPLEMENTATION RESULTS

In this section, the proposed MPC and O-MPC are tested and compared through hardware in the loop (HIL) system. Where, the HIL system includes an independent control-processing unit (CPU) to run the MPC or O-MPC algorithms and real-time simulator to simulate the grid-tied six-level inverter. The communication between the simulator and CPU is assured by a communication channel [77].

The CPU receives the actual grid currents, grid voltages and DC-link capacitor voltages from the real-time simulator through the communication channel at the beginning of each sampling time. From these state variables, the CPU calculates the optimal switching state and drives it to the real-time simulator to be employed during the next sampling time.

In order to facilitate the HIL implementation, PV array, boost converter with VO-MPPT and DC-link voltage control are replaced by a battery in series with a diode. The grid-tied six-level NPC inverter and its controller parameters are identical to those used in the simulations. The real time HIL results are recorded using a 500 MHz Instek oscilloscope.

Both MPC and O-MPC algorithms are tested under several step changes in active and reactive power references where the obtained results are illustrated in Figures 4.12, 4.13, 4.15 and 4.16. In the first case, two step changes in active power reference are performed from 0.09 MW to 0.18 MW and from 0.18 MW to 0.135 MW, while the reactive power reference is set to zero. By using the two algorithms, the active power reference is well tracked as well as the error in DC-link capacitor balancing voltages E_{vc} is obtained small and around zero which confirms the perfect balancing as shown in Figures 4.12 and 4.15. Moreover, the grid currents are increased and decreased while keeping their balanced as shown in Figures 4.13 and 4.16. From that, the O-MPC algorithm provides the same performance as the MPC algorithm under this case.

In the second case, two step changes in reactive power reference are performed from 0 MVar to 0.1 MVar and from 0.1 MVar to -0.1 MVar, while the active power reference is remained at 0.135 MW.

Despite the phase change in grid currents during the first step change, the O-MPC guarantees the injection of reactive power into the grid as the MPC algorithm as well as the balance of the DC-link capacitor voltages as depicted in Figures 4.12 and 4.15. Moreover, the grid currents change the phase and increased rapidly as showing in Figures 4.14(a) and 4.17(a).

When the second change in reactive power reference is occurred, the O-MPC algorithm provides a small overshoot of the measured active power over its reference as showing in Figure 4.15. Furthermore, in contrast to the MPC algorithm, the O-MPC tracks the reactive power after a small delay as shown in Figure 4.17(b). On the other hand, this change has no effect on the five DC-link capacitor voltages balancing by employing the two MPC algorithms.

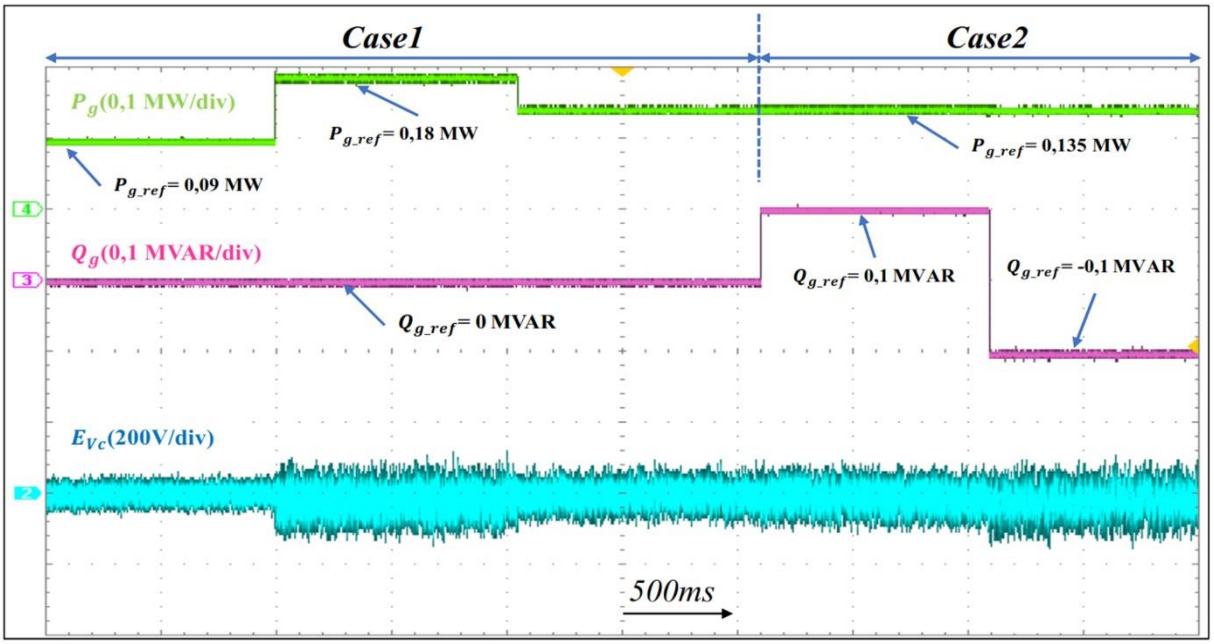

Figure 4.12: Real-time HIL results with MPC algorithm.

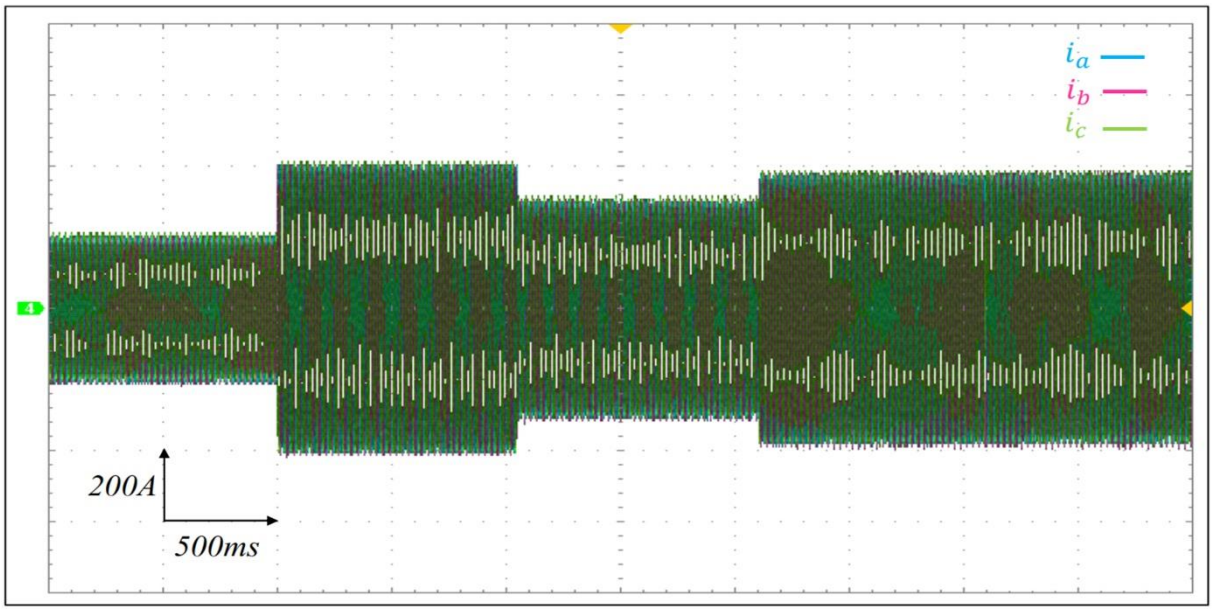

Figure 4.13: Grid currents under active and reactive power step changes with MPC algorithm.

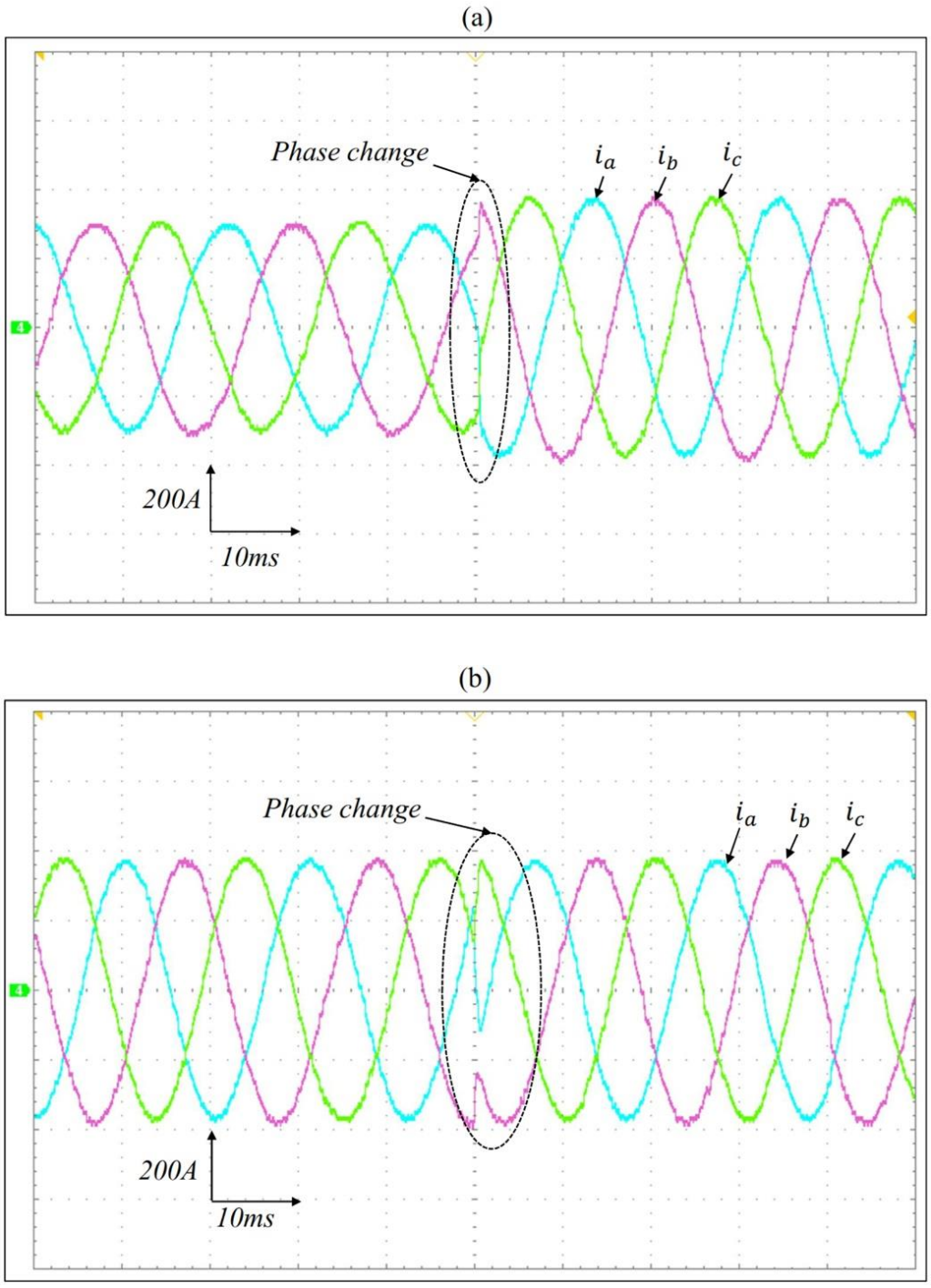

Figure 4.14: Zoom of grid currents under reactive power reference change with MPC algorithm.

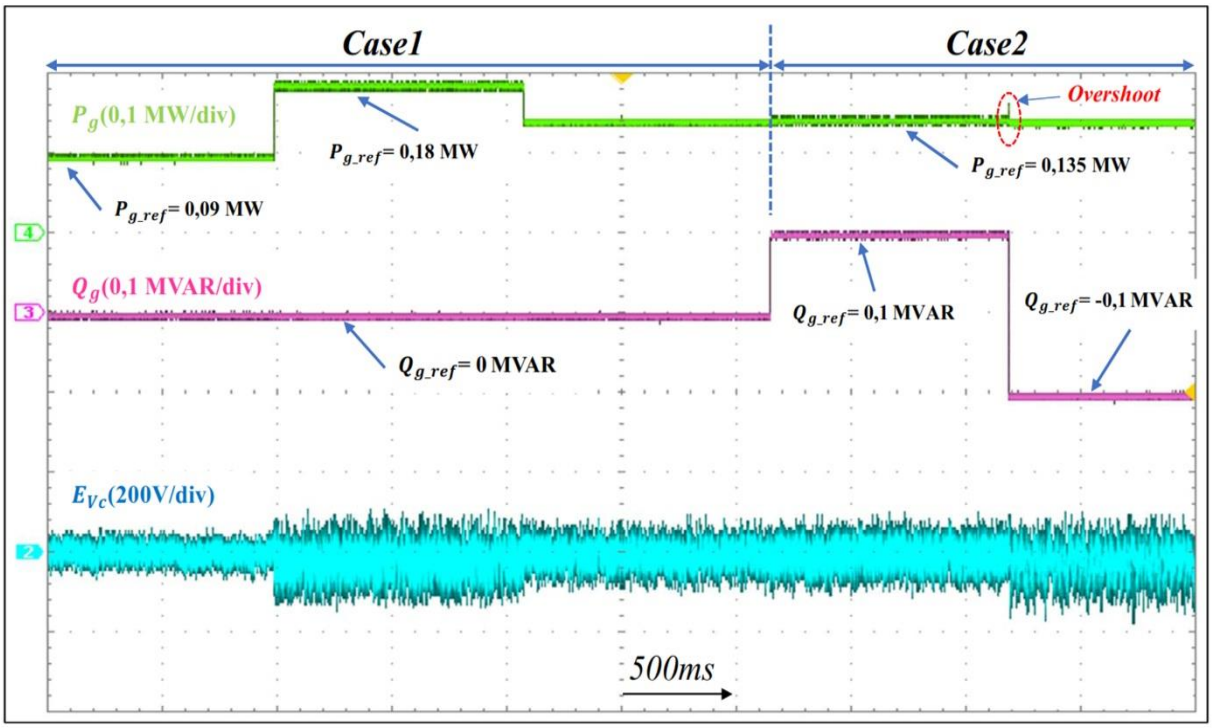

Figure 4.15: Real-time HIL results with O-MPC algorithm.

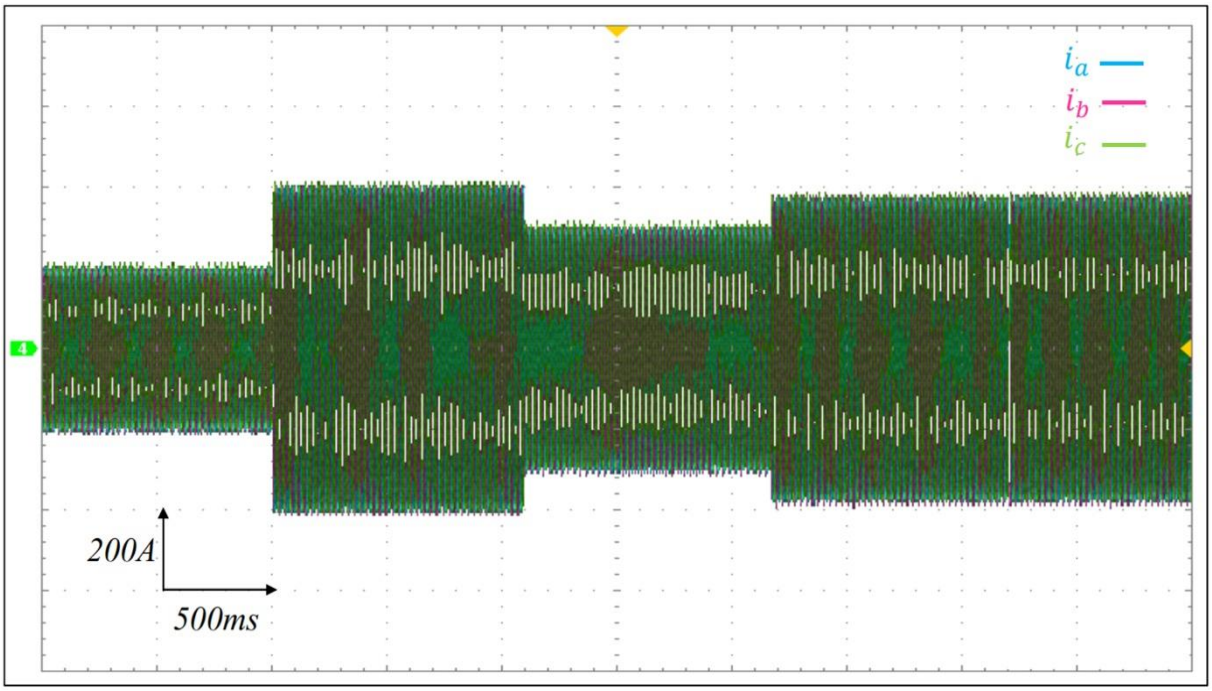

Figure 4.16: Grid current under active and reactive power step changes with O-MPC.

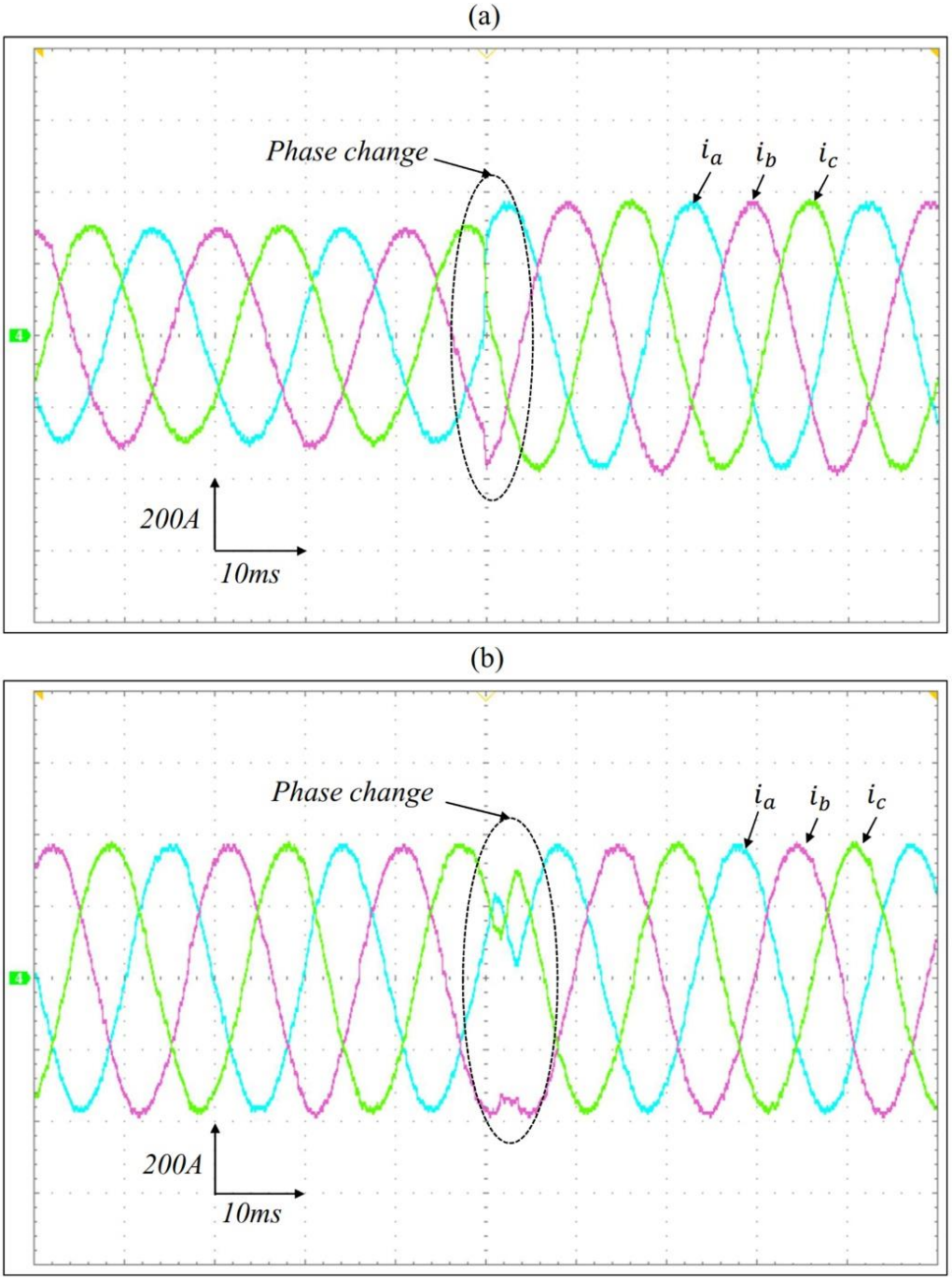

Figure 4.17: Zoom of grid currents under reactive power reference change with O-MPC.

The grid currents quality obtained by employing the two MPC algorithms under all active and reactive power reference levels is summarized in Table VI. From this comparison, we can note that the O-MPC provides almost the same grid current quality under all active and reactive power reference levels as the conventional MPC. This current quality is in compliance with the international standards (IEEE-519, THD < 5%), which confirms the effectiveness of the two proposed algorithms.

TABLE 4.5: THD under different irradiation reactive power reference levels.

Active and reactive power reference Level	0.09 MW & 0 Mvar	0.18 MW & 0 Mvar	0.135 W & 0 Mvar	0.1 Mvar & 0.135 MW	-0.1 Mvar & 0.135 MW
THDi % Proposed O-MPC	4.32	2.12	2.53	2.19	2.27
THDi % Proposed MPC	4.37	2.08	2.59	2.18	2.23

On the other hand, the average execution time for the proposed O-MPC algorithm and the MPC algorithm is measured when the two algorithms are coded in C language and implemented using dSPACE DS1104 R&D controller board with ControlDesk. The required average execution time for the O-MPC is 37.2 μs. However, the MPC has required 83.62 μs. Hence, the average execution time is reduced by 43% by using the O-MPC compared to MPC algorithm.

4.10 CONCLUSION

Control of grid-tied PV system using multilevel NPC inverter based on FCS-MPC has been proposed in this chapter. Where, a decoupled active and reactive power model predictive (MPC) and an optimized model predictive decoupled active and reactive power control (O-MPC) has been employed for grid-tied PV system using six-level NPC inverter. The O-MPC aims to inject the active power generated by the PV system and reactive power demanded by the network operator as well as guarantees the balance of the DC-link capacitor voltages as the MPC algorithm. In addition, the O-MPC decreases the computational burden by reducing the number of voltage vectors for prediction by 57% compared to the MPC algorithm. Despite this reduction of computational burden, the obtained simulation and real-time HIL implementation results prove that the O-MPC as the MPC algorithm, achieved high performance of power control and perfect DC-link capacitor voltages balance under sudden changes in the solar irradiation and reactive power reference and steady state operating conditions. Moreover, the grid current quality of the O-MPC at different solar irradiation and reactive power reference levels is almost the same as the MPC algorithm.

Chapter 5

Finite Control Set Model Predictive Control for Large-Scale Grid-Connected Photovoltaic Systems using High-Level NPC-Inverter

5.1 INTRODUCTION

In medium and high power rang, Multi-MPPTs with centralized inverter topology significantly contribute to the worldwide solar energy development and penetration in order to enhance the energy harvesting from the PV arrays and to inject the produced PV power into the grid with high grid current quality [95-100]. This category of large-scale PV systems has a two conversion stages, the first stage contains a number of PV arrays, each one connected to an individual DC-DC converter (usually boost converter). While, a centralized high-level NPC inverter tied to the grid is employed as a second conversion stage. Each DC-link capacitor input of the NPC inverter is connected to the output of one DC-DC boost converter. The PV arrays are divided into a number of subsections, where each one has an autonomous maximum power point tracking (MPPT) to provide more advanced capabilities in the harvesting of the PV power under climatic changes. In addition, the centralized high-level NPC inverter uses the

semiconductor switches connected in series, which allow the operation at higher DC voltages. However, Multi MPPTs with centralized high-level NPC inverter topology possess major weaknesses, which are: bad MPP tracking under sudden irradiation changes which reduces the energy harvesting capability, unbalancing capacitor potential of DC-link voltage, complexity and hard implementation of the control design [95-100].

In this context, the present chapter offers a simple and effective controller for Multi-MPPTs with centralized high-level NPC inverter topology based on finite control set model predictive control (FCS-MPC) strategy. A voltage oriented maximum power point tracking (VO-MPPT) performed by FCS-MPCC is applied for each boost converter to draw the maximum power point from each PV array. In addition, a FCS-MPC controller is proposed to control the centralized five-level NPC inverter connected to the grid. The main goals of the proposed controller are to achieve a good performance of the MPP tracking under sudden irradiation changes, assure the balance of the four DC-link capacitor voltages whatever the difference between extracted powers of each PV system unit, inject the reactive power on demand, and minimize the switching frequency of the five-level NPC inverter. The proposed control scheme is evaluated versus the conventional control scheme based on PI regulators through Matlab/Simulink and Simpower packages simulations.

5.2 STATE OF THE ART OF LARGE SCALE GRID-CONNECTED PV SYSTEM CONTROLLERS

To improve the energy harvesting capability, many conventional MPPT techniques can be employed such as: fractional short-circuit current and open-circuit voltage [101-102], perturbation and observation (P&O) [103] and incremental conduction (IncCon) [3, 71]. However, these tracking methods possess undesirable drawbacks which are the insufficient MPP tracking accuracy, slow response and large fluctuations at the MPP. Recently, several modifications have been introduced to the conventional MPPT algorithms by using artificial intelligence techniques such as fuzzy logic [104, 105], neural networks [106, 107] and neuro-fuzzy [46] in order to overcome the precedent drawbacks. But, the application of these techniques in large systems will make the global system control hard to be implemented practically. Furthermore, other research works are focused on the development of MPPT without using the artificial intelligence techniques such as voltage oriented loop (VO-MPPT) [108] and current oriented loop (CO-MPPT) [57-59]. The VO-MPPT presents a fast MPP tracking under sudden irradiation change. But it shows an inaccurate tracking, particularly

under step decrease in the irradiation and a significant power oscillation in steady-state. The CO-MPPT affords in addition to an accurate tracking, an important oscillation reduction at the MPP. This technique is performed by using several current control techniques such as conventional PI [57], predictive [58, 59] and sliding mode [60] current controllers. The CO-MPPT reached slowly the new MPP under sudden irradiation change in contrast to the VO-MPPT. The authors in [73] proposed a modified VO-MPPT by adding a fast-current controller loop in order to enhance the tracking performance especially under step changes in irradiation. As results, this strategy achieved high performance tracking in dynamic and steady states in comparison with conventional MPPTs.

On the other side, two traditional control categories are suggested and available in the literature dedicated to the centralized high-level NPC grid-tied inverter. The first one is the control methods without modulation stage such as: direct power control (DPC) [80, 81] and virtual flux direct power control (VF-DPC) [82] based on switching table. In high-level inverter cases (three-level and more), the complexity of switching table design is increased. Furthermore, the obtained control performance by applying these methods are not considered as of high quality. While, the second category represents the control methods with modulation stage such as: voltage-oriented control (VOC) [83], Voltage-based direct power control (V-DPC) [84], Virtual flux oriented control [83]. These techniques employ an internal current loop based on PI controller in addition to a pulse width modulation (PWM) or space-vector modulation (SVM) stage [28, 32]. The DC-link capacitor voltages balance must be included in the design of the modulation stage which makes it more complicated. Moreover, the PI controller weaknesses and control delay will reduce the system performance.

Nowadays, FCS-MPC strategy is widely engaged in power electronics converters control due to its simplicity in control design as well as in experimental implementation [31-32, 109-110]. This technique offers the ability to add nonlinearities and constraints in the design of the controller and removes the need for PI controllers and modulation stage. In renewable energy system applications, FCS-MPC strategy has been emerged for different systems such as: stand-alone systems [58, 59] and grid-connected systems [30-32, 85-90]. As presented in [58-59, 30-32, 85-90], whatever the purposes for which the FCS-MPC has been applied, a high performance control is achieved in comparison to the conventional methods. To control complicated PV systems, especially those based on high-level NPC inverters, FCS-MPC is selected as the best solution between the other control methods. Where, it is easy to be designed

and implemented practically. Furthermore, it is easy to include the DC-link capacitor voltages balancing in the objective control.

5.3 OVERALL SYSTEM CONFIGURATION AND MODELLING

As shown in Figure 5.1, the global system consists of the following components: four subsection PV arrays, four DC-DC boost converters, five-level NPC inverter, and R_g, L_g filter tied to the grid.

The four PV array subsections generate the power depending on solar irradiations. While, each one of the four DC-DC converters is tied to one PV subsection, they are used to extract the MPP by operating their switches through an individual MPPT technique. Centralized five level NPC inverter is connected to the grid through R_g, L_g filter, to inject the produced PV power, as well as, the demanded reactive power into the grid with high grid current quality.

The design of FCS-MPC controllers for large-scale grid connected PV system using high-level NPV inverter is based on the discrete time model of power converters. For this reason, the mathematical model of DC-DC boost converter and the centralized five level NPC inverter connected to the grid are presented in this chapter.

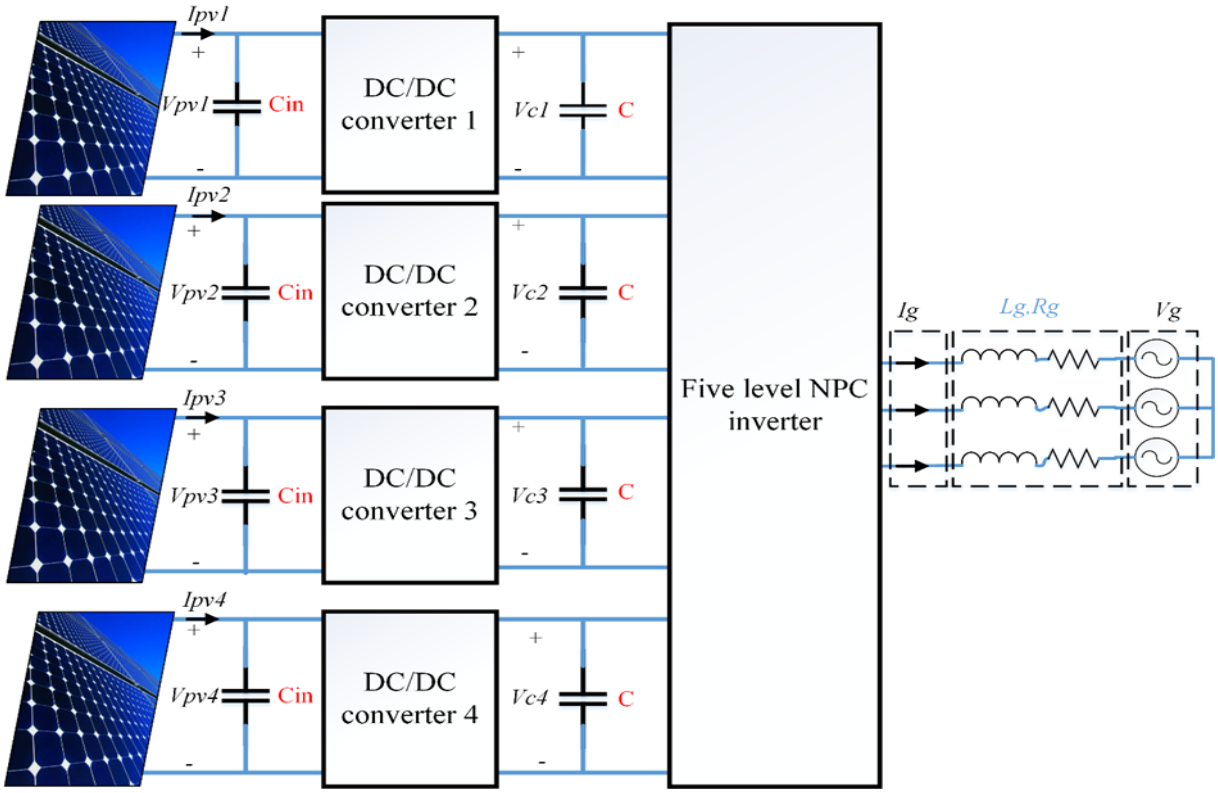

Figure 5.1: Proposed PV system configuration.

5.3.1 DC-DC BOOST CONVERTER MODEL

The boost converter is the most DC-DC converter used in grid-connected PV systems, it allows to track the maximum power point and to elevate the PV voltage to a value higher than the peak of the grid voltage, then allowing the injection of the produced PV power into the grid. The equivalent circuit of the boost converter during two switching intervals is shown in Figure 5.2, in case of continuous mode.

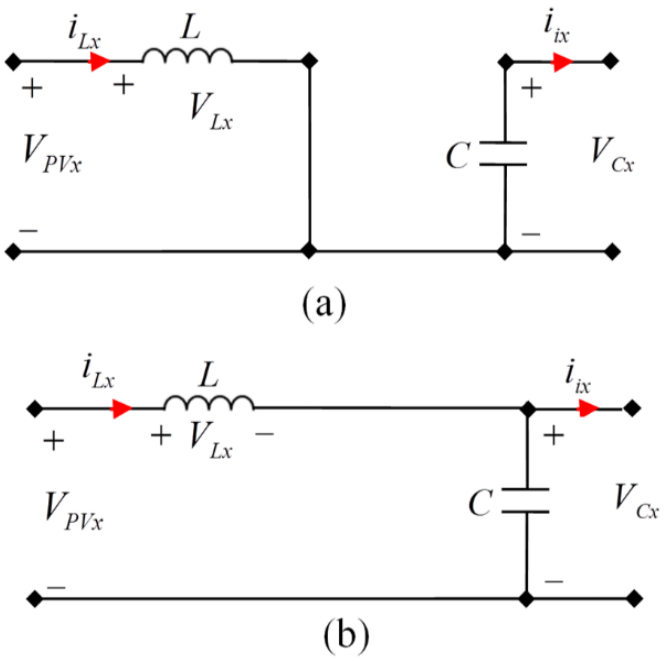

Figure 5.2: Equivalent DC-DC boost converter circuits (a) switch on (b) switch off.

When the switch is ON, the boost converter can be described as follows:

$$\begin{cases} L\dfrac{di_{Lx}(t)}{dt} = v_{pvx}(t) \\ C\dfrac{dv_{cx}(t)}{dt} = -i_{ix}(t) \end{cases} \tag{1}$$

When the switch is OFF, the boost converter equations yield:

$$\begin{cases} L\dfrac{di_{Lx}(t)}{dt} = v_{pvx}(t) - v_{cx}(t) \\ C\dfrac{dv_{cx}(t)}{dt} = i_{Lx}(t) - i_{ix}(t) \end{cases} \tag{2}$$

Equations 1 and 2 can be rewritten in term of boost switch control s as:

$$\begin{cases} L\dfrac{di_{Lx}(t)}{dt} = -(1-s)v_{pvx}(t) - v_{cx}(t) \\ C\dfrac{dv_{cx}(t)}{dt} = (1-s)i_{Lx}(t) - i_{ix}(t) \end{cases} \quad (3)$$

By approximating the derivatives in Equation 3 using Euler forward method presented in [45], the discrete time model of DC-DC boost converter considering the sampling frequency *Ts*, is given as follows [59-58]:

$$\begin{cases} i_{Lx}(k+1) = \dfrac{T_s}{L}((s-1)v_{pvx}(k) - v_{cx}(k)) + i_{Lx}(k) \\ v_{cx}(k+1) = \dfrac{T_s}{C}((1-s)i_{pvx}(k) - i_{ix}(k)) + v_{cx}(k) \end{cases} \quad (4)$$

5.3.2 GRID-TIED CENTRALIZED FIVE LEVEL NPC INVERTER MODEL

The circuit of five-level inverter NPC connected to the grid through an inductive filter L_g with a parasitic resistor R_g is shown in Figure 5.3. The objective of this inverter is to inject into the grid the generated PV power in addition to the demanded reactive power with high grid current quality. For this reason, DC-link voltage V_{dc}, DC-link capacitor voltages v_{cx} and the $i_{gd} - i_{gq}$ currents are considered to be controlled by the inverter. The switching states which generate the five-level voltage at the inverter output in single phase is presented in Table 5.1. For three phases, the five-level NPC inverter generates 125 switching states which give 61 voltage vectors, as illustrated in Figure 5.3.

TABLE 5.1: Switching states for one phase of five level NPC inverter.

Voltage levels	**Switching state**							
	S_{1x}	**S_{2x}**	**S_{3x}**	**S_{4x}**	**S_{5x}**	**S_{6x}**	**S_{7x}**	**S_{8x}**
a) V_{dc}	1	1	1	1	0	0	0	0
b) $3V_{dc}/4$	0	1	1	1	1	0	0	0
c) $V_{dc}/2$	0	0	1	1	1	1	0	0
d) $V_{dc}/4$	0	0	0	1	1	1	1	0
e) 0	0	0	0	0	1	1	1	1

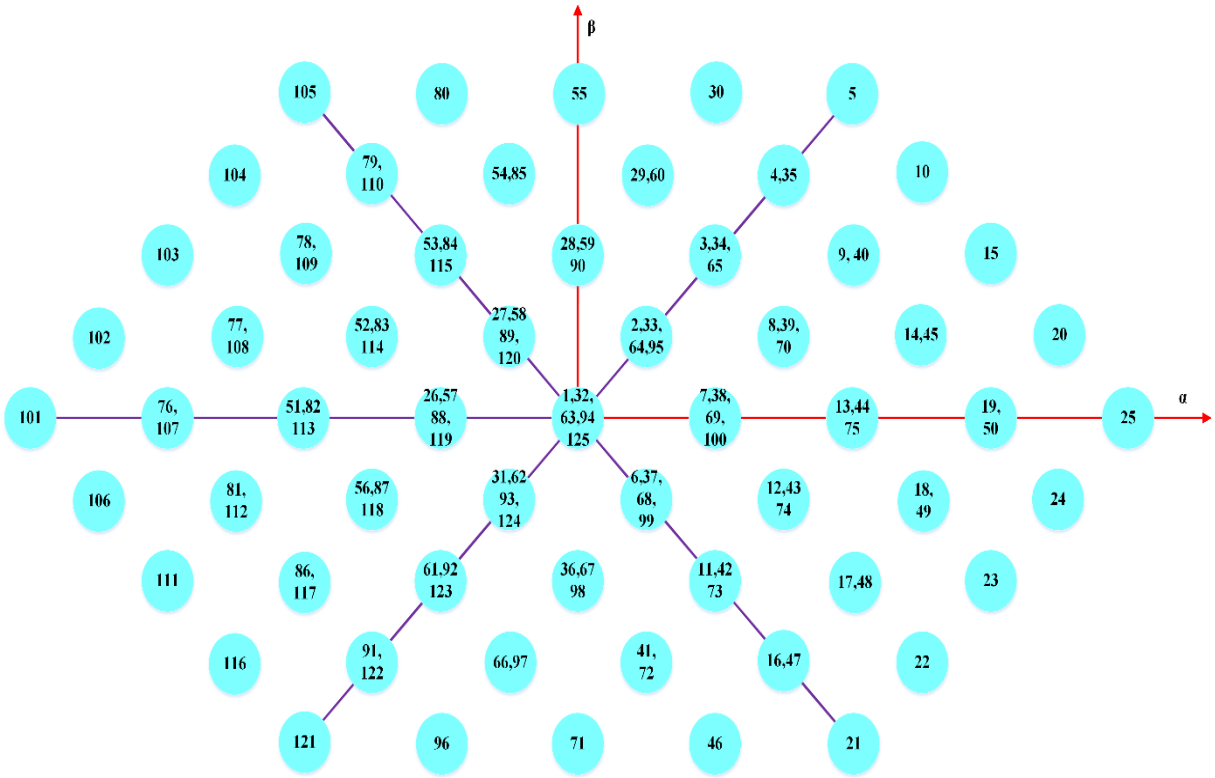

Figure 5.3: Switching states for five level inverter NPC in αβ stationary.

A. Modelling of grid currents in synchronous frame

From Figure 5.4, the mathematical model of grid currents in natural frame abc can be expressed as [86]:

$$\frac{di_g(t)}{dt} = \frac{1}{L}[V - v_g - Ri_g] \tag{5}$$

Where i_g is the grid current, V is the voltage vectors generated by five-level NPC inverter, v_g is the grid voltage and R_g, L_g are the filter value parameters.

From Equation 5, the grid tied inverter model in rotating frame d-q can be defined as [28]:

$$\begin{cases} \dfrac{di_{gd}(t)}{dt} - wi_{gq}(t) = \dfrac{1}{L}[-Ri_{gd}(t) - v_{gd}(t) + V_d] \\ \dfrac{di_{gq}(t)}{dt} + wi_{gd}(t) = \dfrac{1}{L}[-Ri_{gq}(t) - v_{gq}(t) + V_q] \end{cases} \tag{6}$$

Where V_d and V_q are the voltage vectors generated by the inverter in rotating axis d-q respectively, which can be obtained by the conversion of voltage vectors in stationary frame α-β illustrated in Figure 5.3 to rotating frame d-q.

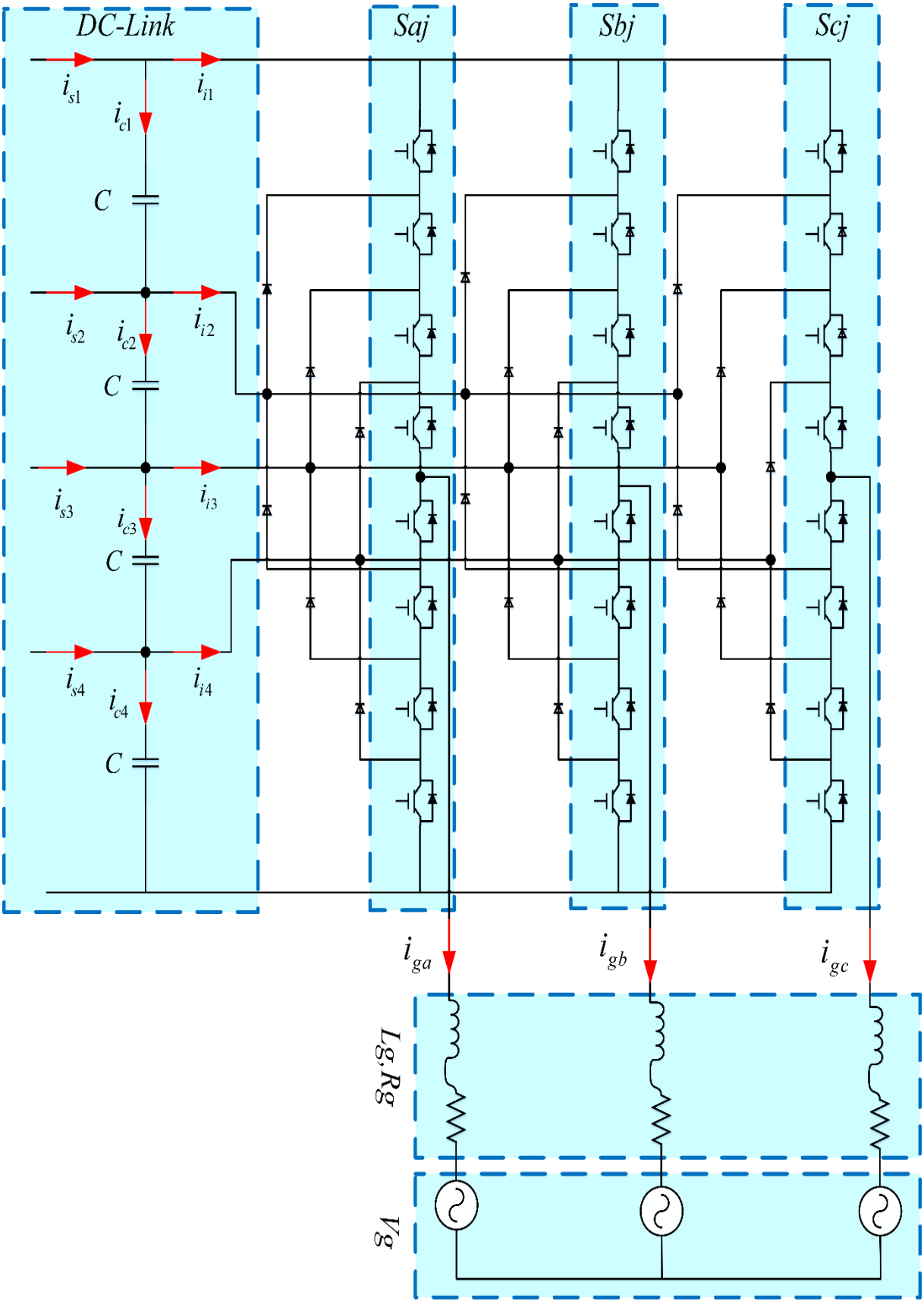

Figure 5.4: Topology of grid-tied five-level NPC inverter.

By using Euler forward method, the discrete time model of Equation 6 yields [28]:

$$\begin{cases} i_{gd}(k+1) = \dfrac{T_s}{L}[-Ri_{gd}(k) - v_{gd}(k) + V_d(k)] + T_s w i_{gq}(k) - i_{gd}(k) \\ i_{gq}(k+1) = \dfrac{T_s}{L}[-Ri_{gq}(k) - v_{gq}(k) + V_q(k)] - T_s w i_{gd}(k) - i_{gq}(k) \end{cases} \tag{7}$$

B. Modelling of DC-link capacitor voltages

The DC-link capacitor voltages model can be defined in terms of the DC-link capacitor currents i_{sx} by the following equation [86]:

$$\frac{dv_{cx}}{dt} = \frac{1}{C} i_{cx} \tag{8}$$

where C is capacitor value.

As shown in Figure 5.4, the capacitor currents can be expressed as [28, 32]:

$$\begin{cases} i_{c1} = i_{s1} - i_{i1} \\ i_{c2} = i_{s2} + i_{c1} - i_{i1} \\ i_{c3} = i_{s3} + i_{c2} - i_{i2} \\ i_{c4} = i_{s4} + i_{c3} - i_{i4} \end{cases} \tag{9}$$

Under equal energy among the capacitors condition, the i_{sx} currents become null and Equation 9 can be rewritten as [28, 32]:

$$\begin{cases} i_{c1} = -i_{i1} \\ i_{c2} = i_{c1} - i_{i1} \\ i_{c3} = i_{c2} - i_{i2} \\ i_{c4} = i_{c3} - i_{i4} \end{cases} \tag{10}$$

The current i_{ix} can be described in terms of the actual grid currents and switching inverter control S_{xy} as:

$$\begin{cases} i_{i1} = \sum\limits_{x=a,b,c} (S_x = 1) i_{xg} \\ i_{i2} = \sum\limits_{x=a,b,c} (S_x = 2) i_{xg} \\ i_{i3} = \sum\limits_{x=a,b,c} (S_x = 3) i_{xg} \\ i_{i4} = \sum\limits_{x=a,b,c} (S_x = 4) i_{xg} \end{cases} \tag{11}$$

From Equation 8, the discrete time model of DC-link capacitor voltages can be expressed as follows [28]:

$$v_{cx}(k+1) = v_{cx}(k) + \frac{T_s}{C} i_{cx}(k) \tag{12}$$

5.4 PROPOSED SYSTEM CONTROL

The large-scale grid-connected PV system using high-level NPC inverter topology discussed in this chapter is controlled by three controllers:

1) A VO-MPPT based on FCS-MPCC is employed to track the maximum power point delivered by the PV system under sudden irradiation change.

2) A simple PI with gains (k_i, k_p) is used to control the DC-link voltage and generate the i_{gd} current reference.

3) A FCS-MPC controller is proposed to control the grid-tied centralized five-level NPC inverter.

5.4.1 INDIVIDUAL MAXIMUM POWER POINT TRACKING

The basic idea of the individual MPPT is to take profit of the fast current tracking capability of the current loop in addition to the fast tracking of MPP voltage under sudden irradiation changes. As shown in Figure 5.5, the MPPT control scheme is based on the integration of the FCS-MPCC with a PI compensator and IncCon voltage MPPT technique. Where, the error between the MPP tracker voltage reference and actual PV voltage entering through PI compensator in order to estimate the current error i_{vx}. This latter is added to the actual PV current in order to estimate the current inductor reference i_{Lx_ref}, while the role of FCS-MPCC is to regulate the inductor current to its reference.

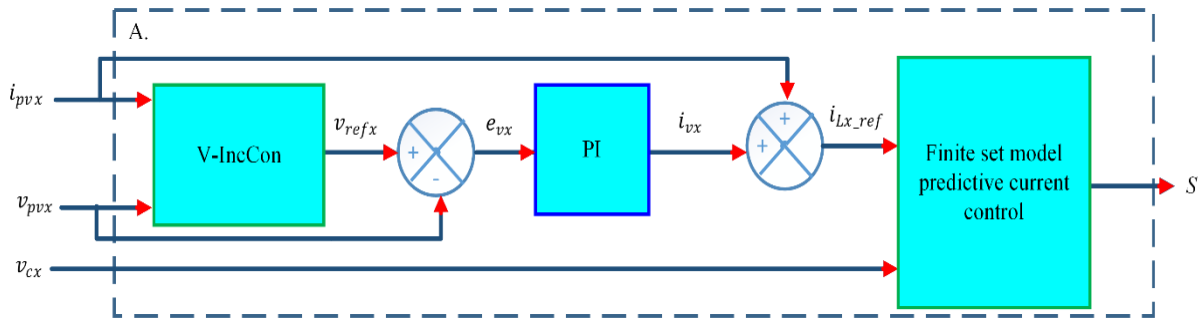

Figure 5.5: The proposed MPPT control.

A. IncCon voltage algorithm

The incremental voltage algorithm (V-IncCon) is based on the slope of the PV power curve. It identifies the instantaneous position value to the maximum power point; zero at the MPP, positive on the left-hand side of the MPP and negative on the right-hand side of the MPP. The basic equations of this method are given as follows [3, 108]:

$$\frac{dP_{pvx}}{dv_{pvx}} > 0 \qquad \text{at left of MPP} \tag{13}$$

$$\frac{dP_{pvx}}{dv_{pvx}} < 0 \qquad \text{at right of MPP} \tag{14}$$

$$\frac{dP_{pvx}}{dv_{pvx}} = 0 \qquad \text{at MPP} \tag{15}$$

Since

$$\frac{dP_{pvx}}{dv_{pvx}} = \frac{d(v_{pvx} * i_{pvx})}{dv_{pvx}} = \frac{di_{pvx}}{dv_{pvx}} v_{pvx} + i_{pvx} \tag{16}$$

Equation 16 can be expressed as:

$$\frac{di_{pvx}}{dv_{pvx}} > -\frac{i_{pvx}}{v_{pvx}} \qquad \text{at left of the MPP} \tag{17}$$

$$\frac{di_{pvx}}{dv_{pvx}} < -\frac{i_{pvx}}{v_{pvx}} \qquad \text{at right of the MPP} \tag{18}$$

$$\frac{di_{pvx}}{dv_{pvx}} = -\frac{i_{pvx}}{v_{pvx}} \qquad \text{at the MPP} \tag{19}$$

As illustrated in the flowchart presented in Figure 5.6, the objective is to adjust the PV voltage reference v_{ref} even equals to v_{MPP} by a comparison between the instantaneous conductance (I/V) and incremental conductance (ΔI/ΔV) [3].

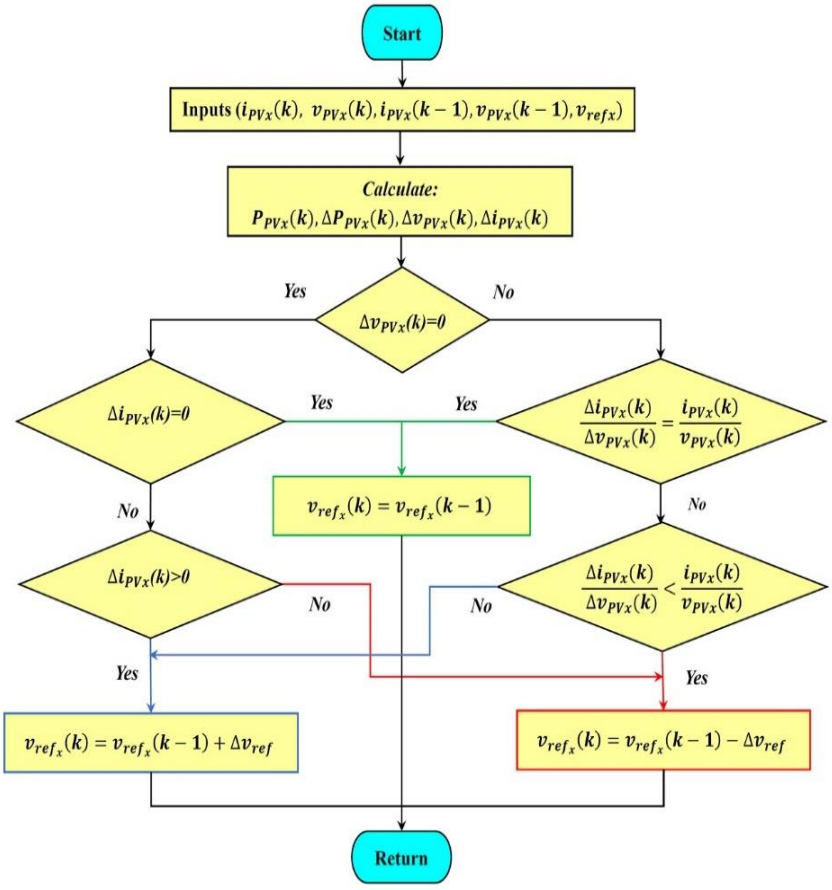

Figure 5.6: Flowchart of IncCon voltage algorithm.

B. PI compensator design

In order to estimate the reference inductor current i_{Lx_ref}, as expressed in Equation 20, the error signal e_{vx} between the voltage reference delivered by V-IncCon and the measured PV voltage v_{pvx}, is considered as input of a PI compensator with the transfer function $G_v(s)$ described in Equation 21. As a result, the current error signal i_{vx} is obtained and added to the measured PV current i_{pvx}.

$$i_{Lx\_ref} = i_{pvx} + i_{vx} \tag{20}$$

$$G_v(s) = k_p + \frac{k_i}{s} \tag{21}$$

The proper calculation of the PI compensator gains ensures high performance control. This calculation is based on the transfer function of the system $v_{pvx}(s)/v_{refx}(s)$. Regarding the transfer function between the PV voltage and the current error signal i_{vx} in addition to the voltage error e_{vx} given as [60, 73]

$$\frac{v_{pvx}(s)}{i_{vx}(s)} = -\frac{1}{C_{in}s} \tag{22}$$

$$e_{vx}(s) = (v_{refx}(s) - v_{pvx}(s)) \tag{23}$$

where C_{in} is the capacitor input of each boost converter.

The closed loop transfer function $v_{pvx}(s)/v_{refx}(s)$ of the system can be written as [60, 73]:

$$T(s) = \frac{v_{pvx}(s)}{v_{refx}(s)} = \frac{k_p s + k_i}{C_{in}s^2 + k_p s + k_i} \tag{24}$$

The transfer function T(s) is a second order transfer function with a damping ratio $\zeta = k_p/2C_{in}\omega_n$ and $\omega_2 = k_i/C_{in}$. Thus, the parameters of the PI compensator can be designed as follows [60, 73]:

$$k_p = 2C_{in}\zeta\omega_n \tag{25}$$

$$k_i = C_{in}\omega_n^2 \tag{26}$$

Equations 25 and 26 can be rewritten as

$$k_p = \frac{8C_{in}}{t_s} \tag{27}$$

$$k_i = \frac{16C_{in}}{t_s^2\zeta^2} \tag{28}$$

where t_s is the closed-loop setting time, which can be calculated in term of the maximum switching frequency T_{sc} by choosing t_s/T_{sc} =10. The damping of the system can be also adjusted by choosing $\zeta = 0.707$ [60].

C. FCS-MPCC for DC-DC boost converter

The FCS-MPCC algorithm employed for each boost converter is presented in Figure 5.7. This method uses the inherent discrete nature of the boost converter to predict the next sampling time behavior of the input boost current $i_{Lx}(k+1)$. Then, a cost function expressed in Equation 29 is defined in order to minimize the error between the predicted current $i_{Lx}(k+1)$and its reference [59].

$$J = \left| i_{Lx\_ref} - i_{Lx}(k+1) \right| \tag{29}$$

From The discrete time model presented in Equation 4, the predicted inductor current $i_{Lx}(k+1)$ is calculated for the two switching states (s=1, 0) in terms of the measured output voltage v_{cx}, actual PV voltage v_{pvx} and actual inductor current of the boost converter i_{Lx}. Next, the two results are compared to the inductor current reference using the cost function. Where, the switch state corresponding to the minimum value of the cost function will be selected as the optimal control action as illustrated in Figure 5.7.

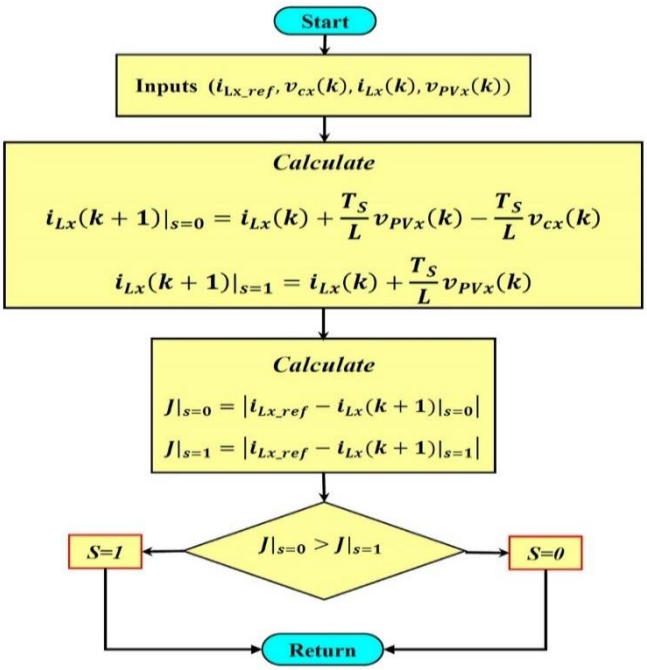

Figure 5.7: Flowchart of FCS-MPC.

5.4.2 FCS-MPC ALGORITHM FOR GRID-TIED FIVE-LEVEL INVERTER

To inject the produced PV power from each PV system in addition to the reactive power demanded by the grid operator with high grid current quality, the control of the centralized five-level NPC inverter should be performed with high accuracy and by taking in account the balancing of DC-link capacitor voltages. Depending on the model predictive control (FCS-MPC) proposed in [75], a proposed FCS-MPC is applied to control the centralized five level NPC inverter in large scale PV system. The aims of the proposed FCS-MPC are:

- Enforce the measured grid current i_{gd} to track the reference i_{gd_ref} delivered by the DC-link voltage control.

- Enforce the measured grid current i_{gq} to track the reference i_{gq_ref} in order to inject the reactive power requested by the grid operator.

- Assure the balance of four DC-link capacitor voltages under irradiation, reactive power reference and contrast of extracted powers of each PV system changes.

- Minimize the switching frequency.

Those objectives are included in the cost function which is defined as:

$$\begin{aligned} g &= (i_{gd\_ref} - i_{gd}(k+1))^2 + (i_{gq\_ref} - i_{gq}(k+1))^2 \\ &+ \lambda_{dc}\left[\sum_{j=1}^{3}\left|v_{cj}(k+1) - v_{cj+1}(k+1)\right| + \sum_{k=1}^{2}\left|v_{ck}(k+1) - v_{ck+2}(k+1)\right| + \left|v_{c3}(k+1) - v_{c4}(k+1)\right|\right] \\ &+ \lambda_{swc}(SWC_a + SWC_b + SWC_c) \end{aligned} \quad (30)$$

where the cost function terms are described as follow:

1) The current i_{gd_ref} is generated by a PI controller according to the produced PV power. While, the i_{gq_ref} is estimated in term of reactive power reference using the following equation [28, 32]:

$$i_{gq\_ref} = \frac{Q_{g\_ref}}{V_{gd} * 1.5} \quad (31)$$

2) $i_{gd}(k+1)$ and $i_{gq}(k+1)$ are the predicted grid currents in synchronous reference frame. After measuring the instantaneous grid currents, the $i_{gd}(k+1)$ and $i_{gq}(k+1)$ are calculated from Equation 7.

TABLE 5.2: Number of switch changes calculation (x = a, b, c).

SWC_x	**Sx (k+1)**				
	1	**2**	**3**	**4**	**5**
$S_x(k)=1$	0	2	4	6	8
$S_x(k)=2$	2	0	2	4	6
$S_x(k)=3$	4	2	0	2	4
$S_x(k)=4$	6	4	2	0	2
$S_x(k)=5$	8	6	4	2	0

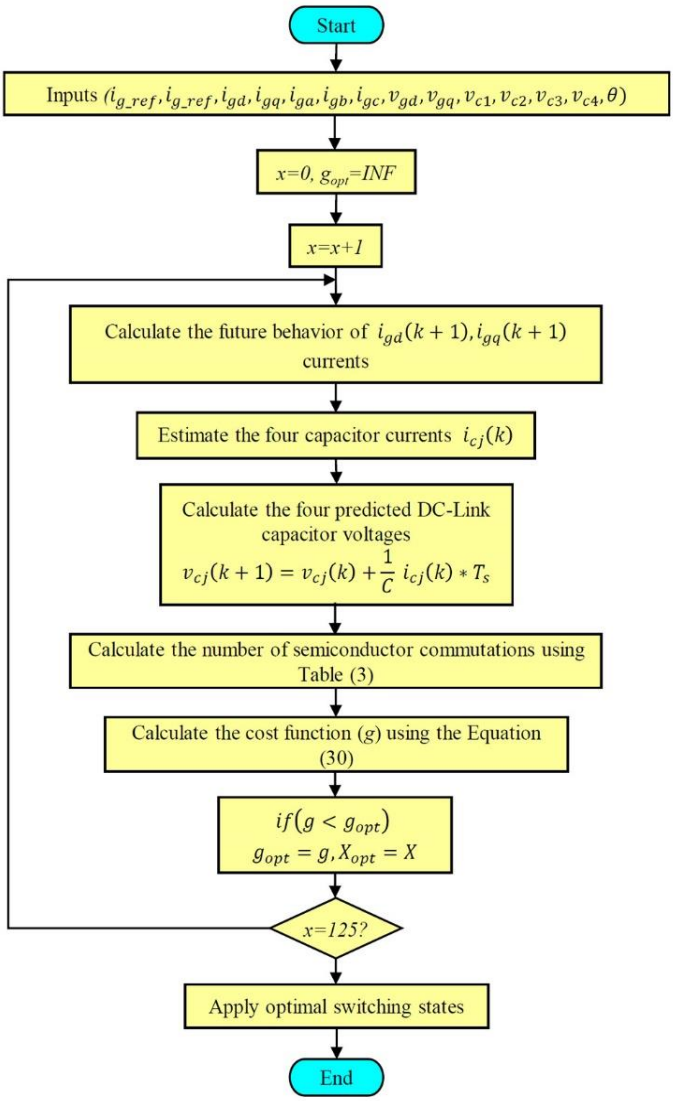

Figure 5.8: Flowchart of the proposed model predictive control (FCS-MPC).

1) $V_{cx}(k+1)$ are the predicted DC-link capacitor voltages. From Equation 12, the measured DC-link capacitor voltages with the measured grid currents in natural frame (abc) are necessary for calculation of the future behaviour of DC-link capacitor voltages.

2) The SWC_x is the difference between the actual number of NPC inverter switch commutations and the switching of the predicted vector involved in phase-x, which can be calculated as detailed in Table 5.2.

3) λ_{dc} and λ_{swc} are the weighting factor for the DC-link capacitor voltages balance and switching frequency minimization respectively.

After calculation of the future behaviors of i_{gd-q} currents and DC-link capacitor voltages for all 125 possible switching states from the measured grid currents and voltages,

in addition to the four DC-link capacitor voltages, a cost function g is evaluated for all switching states. The switching state that minimizes the cost function is selected and applied during the next sampling time. The operating of the proposed FCS-MPC is summarized in Figure 5.8.

TABLE 5.3: Proposed system parameters.

PV subsection electrical parameters (Siemens SM110)	**Value**
Maximum power (Pmpp)	120*Watts*
Open circuit voltage (Voc)	42.1*V*
Short circuit current (Isc)	3.87*A*
Voltage at Pmax	*33.7*
current at Pmax	*3.56*
Number of cells connected in parallel (Np)	1
Number of cells connected in series (Ns)	72
Number of modules connected in series (Nss)	36
Number of modules connected in parallel (Npp)	36
Boost converter electrical parameters	**Value**
Input Capacitor C_{in}	330 µF
Inductor L	1 *mH*
DC-link Capacitors value C	4700*µF*
Grid electrical parameters	**Value**
Grid inductance *Lg*	4 mH
Grid resistance *Rg*	0.1 Ω
Grid Peak Voltage *Vg*	1000 V
Grid frequency *Fg*	50 Hz
Simulation Parameters	**Value**
V-IncCon sampling Time *Ts_MPPT*	1 ms
FCS-MPCC sampling Time Tsc	25 µs
FCS-MPC sampling Time Ts	0.1 ms
DC-Link PI controller parameters	**Value**
Proportional gain K_p	-0.5
Integral gain K_i	-3.5

5.5 RESULTS ANALYSIS

Simulation of the proposed system is performed using MATLAB/Simulink and Simpower system packages with the parameters for each PV subsection, each boost converter and the Rg, Lg filter are illustrated in Table 5.3. The system performance is evaluated under the following conditions: fixed temperature 25 °C, several sudden changes and steady state levels in the solar irradiation and reactive power reference.

To demonstrate the improvement from applying the proposed control scheme, two studies are considered in this section. The aim of the first study is to show the enhancement obtained by applying the proposed control scheme based on FCS-MPC in comparison with the conventional scheme based on PI regulators in terms of MPP tracking, DC-link capacitor voltage balancing, d-q axes current control, and grid current quality. While, in the second study, the proposed control scheme is tested under contrast of powers extraction from each PV system in order to evaluate the DC-link voltage balancing and grid current THD%.

5.5.1 PROPOSED CONTROL SCHEME VERSUS CONVENTIONAL CONTROL SCHEME COMPARISON

Under irradiation and reactive power reference changes represented in Figure 5.9 (a) and Figure 5.9 (f), the large-scale grid-connected PV system using high-level NPC inverter with the proposed control scheme based on FCS-MPC and the conventional control scheme (conventional VO-MPPT presented in [108], and VOC based on PI regulators presented in [83]) are tested by numerical simulations through Matlab/Simulink and Simpower system packages.

The proposed and conventional control schemes performances are compared in dynamic states regarding MPPT tracking speed, DC-link capacitor balancing and d-q grid currents control. While, the following parameters: percentage PV power output oscillation $\%e_{Ppv}$, percentage mean absolute i_{gd} current tracking error$\%e_{dg}$, percentage mean absolute i_{gq}current tracking error $\%e_{gq}$, percentage mean absolute DC-Link voltages deviation $\%e_{dc}$, percentage total harmonic distortion $\%THD$ are observed in steady-state.

As shown in Figures 5.9 and 5.10, a sudden decrease in solar irradiation from 800 to 400 W/m² at instant 0.6 s is applied. The proposed MPPT reaches the new MPP rapidly without any deviation compared to the conventional MPPT (Figures. 5.9(b) and 5.10(b)). Moreover, this change leads to undershoot and small rising time in V_{dc} over its reference as shown in Figures.

5.9 (c) and 5.10 (c). Despite that, the capacitor voltages are balanced perfectly using the proposed control scheme in contrast to the conventional control scheme as illustrated in Figures. 5.9 (d) and 5.10 (d). However, the i_{gd-q} currents track their references in both methods accurately (Figures. 5.9(e, f) and 5.10(e, f)). Whereas the grid currents decreased and remain sinusoidal as shown in Figures. 5.9(g) and 5.10(g).

Then, a large sudden increase in the solar irradiation from 400 to 1000 W/m² at instant 1.4 s is performed. The proposed MPPT exhibits a fast and accurate MPP tracking compared to the conventional MPPT. In spite of the overshoot and settling time in V_{dc} over its reference as shown in Figures. 5.9 (c) and 5.10 (c), the i_{gd-q}currents are regulated very well in both methods. In addition, as presented in Figure 5.10 (d), the proposed control scheme guarantees a perfect balance of the four DC-link capacitor voltages compared to the conventional control scheme, as well as, the grid currents are increased and kept sinusoidal.

Next, two step changes in reactive power reference from 0 to 0.45 Mvar and 0.45 Mvar to -0.45 Mvar are occurred at instant 1.5 s and 2.5 s respectively. The i_{gq} reference is estimated to change suddenly from 0 A to 300 A in the first case and 300 A to -300 A in the second case as presented in Figures 5.9(f) and 5.10(f). The PV power output remained constant under these changes due to constant solar irradiation.

The first step change in i_{gq} current reference leads to a small undershoot in V_{dc} over its reference as shown in Figures 5.9(c) and 5.10(c). The proposed control scheme takes only 0.5 ms to track the i_{gq} current reference. While, the conventional control scheme takes 1.2 ms. Hence, the i_{gd} current is well regulated in both control schemes. Otherwise, a perfect DC-link capacitor voltages balance is assured by the proposed control scheme unlike the conventional one. Moreover, the grid currents are increased rapidly, change the angle and kept the sinusoidal form as shown in Figures 5.11 (a) and 5.12(a). The increases in grid currents are due to the increases in grid apparent power S_g, where the grid current amplitude is proportional to S_g. While, a small overshoot in V_{dc} over its reference is occurred as shown in Figures 5.9(c) and 5.10(c), due the second change in i_{gq}current reference. A fast i_{gq} current regulating and a perfect DC-link capacitor voltages balancing are assured by the proposed control scheme in comparison to classical method. The latter takes 1.6 ms to track the i_{gq} current reference. While, the proposed control scheme takes only 0.8 ms. Besides, the current i_{gd} is well controlled using

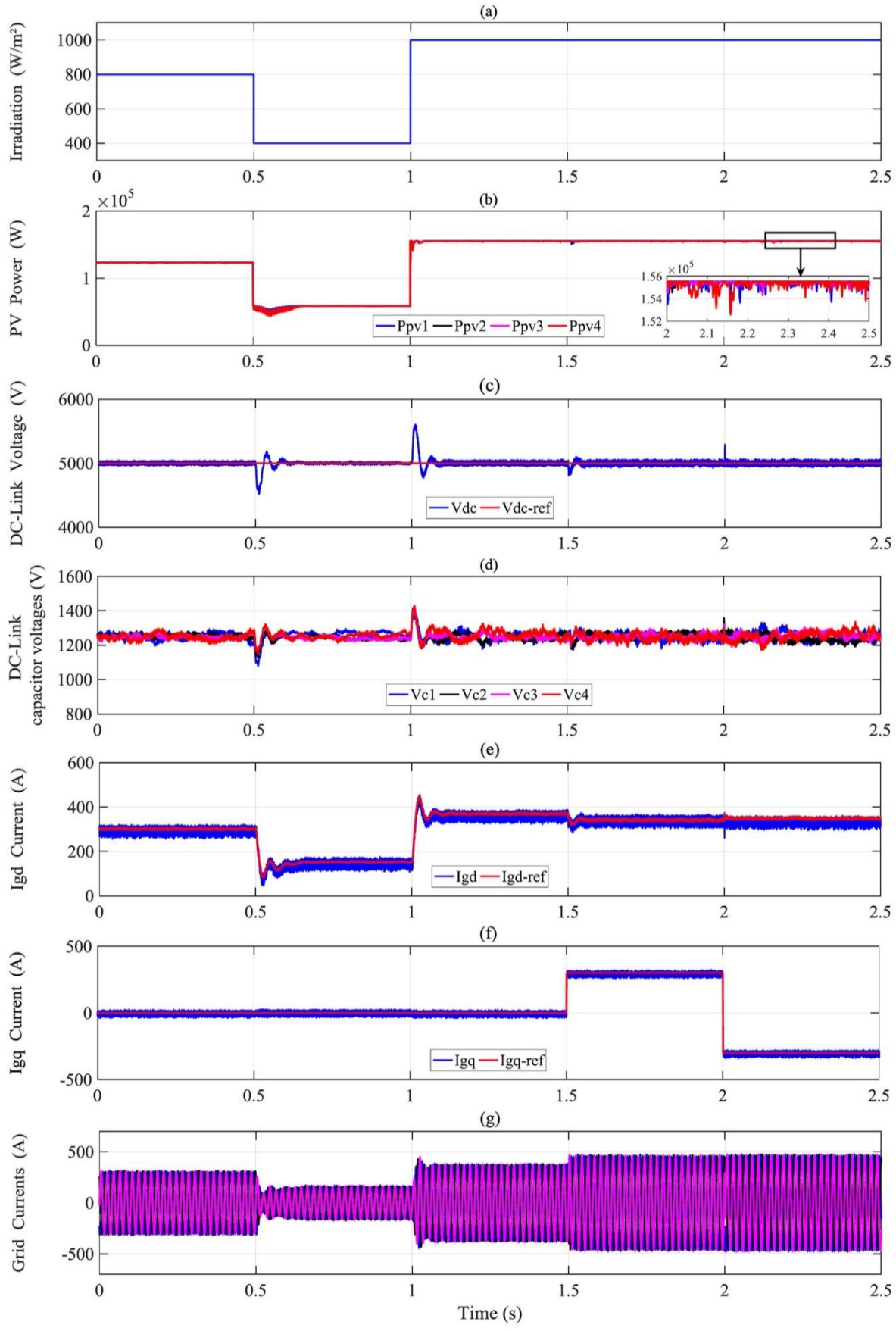

Figure 5.9: Simulation results with proposed control scheme.

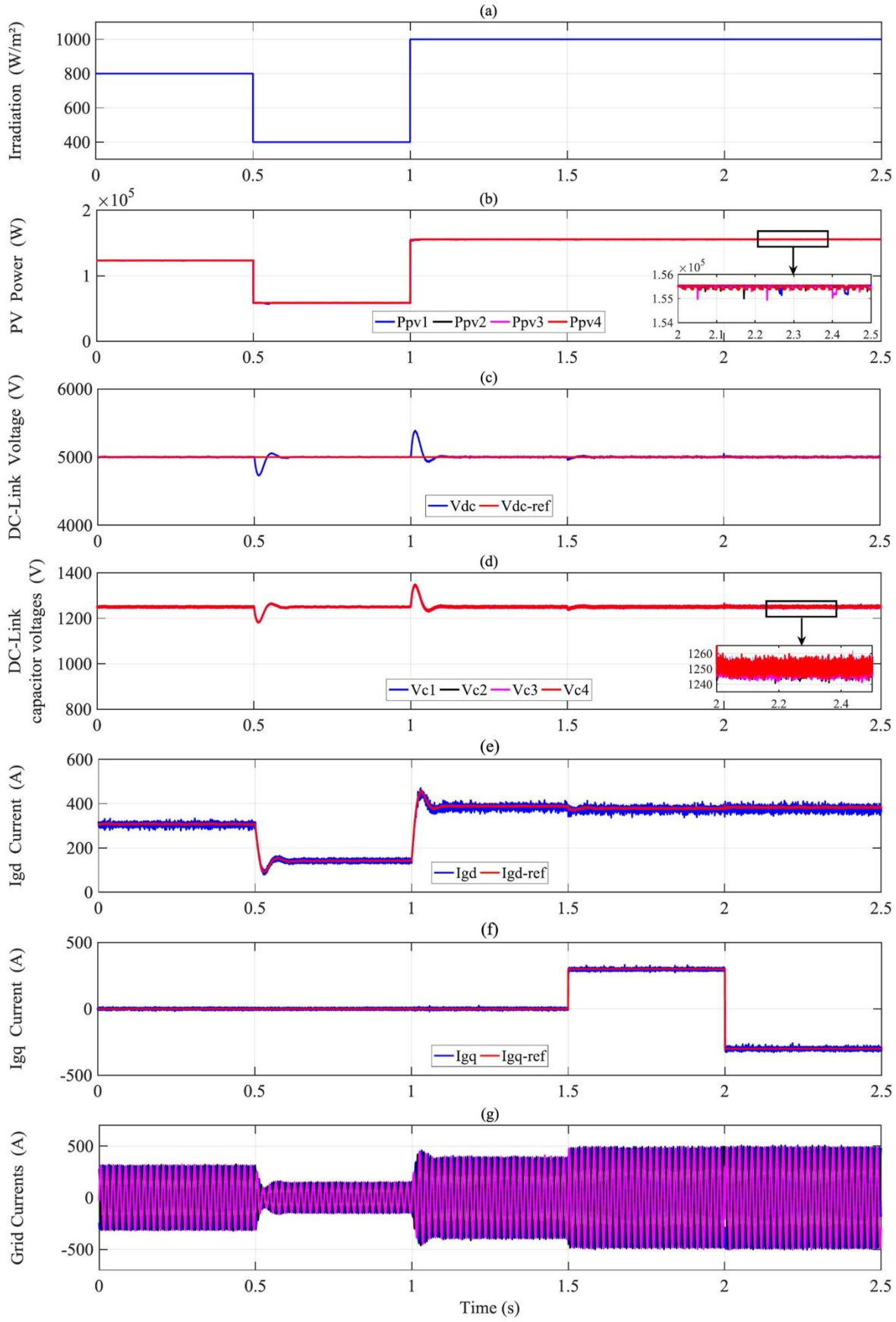

Figure 5.10: Simulation results with proposed control scheme.

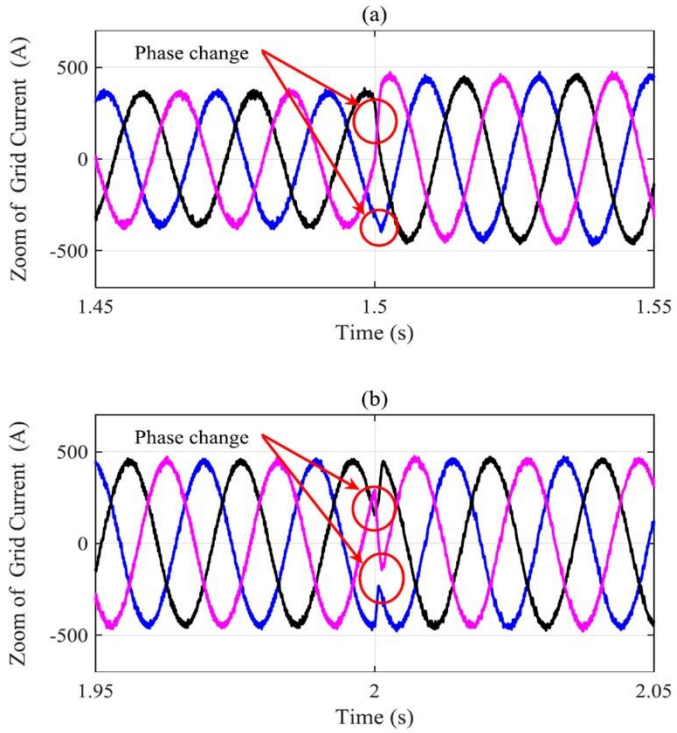

Figure 5.11: Zoom of grid currents under reactive power reference change with conventional control scheme.

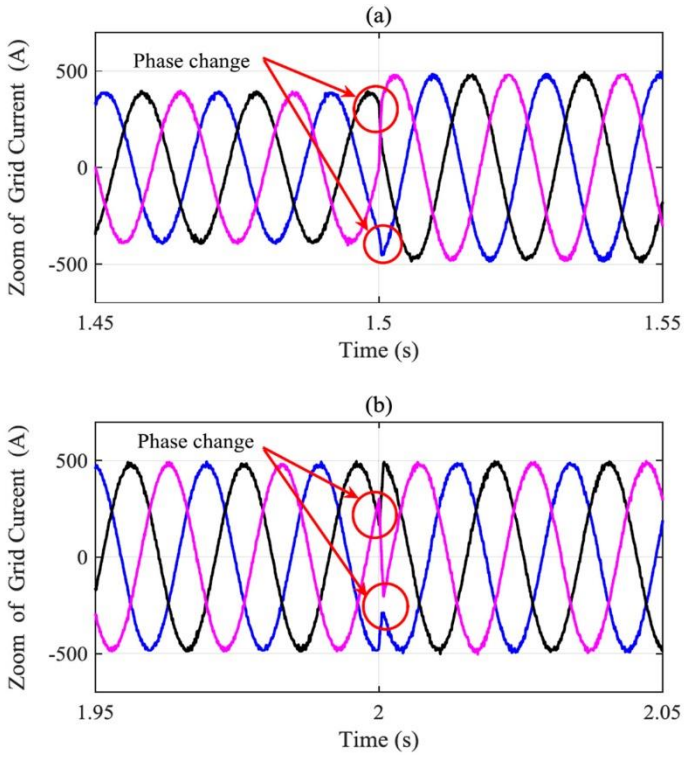

Figure 5.12: Zoom of grid currents under reactive power reference change with proposed control scheme.

both control schemes. Otherwise, the grid currents change their angle and kept the sinusoidal form as illustrated in Figures 5.11 (b) and 5.12(b).

The measured performance of the classical and proposed methods during steady-state are summarized in Table 5.4 and 5.5 respectively. It is clear that the proposed control scheme provides better performance during the five irradiation and reactive power cases compared to conventional control scheme. Where, the percentage PV power output oscillation $\%e_{Ppv}$ for the proposed MPPT is found to be lesser than the $\%e_{Ppv}$ for the classical MPPT method under all irradiation and reactive power levels. Also, the proposed FCS-MPC offers a lower percentage mean absolute i_{gd}current tracking error$\%e_{gd}$, percentage mean absolute i_{gq} current tracking error $\%e_{gq}$ and percentage mean absolute DC-link voltages deviation $\%e_{dc}$ than the conventional VOC during all cases. In addition to that, a perfect DC-link capacitor voltages and high grid current quality are assured from the proposed control scheme in contrast to the conventional VOC.

TABLE 5.4: Steady-state analysis with conventional control scheme results.

Cases	G (W/m²)	Qref (Mvar)	$\%e_{Ppv}$	$\%e_{dc}$	$\%e_{gd}$	$\%e_{gq}$	THD (%)
Case 1	800	0	0.6	1.8	3.31	1.7	2.49
Case 2	400	0	1.56	1.2	5.22	1.1	4.96
Case 3	1000	0	1.41	2.1	2.7	2.26	1.90
Case 4	1000	0.45*	1.73	2.4	1.75	2.66	2.04
Case 5	1000	-0.45*	2.69	2.46	3.45	1.63	1.50

TABLE 5.5: Steady-state analysis with proposed control scheme results.

Cases	G (W/m²)	Qref (Mvar)	$\%e_{Ppv}$	$\%e_{dc}$	$\%e_{gd}$	$\%e_{gq}$	THD (%)
Case 1	800	0	0.56	0.41	0.74	0.83	1.37
Case 2	400	0	0.73	0.26	1.05	0.61	3.77
Case 3	1000	0	0.51	0.46	0.87	0.69	1.31
Case 4	1000	0.45*	0.45	0.64	0.53	1.16	1.21
Case 5	1000	-0.45*	0.58	0.61	0.61	0.67	1.32

5.5.2 PERFORMANCE OF PROPOSED CONTROL SCHEME UNDER CONTRAST OF POWER EXTRACTION FROM EACH PV SYSTEM

In this section, more tests are achieved for the large-scale grid-connected PV system using high-level NPC inverter with the proposed FCS-MPC under contrast of power extraction from each PV system. The DC-link voltage balancing, grid current THD% in addition to i_{gd-q}currents regulation is observed and discussed. As depicted in Figure 5.13, three cases of contrast in irradiation condition are applied to the four PV system. These cases are performed as follows: the contrast is null during the first case (G1=G2=G3=G4=600 W/m²), while the second and third cases are (G1=1000 W/m², G2=800 W/m², G3=600 W/m², G4=400 W/m²) and (G1=800 W/m², G2=600 W/m², G3=400 W/m², G4=1000 W/m²) respectively (Figure 5.13 (a)).

During the first case, the proposed FCS-MPC provides a perfect DC-link capacitor balancing, accurate i_{gd-q}currents control and high grid current quality as presented in Table 6.

At instant 0.5 s, a contrast in irradiation condition is occurred (case2). V_{dc} is overlapped to its reference as depicted in Figure 5.13(c). Despite this change, the proposed FCS-MPC shows a complete balance of DC-link capacitor voltages and high performance i_{gd-q} currents control during dynamic and steady states as illustrated in Figures 5.13(d, e, f) and Table 5.6. Furthermore, the grid currents are increased and remained in sinusoidal form due to the increase in the produced PV power (Figure 5.13(g)).

The second contrast in irradiation conditions is applied at instant 1.5 s, (case3). Figure 5.13 (c) shows an overshoot of V_{dc} over its reference. As the previous cases, the four DC-link capacitor voltages have maintained their balance, i_{gd-q} currents are accurately controlled during dynamic and steady states and the grid currents are well balanced with sinusoidal form.

Despite the contrast of extracted powers from each PV system, the proposed control scheme provides high grid current quality under all scenarios as depicted in Table 5.6.

TABLE 5.6: Steady-state analysis with proposed control scheme results under contrast of extract powers from each PV system.

Cases	$\%e_{dc}$	$\%e_{gd}$	$\%e_{gq}$	THD (%)
Case 1	0.3	1.1	0.66	1.77
Case 2	0.29	0.98	0.87	2.04
Case 3	0.31	1.3	0.83	1.82

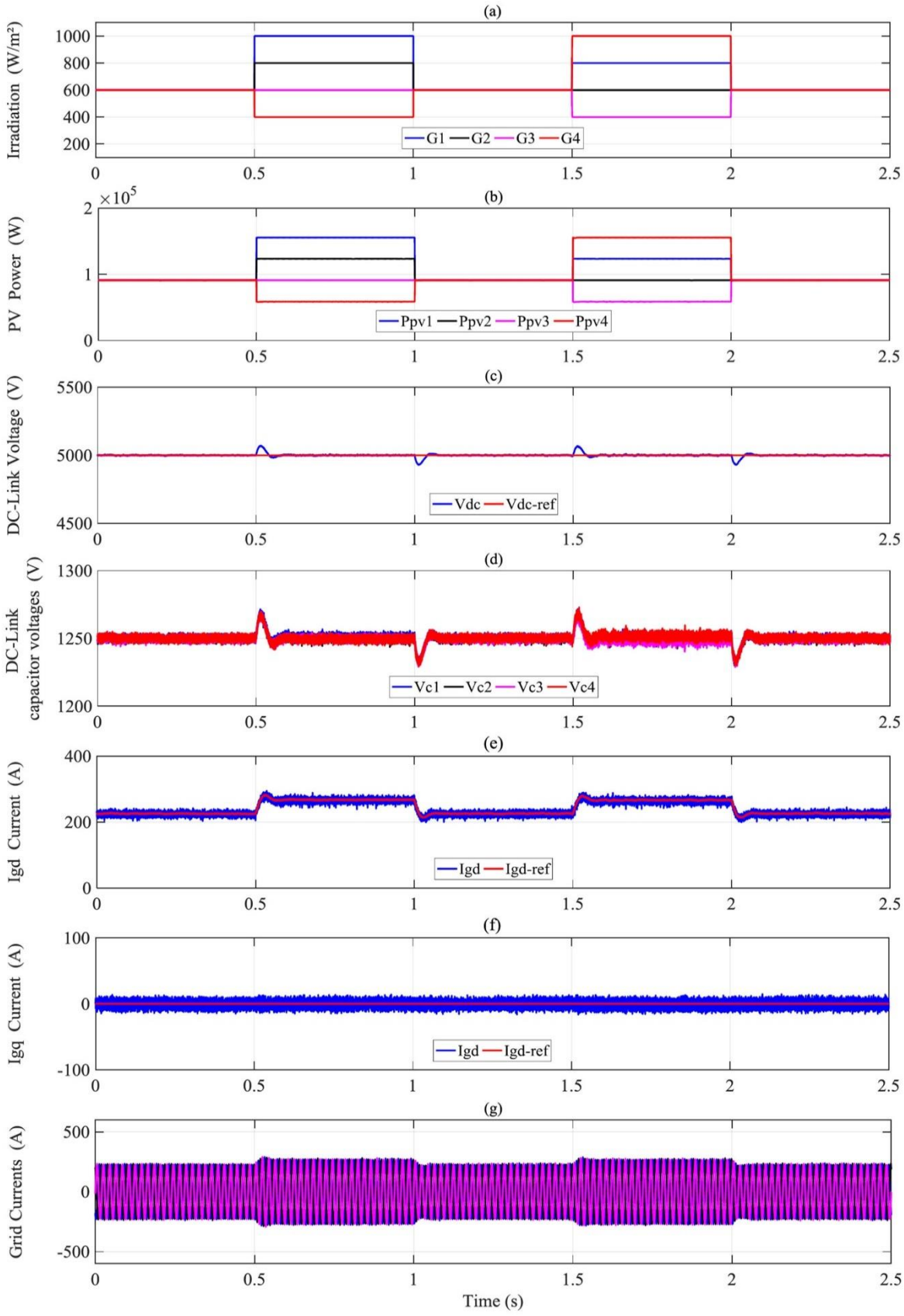

Figure 5.13: Simulation results with proposed control scheme under contrast of power extraction from each PV system.

5.6 CONCLUSION

An improved control scheme of large-scale grid-connected PV system using high-level NPC inverter based on FCS-MPC controllers has been presented in this chapter. A fast voltage oriented maximum power point tracking (VO-MPPT) employing FCS-MPCC is applied to each boost converter to maximize the extracted power from each PV array. In addition, an FCS-MPC is proposed to control the centralized five-level NPC inverter. The main goals of the developed controllers are: tracking the MPP rapidly and accurately under sudden irradiation changes, making the balance of the four DC-link capacitor voltages whatever the difference between extracted powers from each PV system unit, injecting the reactive power demanded by the grid operator and minimizing the switching frequency.

As presented in the simulation results, a significant enhancement by applying the proposed control scheme has been achieved in comparison with the conventional control scheme. Where, the proposed MPPT provides a high performance tracking in term of power oscillations, speed and tracking accuracy. Furthermore, i_{gd-q} currents are tightly regulated, DC-link capacitor voltages are perfectly balanced and high grid current quality has been provided in comparison with the conventional control scheme during different irradiation and reactive power reference scenarios. Under contrast of extracted powers from each PV system, perfect DC-link capacitor voltages balancing, tightly i_{gd-q} currents regulating and high gird current THD% have been provided by the proposed control scheme.

Chapter 6

Conclusions

6.1 General conclusion

Grid-connected PV systems have been widely investigated in numerous research works, in order to enhance the energy harvesting from the PV arrays and to inject the produced PV power into the grid with high grid current quality. In this dissertation, the presented research works have brought several investigations of suitable conversion topologies and effective control schemes for low, medium and high-power grid-connected PV systems.

Numerous grid-connected PV system topologies have been investigated in this dissertation to obtaining the best way to achieve a high energy harvesting capability and a high-performance operation as well as maintaining the simplicity of the control design for these topologies. From these topologies, the dual-stage configuration has been considered in low power grid-connected PV system. Furthermore, the advantages provided by dual-stage configuration have been combined with efficient grid-side multilevel converters in order to inject the produced PV power with high performance operation, as well as ensure the operation in medium and high power range. Also, a topology that divides the large PV array into string modules with individual DC-DC converter connected to a centralized multilevel inverter has been investigated in order to overcome the problems resulting from connecting the PV modules as large PV array.

On the other hand, several controllers based on Finite control set model predictive control have been proposed for the presented topologies. The purposes of the developed controllers are: track the MPP rapidly and accurately under sudden irradiation changes, regulate the DC-link voltage to its desired value, guarantee the balance of DC-link voltage capacitors in case of using multilevel NPC inverters, and inject the produced PV power and the reactive power requested by the grid operator into the grid with achieving a high grid current quality. The major weaknesses of the MPC (variable inherent switching frequency and computational burden, especially in case of high-level inverters) have been taken into account in the proposed controllers.

The proposed control schemes for the investigated grid-connected PV topologies have been validated through numerical simulations and real time HIL implementations. The research results presented in this dissertation promote the proposed control schemes based on FCS-MPC as a simple, efficient and high performance control tool for low, medium and high power grid-connected PV systems in comparison with conventional control schemes.

The topologies and control schemes presented in this dissertation can be employed in other power electronics and energy system applications.

6.2 Author's contributions

The main contributions presented in this dissertation can be summarized as follows:

1. A review of control schemes for dual-stage grid-connected PV system is presented.

Various conventional and advanced MPPT techniques, DC-link voltage regulators and grid power/current control techniques are discussed and compared in brief.

2. A fast current oriented MPPT with a variable incremental current step size employing fixed switching predictive current control is proposed.

This control strategy has been developed to track the MPP quickly and accurately under irradiation changes. The simulation and real time HIL implementation results show clearly a significant enhancement by applying the proposed MPPT method in comparison with the conventional INC and INC through PCC methods in terms of accuracy tracking, response time and stability around the maximum power point under irradiation changes.

3. A voltage oriented control VOC based on both predictive control strategy and space vector modulation SVM (PS-VOC) is proposed.

The PS-VOC proposed and applied to control the grid-tied two-level inverter. The major goals of this control strategy are to improve the regulation of i_d-i_q currents under irradiation and reactive power demanded by the grid operator changes, as well as achieving a high grid current quality. The results obtained from simulation and real time HIL implementation prove that the proposed PS-VOC provides high grid current quality in accordance with international standards (IEEE-519) for any irradiation and reactive power levels.

4. High-level NPC inverters are investigated in grid-connected PV system.

The features of high-level NPC inverters have been exploited in order to inject the medium and high produced PV power with high performance operation.

5. Decoupled active and reactive power control strategy based on finite set model predictive control is proposed to control grid connected six-level NPC inverters for PV application.

The purposes of this strategy are: inject the active power produced by PV system, as well as the reactive power requested by the grid operator with high performance operation, assure the balance of DC-link capacitor voltages and achieve high grid current quality. The proposed strategy has been evaluated through Numerical simulation and HIL implementation. The obtained results indicate that high performance operation in power control and perfect DC-link capacitor voltages balancing have been achieved under sudden changes and steady-state operating conditions in the solar irradiation and reactive power reference. Moreover, a high grid current quality at different solar irradiation and reactive power reference levels in accordance with international standards (IEEE-519) has been achieved.

6. An optimized model predictive decoupled active and reactive power control (O-MPC) is proposed to control grid-connected six-level neutral-point-clamped (NPC) inverter for PV application.

The objective of this MPC strategy is to achieve the same performance operation as an MPC strategy with reduced computational burden. The proposed strategy reduces by 57% the number of voltage vectors for prediction compared to the conventional MPC. Despite this

reduction of computational burden, the obtained simulation and real-time HIL implementation results prove that the O-MPC as the MPC algorithm, achieved high performance operation in power control and perfect DC-link capacitor voltages balancing under sudden changes in the solar irradiation and reactive power reference and steady-state operating conditions. Moreover, the grid currents quality of the O-MPC at different solar irradiation and reactive power reference levels is almost the same as the MPC algorithm.

7. Multi MPPTs with centralized multilevel NPC inverter topology is investigated for high produced PV power range.

This topology composed of two conversion stages, the first stage contains four PV arrays, each one connected to an individual DC-DC converter (boost converter). In the second stage, a five level NPC inverter tied to the grid is employed. Each DC-Link capacitor input of the NPC inverter is connected to the output of the DC-DC boost converter.

8. Effective controllers based on finite set model predictive control (FS-MPC) are proposed for multi MPPTs with centralized multilevel NPC inverter topology.

A fast voltage oriented maximum power point tracking (VO-MPPT) performed by FS-MPC current controller is applied for each boost converter to maximize the produced power from each PV array. In addition, a FS-MPC is proposed to control the centralized five-level NPC inverter. The purposes of the developed controllers are: track the MPP rapidly and accurately under sudden irradiation changes, assure the balance of the four DC-Link capacitor voltages whatever the difference between extract powers of each PV system unit, inject the reactive power requested by the grid operator and minimize the switching frequency. The obtained results demonstrate that, a significant enhancement by applying the proposed control scheme has been achieved in comparison with the conventional control schemes. Where, the proposed MPPT provides a high performance tracking in term of power oscillations, speed and accurate tracking. Furthermore, i_{gd-q} currents are tightly regulated; DC-Link capacitor voltages are perfectly balanced and high grid current quality has been provided in comparison with the conventional control scheme during different irradiation and reactive power reference conditions. Under contrast of extract powers from each PV system, the proposed control scheme has provided a perfect DC-Link capacitor voltage balancing, tightly i_{gd-q} currents regulated and high gird current THD%.

6.3 Future works

- Development of new MPPT algorithms that take into consideration the partially shaded condition.
- Application of proposed control schemes to other multilevel inverter topologies such as cascaded H-Bridge modular and flying capacitors multilevel inverters topologies.
- Application of proposed control schemes for stand-alone PV systems using multilevel inverter topologies.
- Investigation of DC-DC multilevel converter topologies for grid-connected PV systems.
- Development of modified model predictive control that achieves more reduction in computational burden.
- Investigation of new multilevel inverter topologies with a low number of switching for grid-connected PV system.
- Investigation of LCL filters for the grid-connection with design of an effective model predictive controller.

List of Publications

The following list includes all the papers published by the author during his graduate studies. Papers designated by " ★ " are directly related with research results presented in this dissertation.

Journal Papers

★[1] **Abdelbaset Laib**, Fateh Krim, Billel Talbi, Abbes Kihal, Hamza Feroura, 2018. Improved Control for Three Phase dual-Stage Grid-Connected PV Systems Based on a Predictive Control Strategy. Journal of Control Engineering and Applied Informatics, 20(3), 12-23. (Impact Factor: 0.698).

★[2] **Abdelbaset Laib**, Fateh Krim, Billel Talbi, Hamza Feroura, Abbes Kihal, 2019. Decoupled active and reactive power control strategy of grid-connected six-level diode-clamped inverters based on finite set model predictive control for photovoltaic application, Revue roumaine des sciences techniques, 64(1),51–56, 2019. (Impact Factor: 1.135).

[3] Billel Talbi, Fateh Krim, Toufik Rekioua, Saad Mekhilef, **Abdelbaset Laib**, Abdesslam Belaout, 2018. A high-performance control scheme for photovoltaic pumping system under sudden irraadaince and load changes. Solar Energy 159, 353–368. (Impact Factor: 4.018).

[4] Billel Talbi, Fateh Krim, Toufik Rekioua, **Abdelbaset Laib**, Hamza Feroura, 2017. Design and hardware validation of modified P&O algorithm by fuzzy logic approach based on model predictive control for MPPT of PV systems. Journal of Renewable and Sustainable Energy 9, 043503–14. (Impact Factor: 1.135).

[5] Hamza Feroura, Fateh Krim, Billel Talbi, **Abdelbaset Laib**, Abdesslam Belaout, 2017. Finite-set model predictive direct power control of grid connected current source inverter. Elektronika ir Elektrotechnika 23(5), 36–40. (Impact Factor: 0.859).

[6] Hamza Feroura, Fateh Krim, Billel Talbi, **Abdelbaset Laib**, Abdesslam Belaout, 2017. Sensorless field oriented control of current source inverter fed induction motor drive. Revue Roumaine Des Sciences Techniques, 63(1), 100-105. (Impact Factor: 1.036).

[7] Abbes Kihal, Fateh Krim, Billel Talbi, **Abdelbaset Laib**, Abdeslem Sahli, 2018. A Robust Control of Two-Stage Grid-Tied PV Systems Employing Integral Sliding Mode Theory. Energies, 11(10), 2791. (Impact Factor: 2.676).

[8] Abbes Kihal, Fateh Krim, **Abdelbaset Laib**, Billel Talbi, Afghoul Hamza, 2018. An improved MPPT scheme employing adaptive integral derivative sliding mode control for photovoltaic systems under fast irradiation changes. ISA transactions. (Impact Factor: 3.370).

Conference Papers

[9] Billel Talbi, Fateh Krim, **Abdelbaset Laib**, Hamza Feroura, 20017. High-Accuracy Sliding Mode Observer for Boost Converter with MPC Switching Control. In: Proc. ICENT'17, M'sila, Algeria, Nov. 2017.

[10] Hamza Feroura, Fateh Krim, Billel Talbi, **Abdelbaset Laib**, 2017. Photovoltaic grid connected current source inverter with resonance active damping method. In: Proc. ICENT'17, M'sila, Algeria, Nov. 2017.

★[11] **Abdelbaset Laib**, Fateh Krim, Billel Talbi, Hamza Feroura, 2017. Current oriented MPPT based on fuzzy logic and predictive controllers for photovoltaic systems with SEPIC converter. In: Proc. ICENT'17, M'sila, Algeria, Nov. 2017.

★[12] **Abdelbaset Laib**, Fateh Krim, Billel Talbi, Abbas Kihal, Abdeslem Sahli, 2017. Predictive control strategy for double-stage grid connected PV systems. In: Proc. ICEECA'17, Constantine, Algeria, Nov. 2017.

[13] Hamza Feroura, Fateh Krim, Billel Talbi, **Abdelbaset Laib**, 2017. Finite-set model predictive voltage control for islanded three-phase current source inverter. In: Proc. ICEE-B, Boumerdes, Algeria, Oct. 2017.

★[14] **Abdelbaset Laib**, Fateh Krim, Billel Talbi, Hamza Feroura, 2017. Fuzzy logic maximum power point tracking through sliding mode current control for PV systems. In: Proc. IC-AIRES'17, Tipasa, Algeria, Oct. 2017.

[15] Hamza feroura, Fateh Krim, Billel Talbi, **Abdelbaset Laib**, Abdesslam Belaout, 2017. Finite-set model predictive direct power control of grid connected current source inverter. In: Proc. 21st international conference electronics, Palanga , Lithuania, Jun.

2017.

[16] Abdesslam Belaout, Fateh Krim, Billel Talbi, Hamza Feroura, **Abdelbaset Laib**, Semcheddine Bouyahia, Abderrazak Arabi, 2017. Development of real time emulator for control and diagnosis purpose of photovoltaic generator. In: Proc. ICSC'17, Batna, Algeria, May. 2017.

★[17] **Abdelbaset Laib**, Fateh Krim, Billel Talbi, 2017. Simulation of variable step size incremental conduction MPPT through Predictive current control. In: Proc. ICESD'17, Adrar, Algeria, Feb. 2017.

★[18] **Abdelbaset Laib**, Fateh Krim, Billel Talbi, 2016. An improved control for two-stage grid-connected photovoltaic systems. In: Proc. ICESTI'16, Annaba, Algeria, Nov. 2016.

[19] Billel Talbi, Fateh Krim, **Abdelbaset Laib**, 2016. An Improved Variable Step Size P&O Current-Based MPPT Employing FSC-MPC for Sudden Irradiance change. In: Proc. Batna, CEE'16, Algeria, Oct. 2016.

★[20] **Abdelbaset Laib**, Fateh Krim, Billel Talbi, 2016. Simulation of variable step size incremental conduction MPPT through sliding mode current control. In: Proc. Batna, CEE'16, Algeria, Oct. 2016.

[21] Hamza Feroura, Fateh Krim, Billel Tabli, **Abdelbaset Laib**. 2017. Finite-set model predictive voltage control for islanded three phase current source inverter. In 5th International Conference on Electrical Engineering (ICEE-B), Boumerdes, Algeria, May, 2017.

[22] Abbes Kihel, Fateh Krim, **Abdelbasset Laib**. 2017. MPPT voltage oriented loop based on integral sliding mode control applied to the boost converter. In: Proc. ICSC'17, Batna, Algeria, May. 2017.

Other

★[23] **Abdelbaset Laib**, Fateh Krim, 2016. Contribution à l'implémentation pratique de la commande MPPT pour des installations photovoltaïques. Participation in the UFAS1 Doctoriales dedicated to innovation, Sétif, Algeria, May. 2016.

References

[1] R. Wai, W. Wang, and C. Lin, 'High-Performance Stand-Alone Photovoltaic Generation System', *IEEE Transactions on Industrial Electronics*, vol. 55, no. 1, pp. 240–250, Jan. 2008.

[2] M. A. A. M. Zainuri, M. A. M. Radzi, A. C. Soh, and N. A. Rahim, 'Development of adaptive perturb and observe-fuzzy control maximum power point tracking for photovoltaic boost dc–dc converter', *IET Renewable Power Generation*, vol. 8, no. 2, pp. 183–194, Aug. 2013.

[3] A. Safari and S. Mekhilef, 'Simulation and Hardware Implementation of Incremental Conductance MPPT With Direct Control Method Using Cuk Converter', *IEEE Transactions on Industrial Electronics*, vol. 58, no. 4, pp. 1154–1161, Apr. 2011.

[4] Renewable Energy Policy Network for the 21st Centuray (REN21), 'Renewables Global Status Report , http://www.ren21.net/', 2017.

[5] E. P. I. A. (EPIA), 'Global Market Outlook for Photovoltaics until 2016', 2012.

[6] L. Hassaine, E. OLias, J. Quintero, and V. Salas, 'Overview of power inverter topologies and control structures for grid connected photovoltaic systems', *Renewable and Sustainable Energy Reviews*, vol. 30, pp. 796–807, Feb. 2014.

[7] O. Ellabban, H. Abu-Rub, and F. Blaabjerg, 'Renewable energy resources: Current status, future prospects and their enabling technology', *Renewable and Sustainable Energy Reviews*, vol. 39, pp. 748–764, Nov. 2014.

[8] S. R. Madeti and S. N. Singh, 'Monitoring system for photovoltaic plants: A review', *Renewable and Sustainable Energy Reviews*, vol. 67, pp. 1180–1207, Jan. 2017.

[9] B. Talbi, "Contribution à l'Amélioration de la commande d'un système de pompage photovoltaïque." Doctoral dissertation, Setif 1 University, 2018.

[10] M. E.-S. Ahmed, M. Orabi, and O. M. AbdelRahim, 'Two-stage micro-grid inverter with high-voltage gain for photovoltaic applications', *IET Power Electronics*, vol. 6, no. 9, pp. 1812–1821, Nov. 2013.

[11] A. Gupta, S. Chanana, and T. Thakur, 'Power quality assessment of a solar photovoltaic two-stage grid connected system: Using fuzzy and proportional integral controlled dynamic voltage restorer approach', *Journal of Renewable and Sustainable Energy*, vol.

7, no. 1, p. 013113, Jan. 2015.

[12] F. M. de Oliveira, S. A. O. da Silva, F. R. Durand, L. P. Sampaio, V. D. Bacon, and L. B. G. Campanhol, 'Grid-tied photovoltaic system based on PSO MPPT technique with active power line conditioning', *IET Power Electronics*, vol. 9, no. 6, pp. 1180–1191, May 2016.

[13] C. Jain and B. Singh, 'A Three-Phase Grid Tied SPV System With Adaptive DC Link Voltage for CPI Voltage Variations', *IEEE Transactions on Sustainable Energy*, vol. 7, no. 1, pp. 337–344, Jan. 2016.

[14] I. E. Commission, 'Characteristics of the utility interface for photovoltaic (PV) systems', *Report of IEC*, vol. 61727, 2002.

[15] H. C. Emissions, 'Limits for Harmonic Current Emission (Equipment Input Current <16 A per Phase), EN 61000-3-2', 2010.

[16] I. S. C. Committee, 'IEEE Standard for Interconnecting Distributed Resources with Electric Power Systems', *IEEE Std*, pp. 1547–2003, 2009.

[17] S. B. Kjaer, J. K. Pedersen, and F. Blaabjerg, 'A review of single-phase grid-connected inverters for photovoltaic modules', *IEEE transactions on industry applications*, vol. 41, no. 5, pp. 1292–1306, 2005.

[18] B. N. Alajmi, 'Design and control of photovoltaic systems in distributed generation', PhD Thesis, University of Strathclyde, 2013.

[19] B. M. T. Ho, S. H. Chung, and S. Y. R. Hui, 'An integrated inverter with maximum power tracking for grid-connected PV systems', in *Nineteenth Annual IEEE Applied Power Electronics Conference and Exposition, 2004. APEC '04.*, 2004, vol. 3, pp. 1559-1565.

[20] Y. Chen and K. M. Smedley, 'A cost-effective single-stage inverter with maximum power point tracking', *IEEE Transactions on Power Electronics*, vol. 19, no. 5, pp. 1289–1294, Sep. 2004.

[21] S. Jain and V. Agarwal, 'A single-stage grid connected inverter topology for solar PV systems with maximum power point tracking', *IEEE transactions on power electronics*, vol. 22, no. 5, pp. 1928–1940, 2007.

[22] W. Xiao, M. S. E. Moursi, O. Khan, and D. Infield, 'Review of grid-tied converter

topologies used in photovoltaic systems', *IET Renewable Power Generation*, vol. 10, no. 10, pp. 1543–1551, Jun. 2016.

[23] V. Yaramasu, 'Predictive control of multilevel converters for megawatt wind energy conversion systems', Ph. D. dissertation, Ryerson Univ., Toronto, ON, Canada, 2014.

[24] D. Picault, B. Raison, and S. Bacha, "Guidelines for evaluating grid connected PV system topologies," in *Industrial Technology, 2009. ICIT 2009. IEEE International Conference on*, 2009, pp. 1–5.

[25] L. Liu, H. Li, Y. Xue, and W. Liu, 'Decoupled Active and Reactive Power Control for Large-Scale Grid-Connected Photovoltaic Systems Using Cascaded Modular Multilevel Converters', *IEEE Transactions on Power Electronics*, vol. 30, no. 1, pp. 176–187, Jan. 2015.

[26] K. Himour, K. Ghedamsi, and E. M. Berkouk, 'Supervision and control of grid connected PV-Storage systems with the five level diode clamped inverter', *Energy Conversion and Management*, vol. 77, pp. 98–107, Jan. 2014.

[27] E. Ozdemir, S. Ozdemir, and L. M. Tolbert, 'Fundamental-Frequency-Modulated Six-Level Diode-Clamped Multilevel Inverter for Three-Phase Stand-Alone Photovoltaic System', *IEEE Transactions on Industrial Electronics*, vol. 56, no. 11, pp. 4407–4415, Nov. 2009.

[28] V. Yaramasu, B. Wu, and J. Chen, 'Model-Predictive Control of Grid-Tied Four-Level Diode-Clamped Inverters for High-Power Wind Energy Conversion Systems', *IEEE Transactions on Power Electronics*, vol. 29, no. 6, pp. 2861–2873, Jun. 2014.

[29] A. Choudhury, 'Three-level neutral point-clamped (NPC) traction inverter drive for electric vehicles', PhD Thesis, Concordia University, 2015.

[30] J. Rodriguez and P. Cortes, *Predictive Control of Power Converters and Electrical Drives*. John Wiley & Sons, 2012.

[31] J. Rodriguez *et al.*, 'State of the Art of Finite Control Set Model Predictive Control in Power Electronics', *IEEE Transactions on Industrial Informatics*, vol. 9, no. 2, pp. 1003–1016, May 2013.

[32] V. Yaramasu and B. Wu, 'Model Predictive Decoupled Active and Reactive Power Control for High-Power Grid-Connected Four-Level Diode-Clamped Inverters', *IEEE*

Transactions on Industrial Electronics, vol. 61, no. 7, pp. 3407–3416, Jul. 2014.

[33] B. Talbi, F. Krim, T. Rekioua, S. Mekhilef, A. Laib, and A. Belaout, 'A high-performance control scheme for photovoltaic pumping system under sudden irradiance and load changes', Solar Energy, vol. 159, pp. 353–368, Jan. 2018.

[34] A. Laib, F. Krim, B. Talbi, A. Kihal, and A. Sahli, 'Predictive Control Strategy for Double-Stage Grid Connected PV Systems', in *Advanced Control Engineering Methods in Electrical Engineering Systems*, 2019, pp. 314–327.

[35] A. Laib, F. Krim, B. Talbi, A. Kihal, and H. Feroura, 'Improved Control for Three Phase dual-Stage Grid-Connected PV Systems Based on a Predictive Control Strategy', *Journal of Control Engineering and Applied Informatics*, vol. 20, no. 3, pp. 12-23–23, Sep. 2018.

[36] E. Koutroulis, K. Kalaitzakis, and N. C. Voulgaris, 'Development of a microcontroller-based, photovoltaic maximum power point tracking control system', IEEE Transactions on power electronics, vol. 16, no. 1, pp. 46–54, 2001.

[37] N. Femia, G. Petrone, G. Spagnuolo, and M. Vitelli, Power electronics and control techniques for maximum energy harvesting in photovoltaic systems. CRC press, 2012.

[38] N. Femia, G. Petrone, G. Spagnuolo, and M. Vitelli, 'Optimization of perturb and observe maximum power point tracking method', IEEE transactions on power electronics, vol. 20, no. 4, pp. 963–973, 2005.

[39] K. H. Hussein, I. Muta, T. Hoshino, and M. Osakada, 'Maximum photovoltaic power tracking: an algorithm for rapidly changing atmospheric conditions', IEE Proceedings-Generation, Transmission and Distribution, vol. 142, no. 1, pp. 59–64, 1995.

[40] N. E. Zakzouk, M. A. Elsaharty, A. K. Abdelsalam, A. A. Helal, B. W. Williams, 'Improved performance low-cost incremental conductance PV MPPT technique', IET Renewable Power Generation, vol. 10, no. 4, pp. 561-574, 2016.

[41] K. S. Tey and S. Mekhilef, 'Modified incremental conductance MPPT algorithm to mitigate inaccurate responses under fast-changing solar irradiation level', Solar Energy, vol. 101, pp. 333–342, Mar. 2014.

[42] N. A. Gounden, S. Ann Peter, H. Nallandula, and S. Krithiga, 'Fuzzy logic controller with MPPT using line-commutated inverter for three-phase grid-connected photovoltaic

systems', Renewable Energy, vol. 34, no. 3, pp. 909–915, Mar. 2009.

[43] B. N. Alajmi, K. H. Ahmed, S. J. Finney, and B. W. Williams, 'Fuzzy-Logic-Control Approach of a Modified Hill-Climbing Method for Maximum Power Point in Microgrid Standalone Photovoltaic System', IEEE Transactions on Power Electronics, vol. 26, no. 4, pp. 1022–1030, Apr. 2011.

[44] W. Lin, C. Hong, and C. Chen, 'Neural-Network-Based MPPT Control of a Stand-Alone Hybrid Power Generation System', IEEE Transactions on Power Electronics, vol. 26, no. 12, pp. 3571–3581, Dec. 2011.

[45] Y.-H. Liu, C.-L. Liu, J.-W. Huang, and J.-H. Chen, 'Neural-network-based maximum power point tracking methods for photovoltaic systems operating under fast changing environments', Solar Energy, vol. 89, pp. 42–53, Mar. 2013.

[46] A. Chaouachi, R. M. Kamel, and K. Nagasaka, 'A novel multi-model neuro-fuzzy-based MPPT for three-phase grid-connected photovoltaic system', Solar Energy, vol. 84, no. 12, pp. 2219–2229, Dec. 2010.

[47] A. Chikh and A. Chandra, 'Adaptive neuro-fuzzy based solar cell model', IET Renewable Power Generation, vol. 8, no. 6, pp. 679–686, Aug. 2014.

[48] A. Chikh and A. Chandra, 'An Optimal Maximum Power Point Tracking Algorithm for PV Systems With Climatic Parameters Estimation', IEEE Transactions on Sustainable Energy, vol. 6, no. 2, pp. 644–652, Apr. 2015.

[49] C. Larbes, S. M. Aït Cheikh, T. Obeidi, and A. Zerguerras, 'Genetic algorithms optimized fuzzy logic control for the maximum power point tracking in photovoltaic system', Renewable Energy, vol. 34, no. 10, pp. 2093–2100, Oct. 2009.

[50] Y. Shaiek, M. Ben Smida, A. Sakly, and M. F. Mimouni, 'Comparison between conventional methods and GA approach for maximum power point tracking of shaded solar PV generators', Solar Energy, vol. 90, pp. 107–122, Apr. 2013.

[51] K. Ishaque, Z. Salam, M. Amjad, and S. Mekhilef, 'An Improved Particle Swarm Optimization (PSO)–Based MPPT for PV With Reduced Steady-State Oscillation', IEEE Transactions on Power Electronics, vol. 27, no. 8, pp. 3627–3638, Aug. 2012.

[52] R. Pradhan and B. Subudhi, 'Double Integral Sliding Mode MPPT Control of a Photovoltaic System', IEEE Transactions on Control Systems Technology, vol. 24, no.

1, pp. 285–292, Jan. 2016.

[53] A. Kihel, F. Krim, and A. Laib, ‘MPPT voltage oriented loop based on integral sliding mode control applied to the boost converter’, In: 2017 6th International Conference on Systems and Control (ICSC), Batna, Algeria, 2017, pp. 205–209.

[54] M. Farhat, O. Barambones, and L. Sbita, ‘A new maximum power point method based on a sliding mode approach for solar energy harvesting’, Applied Energy, vol. 185, pp. 1185–1198, Jan. 2017.

[55] A. Kihal, F. Krim, A. Laib, B. Talbi, and H. Afghoul, ‘An improved MPPT scheme employing adaptive integral derivative sliding mode control for photovoltaic systems under fast irradiation changes’, ISA Transactions, Nov. 2018.

[56] Naghmash, H. Armghan, I. Ahmad, A. Armghan, S. Khan, and M. Arsalan, ‘Backstepping based non-linear control for maximum power point tracking in photovoltaic system’, Solar Energy, vol. 159, pp. 134–141, Jan. 2018.

[57] S. K. Kollimalla and M. K. Mishra, ‘A novel adaptive P&O MPPT algorithm considering sudden changes in the irradiance’, IEEE Transactions on Energy Conversion, vol. 29, no. 3, pp. 602–610, Sep. 2014.

[58] P. E. Kakosimos and A. G. Kladas, ‘Implementation of photovoltaic array MPPT through fixed step predictive control technique’, Renewable Energy, vol. 36, no. 9, pp. 2508–2514, Sep. 2011.

[59] B. Talbi, F. Krim, T. Rekioua, A. Laib, and H. Feroura, ‘Design and hardware validation of modified P&O algorithm by fuzzy logic approach based on model predictive control for MPPT of PV systems’, Journal of Renewable and Sustainable Energy, vol. 9, no. 4, p. 043503, Jul. 2017.

[60] E. Bianconi et al., ‘A Fast Current-Based MPPT Technique Employing Sliding Mode Control’, IEEE Transactions on Industrial Electronics, vol. 60, no. 3, pp. 1168–1178, Mar. 2013.

[61] A. Krama, L. Zellouma, and R. Boualaga, ‘Anti-windup proportional integral strategy for shunt active power filter interfaced by photovoltaic system using technique of direct power control’, Revue roumaine des sciences techniques, vol. 62, no. 3, pp. 252–257, 2017.

[62] A. Sahli, F. Krim, A. Belaout, ‘Energy Management and Power Quality Improvement in Grid-Connected Photovoltaic Systems’, In: 2017 International Renewable and Sustainable Energy Conference (IRSEC), Tangier, Morocco, 2017, pp. 1-7.

[63] A. Krama, L. Zellouma, B. Rabhi, A. Laib, ‘Fuzzy Logic Controller for Improving DC Side of PV Connected Shunt Active Filter Based on MPPT Sliding Mode Control’, in International Conference in Artificial Intelligence in Renewable Energetic Systems, 2017, pp. 224-235.

[64] M. Singh and A. Chandra, ‘Real-Time Implementation of ANFIS Control for Renewable Interfacing Inverter in 3P4W Distribution Network’, IEEE Transactions on Industrial Electronics, vol. 60, no. 1, pp. 121–128, Jan. 2013.

[65] A. Krama, L. Zellouma, A. Benaissa, B. Rabhi, M. Bouzidi, and M. F. Benkhoris, ‘Design and Experimental Investigation of Predictive Direct Power Control of Three-Phase Shunt Active Filter with Space Vector Modulation using Anti-windup PI Controller Optimized by PSO’, Arabian Journal for Science and Engineering, , 1-15. Nov. 2018.

[66] A. Laib, F. Krim, and B. Talbi, ‘An improved control for two-stage grid-connected photovoltaic systems’, in In: Proc. ICESTI’16, Annaba, Algérie, Nov. 2016.

[67] L. Zellouma, R. Boualaga, A. Krama, A. Benaissa, and M. F. Benkhoris, ‘Simulation and real time implementation of three phase four wire shunt active power filter based on sliding mode controller’, Revue roumaine des sciences techniques, vol. 63, no. 1, pp. 77–82, 2018.

[68] A. Kihal, F. Krim, B. Talbi, A. Laib, and A. Sahli, ‘A Robust Control of Two-Stage Grid-Tied PV Systems Employing Integral Sliding Mode Theory’, Energies, vol. 11, no. 10, p. 2791, Oct. 2018.

[69] T. Noguchi, H. Tomiki, S. Kondo, and I. Takahashi, ‘Direct power control of PWM converter without power-source voltage sensors’, IEEE Transactions on Industry Applications, vol. 34, no. 3, pp. 473–479, May 1998.

[70] R. Teodorescu, M. Liserre, and P. Rodriguez, Grid Converters for Photovoltaic and Wind Power Systems. John Wiley & Sons, 2011.

[71] F. Liu, S. Duan, F. Liu, B. Liu, and Y. Kang, ‘A variable step size INC MPPT method for PV systems’, *IEEE Transactions on industrial electronics*, vol. 55, no. 7, pp. 2622–2628,

2008.

[72] A. Loukriz, M. Haddadi, and S. Messalti, ‘Simulation and experimental design of a new advanced variable step size Incremental Conductance MPPT algorithm for PV systems’, *ISA transactions*, vol. 62, pp. 30–38, 2016.

[73] P. E. Kakosimos, A. G. Kladas, and S. N. Manias, ‘Fast photovoltaic-system voltage-or current-oriented MPPT employing a predictive digital current-controlled converter’, *IEEE transactions on Industrial Electronics*, vol. 60, no. 12, pp. 5673–5685, 2013.

[74] E. V. Dijk, J. N. Spruijt, D. M. O’Sullivan, and J. B. Klaassens, ‘PWM-switch modeling of DC-DC converters’, *IEEE Transactions on Power Electronics*, vol. 10, no. 6, pp. 659–665, Nov. 1995.

[75] J. Rodriguez *et al.*, ‘Predictive Current Control of a Voltage Source Inverter’, *IEEE Transactions on Industrial Electronics*, vol. 54, no. 1, pp. 495–503, Feb. 2007.

[76] S. Kouro, P. Cortes, R. Vargas, U. Ammann, and J. Rodriguez, ‘Model Predictive Control—A Simple and Powerful Method to Control Power Converters’, *IEEE Transactions on Industrial Electronics*, vol. 56, no. 6, pp. 1826–1838, Jun. 2009.

[77] J. D. Irwin and B. Wilamowski, *The Industrial Electronics Handbook: control and mechatronics; Second edition.* Taylor & Francis, 2011.

[78] A. K. Gupta and A. M. Khambadkone, ‘A Space Vector PWM Scheme for Multilevel Inverters Based on Two-Level Space Vector PWM’, *IEEE Transactions on Industrial Electronics*, vol. 53, no. 5, pp. 1631–1639, Oct. 2006.

[79] A. Lewicki, Z. Krzeminski, and H. Abu-Rub, ‘Space-Vector Pulsewidth Modulation for Three-Level NPC Converter With the Neutral Point Voltage Control’, *IEEE Transactions on Industrial Electronics*, vol. 58, no. 11, pp. 5076–5086, Nov. 2011.

[80] S. Rivera *et al.*, ‘Multilevel Direct Power Control—A Generalized Approach for Grid-Tied Multilevel Converter Applications’, *IEEE Transactions on Power Electronics*, vol. 29, no. 10, pp. 5592–5604, Oct. 2014.

[81] J. Eloy-García, S. Arnaltes, and J. L. Rodríguez-Amenedo, ‘Extended direct power control for multilevel inverters including DC link middle point voltage control’, *IET Electric Power Applications*, vol. 1, no. 4, p. 571, 2007.

[82] L. A. Serpa, P. M. Barbosa, P. K. Steimer, and J. W. Kolar, ‘Five-level virtual-flux direct power control for the active neutral-point clamped multilevel inverter’, in *2008 IEEE Power Electronics Specialists Conference*, Rhodes, Greece, 2008, pp. 1668–1674.

[83] B. Wu, Y. Lang, N. Zargari, and S. Kouro, *Power conversion and control of wind energy systems*, vol. 76. John Wiley & Sons, 2011.

[84] R. Portillo, S. Vazquez, J. I. Leon, M. M. Prats, and L. G. Franquelo, ‘Model Based Adaptive Direct Power Control for Three-Level NPC Converters’, *IEEE Transactions on Industrial Informatics*, vol. 9, no. 2, pp. 1148–1157, May 2013.

[85] A. K. Bonala, S. R. Sandepudi, and V. P. Muddineni, ‘Model predictive current control with modified synchronous detection technique for three-phase 3L-NPC multi-functional solar photovoltaic system’, in *2016 IEEE International Conference on Power Electronics, Drives and Energy Systems (PEDES)*, 2016, pp. 1–6.

[86] R. Vargas, P. Cortes, U. Ammann, J. Rodriguez, and J. Pontt, ‘Predictive Control of a Three-Phase Neutral-Point-Clamped Inverter’, *IEEE Transactions on Industrial Electronics*, vol. 54, no. 5, pp. 2697–2705, Oct. 2007.

[87] V. Yaramasu, B. Wu, M. Rivera, and J. Rodriguez, ‘Predictive current control and DC-link capacitor voltages balancing for four-leg NPC inverters’, in *2013 IEEE International Symposium on Industrial Electronics*, 2013, pp. 1–6.

[88] F. S. Saeed and P. H. Reza, ‘Predictive control of a five-level NPC inverter using a three-phase coupled inductor’, in *2016 7th Power Electronics and Drive Systems Technologies Conference (PEDSTC)*, 2016, pp. 602–607.

[89] H. Feroura, F. Krim, B. Talbi, A. Laib, and A. Belaout, ‘Finite-Set Model Predictive Direct Power Control of Grid Connected Current Source Inverter’, *Elektronika ir Elektrotechnika*, vol. 23, no. 5, pp. 36-40–40, Oct. 2017.

[90] J. Scoltock, T. Geyer, and U. K. Madawala, ‘Model predictive direct power control for grid-connected NPC converters’, *IEEE Transactions on industrial Electronics*, vol. 62, no. 9, pp. 5319–5328, 2015.

[91] Q. Chen, Q. Wang, L. Cheng, and C. Zheng, ‘Study of predictive direct power control for three-level NPC converter’, in *2016 IEEE 11th Conference on Industrial Electronics and Applications (ICIEA)*, 2016, pp. 1207–1211.

[92] M. Habibullah, D. D. Lu, D. Xiao, J. E. Fletcher, and M. F. Rahman, 'Predictive Torque Control of Induction Motor Sensorless Drive Fed by a 3L-NPC Inverter', *IEEE Transactions on Industrial Informatics*, vol. 13, no. 1, pp. 60–70, Feb. 2017.

[93] P. Cortes, A. Wilson, S. Kouro, J. Rodriguez, and H. Abu-Rub, 'Model Predictive Control of Multilevel Cascaded H-Bridge Inverters', *IEEE Transactions on Industrial Electronics*, vol. 57, no. 8, pp. 2691–2699, Aug. 2010.

[94] A. Laib, F. Krim, B. Talbi, H. Feroura, A. Kihal, 'Decoupled active and reactive power control strategy of grid-connected six-level diode-clamped inverters based on finite set model predictive control for photovoltaic application', Revue roumaine des sciences techniques, vol. 64, no. 1, pp. 51–56, 2019.

[95] R. Mechouma, H. Mebarki, and B. Azoui, 'Behavior of nine levels NPC three-phase inverter topology interfacing photovoltaic system to the medium electric grid under variable irradiance', *Electrical Engineering*, vol. 100, no. 3, pp. 2129–2145, Sep. 2018.

[96] M. Benadja, S. Saad, and B. Ali, 'Sensorless control of inverter dc-bus voltage combined with modified PQ control using extended Kalman filter in a photovoltaic system', *Electrical Engineering*, vol. 99, no. 1, pp. 265–274, Mar. 2017.

[97] A. Menadi, S. Abdeddaim, A. Ghamri, and A. Betka, 'Implementation of fuzzy-sliding mode based control of a grid connected photovoltaic system', *ISA Transactions*, vol. 58, pp. 586–594, Sep. 2015.

[98] G. M. S. Islam, A. Al-Durra, S. M. Muyeen, and J. Tamura, 'Low voltage ride through capability enhancement of grid connected large scale photovoltaic system', in *IECON 2011 - 37th Annual Conference of the IEEE Industrial Electronics Society*, 2011, pp. 884–889.

[99] D. Xu, C. Du, and E. Xie, 'Research and simulation analysis of control strategies for the large-scale grid-connected photovoltaic system', in *2015 Sixth International Conference on Intelligent Control and Information Processing (ICICIP)*, 2015, pp. 167–172.

[100] S. Kouro, K. Asfaw, R. Goldman, R. Snow, B. Wu, and J. Rodríguez, 'NPC multilevel multistring topology for large scale grid connected photovoltaic systems', in *The 2nd International Symposium on Power Electronics for Distributed Generation Systems*, 2010, pp. 400–405.

[101] G. W. Hart, H. M. Branz, and C. H. Cox, 'Experimental tests of open-loop maximum-power-point tracking techniques for photovoltaic arrays', *Solar Cells*, vol. 13, no. 2, pp. 185–195, Dec. 1984.

[102] Z. M. Salameh, F. Dagher, and W. A. Lynch, 'Step-down maximum power point tracker for photovoltaic systems', *Solar Energy*, vol. 46, no. 5, pp. 279–282, Jan. 1991.

[103] A. Belkaid, I. Colak, and K. Kayisli, 'Implementation of a modified P&O-MPPT algorithm adapted for varying solar radiation conditions', *Electrical Engineering*, vol. 99, no. 3, pp. 839–846, Sep. 2017.

[104] M. M. Algazar, H. AL-monier, H. A. EL-halim, and M. E. E. K. Salem, 'Maximum power point tracking using fuzzy logic control', *International Journal of Electrical Power & Energy Systems*, vol. 39, no. 1, pp. 21–28, Jul. 2012.

[105] M. Nabipour, M. Razaz, S. G. Seifossadat, and S. S. Mortazavi, 'A new MPPT scheme based on a novel fuzzy approach', *Renewable and Sustainable Energy Reviews*, vol. 74, pp. 1147–1169, Jul. 2017.

[106] S. A. Rizzo and G. Scelba, 'ANN based MPPT method for rapidly variable shading conditions', *Applied Energy*, vol. 145, pp. 124–132, May 2015.

[107] H. Boumaaraf, A. Talha, and O. Bouhali, 'A three-phase NPC grid-connected inverter for photovoltaic applications using neural network MPPT', *Renewable and Sustainable Energy Reviews*, vol. 49, pp. 1171–1179, Sep. 2015.

[108] M. A. G. de Brito, L. Galotto, L. P. Sampaio, G. d A. e Melo, and C. A. Canesin, 'Evaluation of the Main MPPT Techniques for Photovoltaic Applications', *IEEE Transactions on Industrial Electronics*, vol. 60, no. 3, pp. 1156–1167, Mar. 2013.

[109] H. Feroura, F. Krim, B. Talbi, A. Laib, A. Belaout, 'Sensorless field oriented control of current source inverter fed induction motor drive', Revue roumaine des sciences techniques, vol. 63, no. 1, pp. 100–105, 2018.

[110] H. Feroura, F. Krim, B. Tabli, A. Laib, 'Finite-set model predictive voltage control for islanded three phase current source inverter', In: 2017 5th International Conference on Electrical Engineering-Boumerdes (ICEE-B), Boumerdes, Algeria, 2017, pp. 1-5.

A Robust Control for Grid-Connected PV Systems using Multilevel Inverters

Abstract :

Several grid-connected PV topologies are investigated in this dissertation for low, medium and high power applications. Furthermore, an effective controllers have been proposed for these topologies instead of conventional control strategies. The latter's suffer from several drawbacks such as bad MPPT tracking, inaccurate grid power control, low grid current quality, hard implementation practically and variable switching frequency. To overcome these drawbacks, a model predictive control (MPC) strategy is proposed to control the power converters employed in the investigated grid-connected PV topologies. The major drawbacks of MPC strategy are variable inherent switching frequency and computational burden especially in case of high-level inverters. Therefore, these drawbacks are taking into account in the design of proposed controllers. Firstly, an improved control strategy based on fixed switching predictive control strategy for three-phase dual-stage grid-connected PV system is proposed. A variable incremental current step size of an MPPT current oriented loop based on fixed-switching predictive current control is proposed and employed to control the DC-DC converter. While, a modified VOC based on predictive control strategy and space vector modulation (SVM) is employed to control the DC-AC converter. Afterwards, High-level NPC inverters are employed in grid-connected PV system in order to inject a high produced PV power into the grid with high performance operation. On the other hand, a simple and effective model predictive control (MPC) algorithm is proposed for grid-connected PV system using high-level NPC inverter (six-level) that permits to inject the active power generated by the PV system, the reactive power demanded by the grid operator and assure the balance of DC-link capacitor voltages. Then, an optimized model predictive control (O-MPC) is proposed in order to achieve the same performance control provided by the MPC algorithm but with a significant reduction in computational burden. Finally, a topology that divided the large PV array to string modules with individual DC-DC converter connected to a centralized multilevel inverter is investigated in order to overcome the problems resulted by connecting the PV modules as large PV array. Simple and effective controllers for this topology based on finite control set model predictive control (FCS-MPC) strategy is proposed. A voltage oriented maximum power point tracking (VO-MPPT) performed by an FCS-MPCC is applied for each DC-DC converter to draw the maximum power point from each string PV modules. In addition, an FCS-MPC controller is proposed to control the centralized multilevel NPC inverter connected to the grid. The simulation and HIL results validate the proposed control schemes for the investigated grid-connected PV topologies.

Keywords:photovoltaic energy, grid-connected PV systems, multilevel inverters, maximum power point (MPPT), model Predictive Control.

Commande robuste de systèmes photovoltaïques interconnectés au réseau avec convertisseurs multi niveaux

Résumé :

Différentes topologies des systèmes photovoltaïques (PV) interconnectées au réseau pour des applications faibles, moyennes et hautes puissance sont étudiées dans cette thèse. En outre, des contrôleurs efficaces ont été proposés pour ces topologies au lieu des stratégies conventionnelles. Ces derniers souffrent de plusieurs inconvénients tels que le mauvais suivi du point de puissance maximale, le contrôle imprécis des puissances injectées au réseau, la mauvaise qualité du courant du réseau, la complexité de l'implémentation pratique et la fréquence de commutation variable. Pour surmonter ces inconvénients, une stratégie de commande prédictive est proposée pour contrôler les différents convertisseurs de puissance utilisés dans les topologies étudiées. Toutefois, la commande prédictive présente quelques inconvénients qui sont particulièrement la fréquence de commutation variable et la charge de calcul dans le cas des onduleurs multiniveaux. Par conséquent, ces inconvénients sont pris en compte dans la conception des contrôleurs proposés. En premier lieu, on a proposé un schéma de commande amélioré fondé sur une stratégie de commande prédictive avec une fréquence de commutation fixe pour un système PV interconnectées au réseau à double étage. Un algorithme de l'incrément de conductance à pas variable de courant employé avec un contrôleur prédictif à fréquence de commutation fixe est proposé pour contrôler le convertisseur DC-DC. Tandis qu'une commande VOC modifiée basée sur la commande prédictive et l'algorithme de la MLI vectorielle est employée pour contrôler le convertisseur DC-AC. Par la suite, des onduleurs multiniveaux du type NPC sont employés dans un système PV interconnectées au réseau afin d'injecter une haute puissance dans le réseau avec une bonne performance. D'autre part, un algorithme prédictif simple et efficace est proposé pour le système interconnecté au réseau avec un onduleur NPC (six-niveaux) cela permet d'injecter la puissance active générée par le système PV, la puissance réactive demandée par l'opérateur de réseau et assurer la balance des tensions des condensateurs du bus continu. Ensuite, une commande prédictive optimisée est proposée afin d'obtenir la même performance que l'algorithme prédictif avec une rédaction signifiante de la charge de calcul. Finalement, une topologie qui divise un grand champ PV en des panneaux PV avec un convertisseur DC-DC individuel connecté à un onduleur NPC multi-niveaux (cinq-niveaux) centralisé est développée afin de surmonter les problèmes résultent de la connexion de nombreux modules PV. Des contrôleurs simples et efficaces pour cette topologie bases sur la commande prédictive des éléments finis sont proposés. Une commande MPPT à pilotage de tension effectué par un contrôleur prédictif est appliquée pour chaque convertisseur DC-DC pour suivre le point de puissance maximum de chaque panneau PV. De plus, un contrôleur prédictif est proposé pour contrôler l'onduleur NPC centralisé connecté au réseau. Les résultats de la simulation et l'implémentation sur un banc hardware in the loop valident les schémas de commande proposés pour les topologies PV connectées au réseau étudiées.

Mots clés : Energie photovoltaïque; Système de pompage photovoltaïque; MPPT; La logique floue; La commande prédictive.

تحكم قوي للأنظمة الكهرضوئية الموصلة بالشبكة و المستعملة للعاكسات متعددة المستويات

ملخص:

تم تقديم العديد من طوبولوجيا الكهروضوئية الموصلة بالشبكة لتطبيقات الطاقة المنخفضة، المتوسطة والعالية إضافة الى اقتراح إستراتيجيات تحكم جديدة بديلا للتقليدية. تعاني استراتيجيات التحكم التقليدية للنظام الكهروضوئي المتصل بالشبكة المتصل بالشبكة من عدة عيوب مثل: تتبع سيء للنقطة العظمى للطاقة، التحكم الغير دقيق في طاقة الشبكة، الجودة المنخفضة لتيار الشبكة، التنفيذ الصعب لهذه الإستراتيجيات عمليا والتردد المتغير. للتغلب على هذه العيوب، تم اقتراح استراتيجية تحكم تنبؤية (MPC) للتحكم في محولات الطاقة المستخدمة في طوبولوجيا الكهروضوئية الموصلة بالشبكة. تم أخذ بعين الاعتبار في تصميم مخططات التحكم المقترحة العيوب الرئيسية لهذه الإستراتيجية المتمثلة في التردد المتغير والعبء الحسابي، خاصة في حالة العاكسات متعددة المستويات. أولا، تم اقتراح إستراتيجية تحكم محسنة تعتمد على إستراتيجية التحكم التنبئي مع تردد ثابت لنظام الطاقة الكهروضوئية مزدوج مراحل التحويل الموصل بالشبكة. إستراتيجية تتبع النقطة الأعظمية بخطوات متغيرة موجهة بمتحكم تنبئ ذو تردد ثابت قد اقترحت وطبقت على مرحلة التحويل الأولى (مستمر-مستمر). في حين ان تحكم (VOC) قد تم تعديلها باستخدام إستراتيجية التحكم التنبئي وتضمين المتجه الفضائيSVM وتطبيقها للتحكم في مرحلة التحول الثانية (مستمر-متناوب). بعد ذلك، يتم استخدام العاكسات متعددة المستويات في النظام الكهروضوئي المتصل بالشبكة من أجل حقن كمية الطاقة الكبيرة المستخرجة من الألواح الشمسية مع أداء عالي. من ناحية أخرى، يتم اقتراح نموذج تحكم تنبئي وفعال لنظام الكهروضوئية الموصلة بالشبكة باستخدام العاكسات متعددة المستويات (ستة مستويات) التي تسمح بحقن الطاقة النشطة المولدة من النظام الكهروضوئي والطاقة المتفاعلة المطلوبة من طرف مشغل الشبكة مع ضمان توازن الجهد في المكثفات. بعد ذلك تم اقتراح نموذج محسن لنظام التحكم التنبئي(O-MPC) مناجل تحقيق نفس أداء التحكم التنبئي السابق ولكن مع انخفاض كبير في العبء الحسابي. وأخيرًا، تم تقديم الطوبولوجيا التي تقسم حقل كبير من الألواح الشمسية إلى وحدات صغيرة مع محول (DC-DC)، الكل متصل بعاكس مركزي متعدد المستويات للتغلب على المشكلات الناتجة عن توصيل الوحدات الكهروضوئية كحقل كبير. يتم اقتراح وحدات تحكم بسيطة وفعالة لهذا الهيكل القائم على أساس استراتيجية التحكم المحدد في نموذج التحكم التنبئي (FCS-MPC). يتم تطبيق تتبع جهد أقصى نقطة طاقة بواسطة (VO-MPPT) المعتمدة على التحكم التنبئي للتيار (FCS-MPCC) لكل محول DC-DC لتتبع أقصى نقطة طاقة من كل سلسلة من الوحدات الكهروضوئية. بالإضافة إلى ذلك، يتم اقتراح وحدة تحكم FCS-MPC للتحكم في العاكس المركزي متعدد المستويات NPC المتصل بالشبكة. نتائج المحاكاة والتطبيق العملي باستعمال نظام HIL تحقق صحة خطط التحكم المقترحة.

الكلمات المفتاحية : الطاقة الكهروضوئية، الانظمة الكهروضوئية المتصلة بالشبكة، العاكسات المتعددة المستويات، تتبع نقطة الطاقة القصوى (MPPT)، نموذج التحكم التنبئي (MPC)